Missouri State University

BearWorks

MSU Graduate Theses

Summer 2022

U-Pb Apatite Chronometry of Intrusions in an Accretionary Metamorphic Belt in Western Idaho, USA

Colleen Grace Rankin
Missouri State University, Rankin19@live.missouristate.edu

As with any intellectual project, the content and views expressed in this thesis may be considered objectionable by some readers. However, this student-scholar's work has been judged to have academic value by the student's thesis committee members trained in the discipline. The content and views expressed in this thesis are those of the student-scholar and are not endorsed by Missouri State University, its Graduate College, or its employees.

Follow this and additional works at: https://bearworks.missouristate.edu/theses

 Part of the Geochemistry Commons, Geology Commons, and the Tectonics and Structure Commons

Recommended Citation

Rankin, Colleen Grace, "U-Pb Apatite Chronometry of Intrusions in an Accretionary Metamorphic Belt in Western Idaho, USA" (2022). *MSU Graduate Theses*. 3769.
https://bearworks.missouristate.edu/theses/3769

This article or document was made available through BearWorks, the institutional repository of Missouri State University. The work contained in it may be protected by copyright and require permission of the copyright holder for reuse or redistribution.
For more information, please contact BearWorks@library.missouristate.edu.

U-PB APATITE CHRONOMETRY OF INTRUSIONS IN AN ACCRETIONARY METAMORPHIC BELT IN WESTERN IDAHO, USA

A Master's Thesis

Presented to

The Graduate College of

Missouri State University

In Partial Fulfillment

Of the Requirements for the Degree

Master of Science, Geography and Geology

By

Colleen Grace Rankin

August 2022

Copyright 2022 by Colleen Grace Rankin

U-PB APATITE CHRONOMETRY OF INTRUSIONS IN AN ACCRETIONARY METAMORPHIC BELT IN WESTERN IDAHO, USA

Geography, Geology, and Planning

Missouri State University, August 2022

Master of Science

Colleen Grace Rankin

ABSTRACT

The Salmon River suture zone in west-central Idaho, USA records the tectonic processes where island arcs, similar to modern-day Japan, were accreted to the North American continent in the Jurassic and Cretaceous periods (160-90 million years ago). This suture zone contains metamorphic rocks that were buried deep within the crust at depths of 20 kilometers or more and have subsequently been brought to the surface. The exhuming processes responsible for the metamorphic rocks in the Salmon River suture zone remains unclear. Two competing hypotheses have been proposed to explain the transport of the rocks from the Salmon River suture zone to the surface: (1) buoyancy changes in the crust from lithosphere delamination or (2) thrust faults bringing rocks to the surface. I present apatite closure temperature estimates with apatite, zircon, and rutile ages to test the two competing hypotheses that have been proposed to explain the transport of the rocks from the Salmon River suture zone to the surface. U-Pb radiometric ages and closure temperature estimates have been collected from the mineral's apatite, zircon, and rutile to investigate age and cooling trends in deformed igneous intrusions. U-Pb apatite ages record cooling temperatures from a 350-500 °C cooling window, this can be refined depending on the grain size of apatite. When combined with garnet, hornblende, muscovite and biotite ages and closure temperatures, a full multi-mineral temperature time path can be created to give insight on the exhumation processes of the region.

KEYWORDS: closure temperature, U-Pb, apatite, zircon, geochronology, island-arc terranes, exhumation, salmon river suture zone

U-PB APATITE CHRONOMETRY OF INTRUSIONS IN AN ACCRETIONARY METAMORPHIC BELT IN WESTERN IDAHO, USA

By

Colleen Grace Rankin

A Master's Thesis
Submitted to the Graduate College
Of Missouri State University
In Partial Fulfillment of the Requirements
For the Degree of Master of Science, Geography and Geology

August 2022

Approved:

Matthew P. McKay, Ph.D., Thesis Committee Chair

Gary Michelfelder, Ph.D., Committee Member

Kevin Mickus, Ph.D., Committee Member

Julie Masterson, Ph.D., Dean of the Graduate College

In the interest of academic freedom and the principle of free speech, approval of this thesis indicates the format is acceptable and meets the academic criteria for the discipline as determined by the faculty that constitute the thesis committee. The content and views expressed in this thesis are those of the student-scholar and are not endorsed by Missouri State University, its Graduate College, or its employees.

ACKNOWLEDGEMENTS

First, I would like to thank my thesis advisor Dr. Matthew McKay, this project would not be possible without his guidance. Thank you for dealing with my many “crises” that arose each week with my data. I would also like to thank my two thesis committee members, Dr. Gary Michelfelder, and Dr. Kevin Mickus. Also thank you to Dr. Barry Shaulis at the University of Arkansas for the assistance with the LA-ICPMS. Graduate school would not be possible without the support system of my friends. I would like to thank my field partners: Adelie Ionescu, Oren Redus, JZ Upp, and Jon Cone. Also special thanks to my first office mate and who I shared all graduate classes with, Harrison Birch Richardson, and my roommate Keigon Bruneteau who kept me sane the last year and shared the same love for rocks as me. I would like to acknowledge a few places in Springfield that also kept me sane throughout the last two years: Missouri State University’s rock-climbing wall and Sunshine Lanes. An honorable mention would be for the River Rock Café and Seven Devils Saloon in Riggins, Idaho for providing the BEST food to consume while conducting my field research. This project would not be possible without the funding from the National Science Foundation and the Missouri State Graduate college, so thank you.

I dedicate this thesis to myself.

TABLE OF CONTENTS

Introduction	1
Geologic Background	3
Tectonic Framework of the Blue Mountains Province	3
The Salmon River Suture Zone	7
Study Area	12
Methods	15
U-Pb Zircon	17
U-Pb Rutile	17
U-Pb Apatite	18
Results	20
U-Pb Zircon	20
U-Pb Rutile	23
U-Pb Apatite	24
Discussion	56
Metamorphic History of Zircon	56
Zr-in-Rutile Thermochronology	58
Spatial Cooling Trends in the Salmon River Suture Zone	59
Multi-mineral Temperature-time Paths from the Salmon River Suture Zone	61
Delamination	66
Thrust Propagation	68
Conclusion	72
References Cited	74
Appendices	85
Appendix A. UTM Coordinates for samples found in the Salmon River suture zone in zone 11T using WGS 84 datum	85
Appendix B. U-Pb Zircon Ages	87
Appendix C. U-Pb Rutile Ages	103
Appendix D. U-Pb Apatite Ages and Closure Temperatures	104

LIST OF FIGURES

Figure 1. Regional map of the Blue Mountains province 10

Figure 2. Simplified map of the Salmon River suture zone 11

Figure 3. Sample location map along the Salmon River 13

Figure 4. Sample location map on Pollock Mountain 14

Figure 5. Weighted mean ages and sample photos for U-Pb zircon 30

Figure 6. Zircon crystallization age vs. U/Th ratios 35

Figure 7. Weighted mean ages and sample photos for U-Pb apatite 39

Figure 8. Apatite grain size vs closure temperature 47

Figure 9. Apatite age vs closure temperature 51

Figure 10. Temperature-time cooling paths 70

Figure 11. Mineral grain length uncertainty 71

INTRODUCTION

The Salmon River suture zone records the accretion of oceanic crustal fragments to the North American cordilleran margin (Hamilton, 1963; Lund and Snee, 1988; Snee et al., 1995; Vallier, 1995; McClelland et al., 2000; Fleck and Criss, 2004). The North American Cordillera developed through a series of accretionary orogens, where multiple oceanic terranes collided with the western margin of Laurentia (Fleck and Criss, 1985; Lund and Snee, 1988; McClelland et al., 2000; Tikoff et al., 2001; Giorgis et al., 2008; Zak et al., 2015). Accretional orogens created crustal thickening, metamorphism, and wide-spread magmatism that are recorded in the mid-crustal rocks of the Pacific Northwest (Cawood et al., 2009).

In western Idaho, the Salmon River suture zone separates accreted oceanic island arc rocks with continental rocks and records Cretaceous metamorphism and deformation that began about 120 Ma (Sutter et al., 1984; Criss and Fleck, 1987; Lund and Snee, 1988; Manduca, 1988; McClelland et al., 2000; Giorgis et al., 2008). While the burial conditions and prograde metamorphic history of rocks in the Salmon River suture zone have been investigated, there are very few constraints on the timing and magnitude of exhumation, which could record (1) synorogenic, tectonic exhumation, (2) post-orogenic uplift, and (3) Cenozoic topographic development, including incision of the Salmon and Snake rivers. Limited evidence suggests that the cooling of the Salmon River metamorphic rocks may have been relatively rapid, with cooling rates of 1000 °C/m.y. to less than 5 °C/m.y. for slow cooling (Lund and Snee, 1988). Two hypotheses have been proposed to explain the possible rapid cooling of the Salmon River suture

zone rocks during exhumation to the surface: 1) buoyancy changes in the lithosphere driven by delamination of the lithospheric mantle (Selverstone et al., 1992) and 2) thrust fault exhumation of hanging wall rocks during out-of-sequence thrust propagation (McKay et al., 2017). Understanding how rocks were exhumed is crucial to the construction of an orogen. To test the two proposed models, U-Pb (uranium-lead) isotopic ages and closure temperatures from the mineral's apatite, zircon, and rutile are presented to provide cooling trends through time (temperature-time or T-t paths) for pre-, syn-, and post-kinematic igneous intrusions within the Salmon River suture zone. Using apatite as a thermochronometer, the goal is to apply U-Pb apatite and closure temperature estimates to create a single system, multi-point cooling path. Currently, the window for apatite's closure temperature is 350-500 °C. This range can be refined depending on the mineral's grain size. Peak metamorphism has been previously dated for the rocks in the Salmon River suture zone (McKay et al., 2017), allowing apatite to provide better spatial control of the region.

GEOLOGIC BACKGROUND

Rocks of western Idaho record mid-crustal metamorphism and deformation associated with orogenesis during Mesozoic accretion of volcanic arc terranes to western Laurentia (Armstrong et al., 1977; Manduca et al., 1993; McClelland et al., 2000; LaMaskin, et al., 2015; Stanciu, et al., 2016). The Blue Mountains Province is a group of island arcs that collided with North America to the east. Two tectonic features, the Salmon River suture zone, and the western Idaho shear zone both represent a steep ocean-continent plate boundary that separates Paleozoic-Mesozoic island-arc terranes to the west from the ancestral western Laurentian margin to the east (Dickinson, 2004; Blake et al., 2009; Schwartz, et al., 2011; Gray et al., 2012).

Tectonic Framework of the Blue Mountains Province

The North American Cordillera consists of an assemblage of terranes that were accreted to western Laurentia during the Phanerozoic subduction of the Farallon plate (Coney et al., 1980; Engebretson et al., 1985). The western portion of the North American Cordillera consists of a patchwork of lithotectonic terranes called the Blue Mountains Province that was accreted to the western edge of North America during Mesozoic subduction (Coney et al., 1980; Oldow et al., 1989; Evenchick et al., 2007; Yonkee and Weil, 2015). Within the Blue Mountains region of Idaho, the boundary between cratonic and accreted terranes can be approximated by strontium (Sr) isotopes, where continental/ cratonic rocks to the east have elevated $^{87}Sr/^{86}Sr$ ratios (> 0.706) and island arc and mantle-derived rocks to the west $^{87}Sr/^{86}Sr < 0.706$ (Armstrong

et al., 1977; Fleck and Criss, 2004). To the west of the $^{87}Sr/^{86}Sr$ boundary, the island arc rocks of the Blue Mountains Province, are divided into four lithotectonic assemblages or terranes (Fig. 1): the Olds Ferry island arc, Wallowa island arc, Izee basin, and Baker terrane. The Wallowa terrane is an exotic island arc, Olds Ferry, and Baker are a fringing island arcs that are along the western margin of Laurentia. The Wallowa arc collides with the Olds Ferry terrane, then the entire assemblage of terranes collides with North America (Brooks and Vallier, 1978; Dickinson and Thayer, 1978; Brooks, 1979; Schwartz et al., 2010).

The Olds Ferry island arc terrane (Fig. 1) consists of Middle to Late Triassic weakly metamorphosed volcanic and volcaniclastic rocks with intercalated sedimentary rocks (Brooks and Vallier, 1978; Brooks, 1979; Tumpane and Schmitz, 2009). The metavolcanic rocks (Huntington Formation) within the Olds Ferry terrane are mostly andesitic in composition, but range from basalt to rhyolite (Walker, 1995; Schwartz, et al., 2010). Uranium-lead geochronology studies from the Huntington Formation indicate that volcanism may have lasted into Early Jurassic time (Brooks and Vallier, 1978; Tumpane et al., 2008). The rocks of the Huntington Formation indicate that the arc-affinity rocks of the Olds Ferry terrane are structurally overlain by a deformed Jurassic flysch sequence that has south verging folds (Schwartz et al., 2010).

The Wallowa terrane (Fig. 1) is a composite island-arc system consisting of a Permian island-arc sequence overlain by extensive Triassic volcanic and volcaniclastic rocks (Vallier, 1977; Vallier and Batiza, 1978; Kays et al., 2006; Schwartz et al., 2010). The Salmon River suture zone juxtaposes volcanic arc rocks of the Wallowa terrane directly against cratonic North America creating an interoceanic arc (Selverstone et al.,

1992). Near Riggins, Idaho, Paleozoic, and early Mesozoic arc rocks are juxtaposed against North American rocks across a 20-30 km wide zone of Cretaceous deformation (Selverstone et al., 1992). Previous studies of U-Pb zircon ages from Walker (1986) suggest that parts of the Wallowa arc may be as old as Pennsylvanian age with an Upper Triassic to Lower Jurassic clastic sequence (Walker, 1986; Schwartz et al., 2010), with the plutonic rocks ranging in ages from 264 to 225 Ma (Walker, 1985;1986). A Cretaceous western thrust belt arranges the rocks of the Wallowa terrane.

The Izee Basin terrane (Fig. 1) has Late Triassic to Late Jurassic marine sedimentary rocks that unconformably overlie the Baker terrane (Dickinson and Thayer, 1978; Silberling et al., 1987; Shwartz et al., 2010). Sedimentary rocks of the Izee terrane were accumulated in a Triassic-Jurassic forearc basin between a non-collisional east-dipping subduction zone in the west and a west-facing magmatic arc in the east (Dickinson and Thayer, 1978; Brooks and Vallier, 1978; Dickinson, 1979; Dorsey and LaMaskin, 2006). Sedimentation in the Izee basin persisted from Late Triassic and was terminated by Late Jurassic thrusting, metamorphism, and final accretion of the basin by an underlying terrane to the western margin of North America (Dickinson and Vigrass, 1965; Dickinson, 1979; Vallier, 1995; Dorsey and LaMaskin, 2006). Collisional tectonics by this sedimentation plays a significant role in plate interactions and lithospheric processes that controlled Triassic-Jurassic growth in the western U.S. and Canadian Cordillera (Dorsey and LaMaskin, 2006).

The Baker terrane (Fig. 1) separates Olds Ferry and Wallowa arc systems (Schwartz et al., 2010). It is the oldest terrane containing fragments of the ocean floor and island-arc volcanic, plutonic, and sedimentary rocks that range in ages from Middle

Devonian to Early Jurassic (Coward, 1983; Nestell, 1983; Walker, 1986; Carpenter and Walker, 1992; Schwartz et al., 2010). Upper Triassic depositionaly overlies the Baker terrane to Jurassic marine sedimentary rocks of the Izee terrane (Dickinson and Thayer, 1978; Silberling et al., 1987; Dorsey and LaMaskin, 2006; Schwartz et al., 2010).

A mid-Mesozoic record of sedimentation, magmatism, and metamorphism is exposed in the Blue Mountains Province (Schwartz et al., 2011). U-Pb zircon geochronology records distinct orogenic extensional episodes that occurred during the Jurassic period (Coleman et al., 1988; Wright and Fahn, 1988, Hacker et al., 1995; Schwartz et al., 2011). Deformation in the Blue Mountains post-dates emplacement of Middle Jurassic plutons but pre-dates the Idaho Batholith (Schwartz et al., 2011). Zones of deformation within the Blue Mountains Province contain numerous brittle faults with intense brecciation of footwall rocks and extensive networks of cataclastic shear zones within footwall and hanging wall rocks at greenschist facies metamorphic conditions (Schwartz et al., 2011). The deformation within the Baker terrane is interpreted to preserve shallow to mid-crustal deformation that is related to the inferred arc-arc collision, during which the Baker terrane was thrust over both colliding island arcs (Ferns and Brooks, 1995; Schwartz et al., 2010; 2011). Late Jurassic deformation in the Blue Mountain Province involved faulting and folding. The mechanisms of upper crustal strain and deformation during amalgamation have been interpreted to signify the collision of the Wallowa Island arc terrane with the fringing continental-margin Olds Ferry island-arc terrane (Avé Lallemant, 1995; Ferns and Brooks, 1995; Schwartz et al., 2010; Schwartz et al., 2011).

The Salmon River Suture Zone

The Salmon River suture zone is a steep to vertical tectonic boundary that separates the Blue Mountains Province to the west from the Cretaceous Idaho batholith to the east (Fig. 2; Hamilton, 1969; Lund and Snee, 1988; Getty et al., 1993; Lund, 2004; Blake et al., 2009). Suture zones demark the boundaries between two or more terranes, continents, or other tectonic units that have different geologic histories (Dewey, 1977; Moores, 1981, Fleck and Criss, 2004). Suture zones contain intensely deformed rocks and can commonly transport metamorphic rocks from the middle or deep crust toward the surface. Over time, metamorphic rocks from within suture zones may be exposed by continued uplift and erosion, providing an opportunity to study rocks that record the processes active deep within a mountain belt (Dewey, 1977; Moores, 1981; Busch et al., 1997; Burke et al., 2003). Exhumation history has two parts, burial, and exhumation. The rate at which subduction occurred within the Salmon River suture zone is poorly constrained and understood (Selverstone et al., 1992).

From west to east, the Salmon River suture zone contains a Cretaceous thrust belt, the Late Cretaceous western Idaho shear zone, and the Idaho batholith (McClelland et al. 2000). The Salmon River suture zone contains Cretaceous metamorphic rocks that have experienced midcrustal metamorphism (Hamilton, 1963; Selverstone et al., 1992; Tikoff et al., 2001; Kuntz and Snee, 2007). The western part of the Salmon River suture zone is a thrust belt that contains midcrustal assemblages that may correlate to rocks of the Wallowa terrane (Gray and Oldow 2005; Blake, et al., 2009). Metamorphism and deformation that occurred in the Salmon River suture zone were from the underthrusting of the Wallowa terrane beneath the continental margin

(Lund and Snee, 1988; Selverstone et al., 1992; Manduca et al., 1993; McClelland et al., 2000). Underthrusting was recorded in the prograde metamorphic history of the Pollock Mountain plate. Metamorphic conditions in the middle to lower crust reached its peak at about 128 Ma (Selverstone et al, 1992; Getty et al., 1993; McClelland et al., 2000).

Lithotectonic assemblages within the Salmon River suture zone are internally juxtaposed along thrust faults that place higher grade rocks above lower grade metamorphic rocks in the footwall (Hamilton, 1969; Gray and Oldow, 2005; Kuntz and Snee, 2007; McKay et al., 2017). From west to east, three major thrust faults dissect the Salmon River suture zone: the Heavens Gate fault, the Rapid River fault, and the Pollock Mountain fault. The Pollock Mountain fault carries amphibolite facies rocks in the hanging wall, known as the Pollock Mountain plate, above upper greenschist rocks in the footwall, known as the Rapid River plate. The Rapid River plate structurally overlies the Heavens Gate plate (Hamilton, 1963).

The Heavens Gate plate is the structurally lowest rock consisting of greenschist facies in its hanging wall over lower grade volcanic rocks of the Wallowa terrane (Gray and Oldow, 2005; Gray, 2013). The Heavens Gate fault is dominated by metasedimentary and metavolcanic rocks of island arc affinity that record progressive deformation and metamorphism during the Late Jurassic to Early Cretaceous accretion of the Blue Mountains Province to western Laurentia (Lund and Snee, 1988; Avé Lallemant, 1995; Snee et al., 1995). Island-arc accretion recorded by the Salmon River suture zone predates movement on the western Idaho shear zone (Giorgis et al., 2008).

The Rapid River plate contains the Riggins Group sedimentary and volcanic rocks that were metamorphosed at upper greenschist to amphibolite facies (Hamilton, 1963). Riggins Group rocks contain Squaw Creek Schist, Lightning Creek Schist, and Fiddle Creek Schist. Metasedimentary rocks of the Riggins Group have been correlated with volcaniclastic and sedimentary units of the Wallowa terrane (Vallier, 1977; Lund, 1984; Lund et al. 1993; McKay et al., 2017), Huntington Formation of the Olds Ferry terrane (Brooks and Vallier, 1978; Vallier, 1995), Baker terrane (Vallier, 1977; Brooks and Vallier, 1978), and Izee Basin (Brooks and Vallier, 1978). Pressure and temperatures calculated for the Rapid River plate range from 480- 500 °C at about 6 kbar (Selverstone et al., 1992). Ages of the rocks in the Riggins Group and Seven Devils Group record cooling through ~550-500 °C at 244-226 Ma. Cooling ages show that metamorphism occurred before suturing (Snee et al., 1995). Hornblende 40Ar/39Ar ages range from 118 to 88 Ma across the Western Idaho shear zone, with cooling ages becoming progressively younger toward the North American continent (Snee et al., 1995). McKay et al. (2017) recorded metamorphism that began in the Salmon River suture zone from 141 to 124 Ma.

The Pollock Mountain plate is structurally highest with medium to high-grade gneissic amphibolite and orthogneiss (Alberti, 1988). Pollock Mountain thrust fault dips southeast and overlies the Rapid River plate. Metamorphic rocks in the Pollock Mountain plate were intruded by the Hazard Creek Complex between 118 and 114 Ma (Manduca et al., 1993; Unruh et al., 2008). Metamorphic conditions in the Pollock Mountain plate were estimated to be 8-11 kbar and at temperatures of about 600-625 °C (Selverstone et al., 1992).

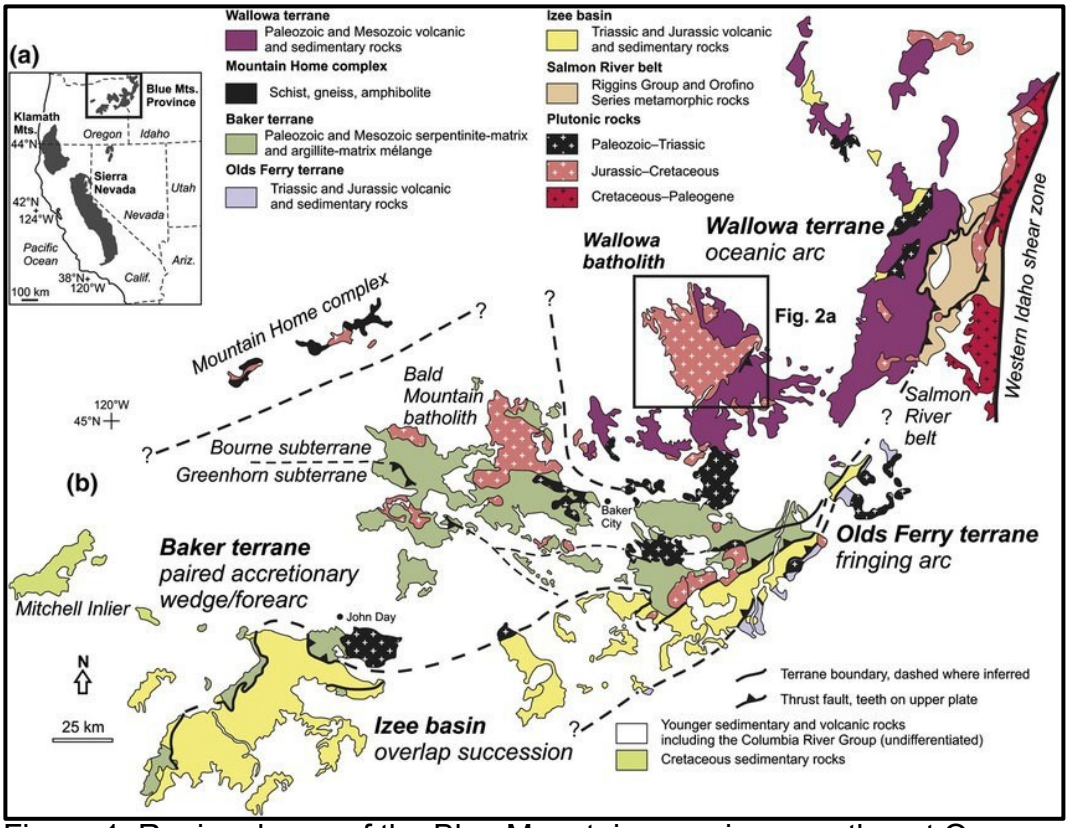

Figure 1. Regional map of the Blue Mountains province, northeast Oregon, and western Idaho, showing the locations of the four terranes and their rock types (Schwartz et al., 2011; Zak et al., 2012).

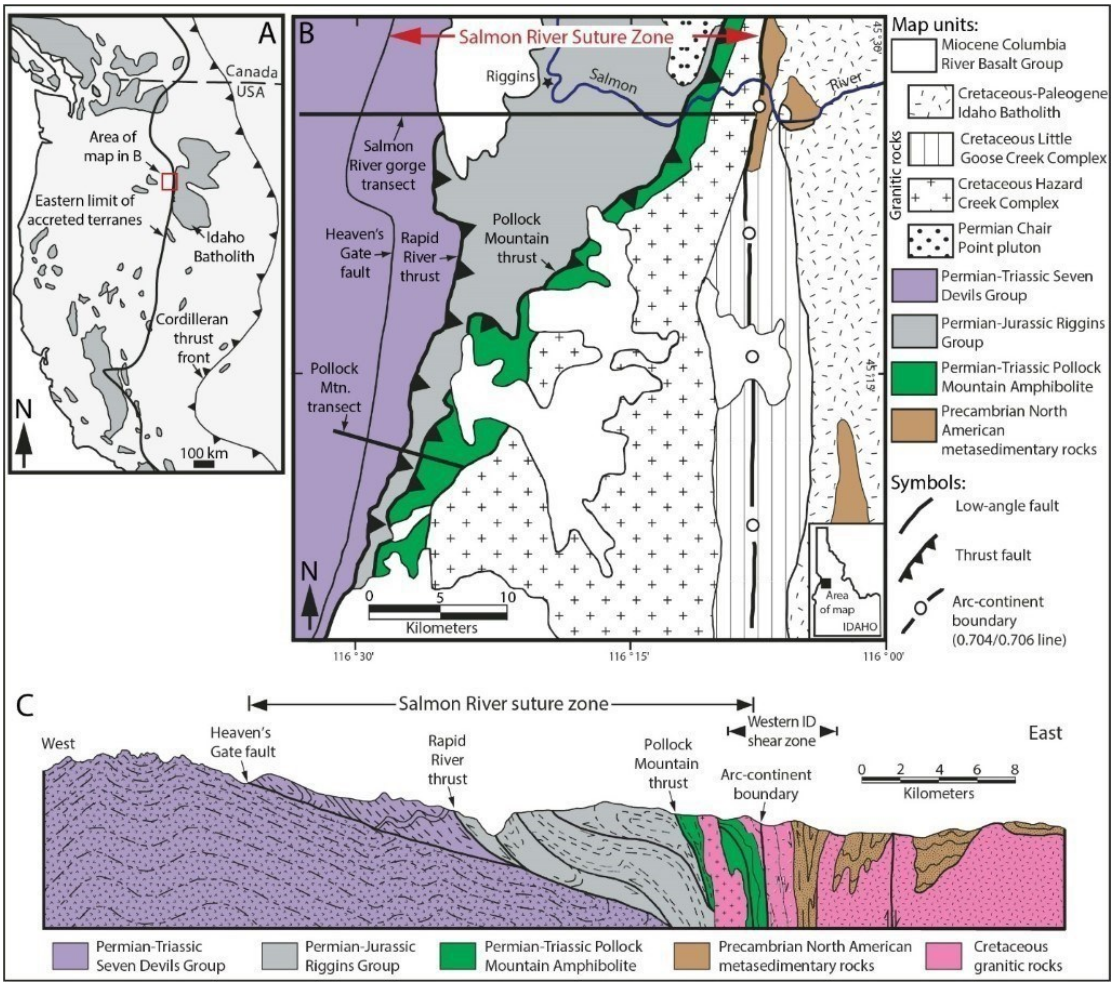

Figure 2. A) map of the Western U.S. Cordillera showing accreted terranes and thrust faults. B) Simplified geologic map of west-central Idaho also showing the two transects, Salmon River and Pollock Mountain. C) Schematic cross section across the Salmon River suture zone. Modified from Blake et al. (2009).

STUDY AREA

To detail the post-metamorphic cooling history of the Salmon River suture zone, samples were collected along a 16-kilometer transect (Fig. 3) that roughly parallels the Salmon River from Riggins, ID to about French Creek, ID for U-Pb apatite, zircon, and rutile geochronology. Geologic map unit identification is based on 1:24,000 scale geologic mapping by Gray (2013) and Blake et al. (2016), as well as regional compilation mapping by Lund (2004). The transect is approximately perpendicular to the strike of major structures and traverses all major lithotectonic units in the Salmon River suture zone. The samples collected along the Salmon River were collected from Riggins Group rocks that lie in the Rapid River plate. Riggins Group lithology is a garnet biotite muscovite schist (Gray, 2013) including the formations: Squaw Creek Schist, Lightning Creek Schist, and Fiddle Creek Schist. Pollock Mountain plate includes the Pollock Mountain amphibolite that is Triassic in age and dioritic orthogneiss and migmatite that is Triassic- Cretaceous (Lund, 2004; Gray, 2013; Blake et al., 2016; Nandi et al., 2018). Along the Salmon River are two other geologic structures, the Riggins synform and the Lake Creek antiform (Lund, 2004). Another location samples were collected from was Pollock Mountain (Fig. 4). Zircon and apatite were collected from the Pollock Mountain amphibolite (Nandi et al., 2018).

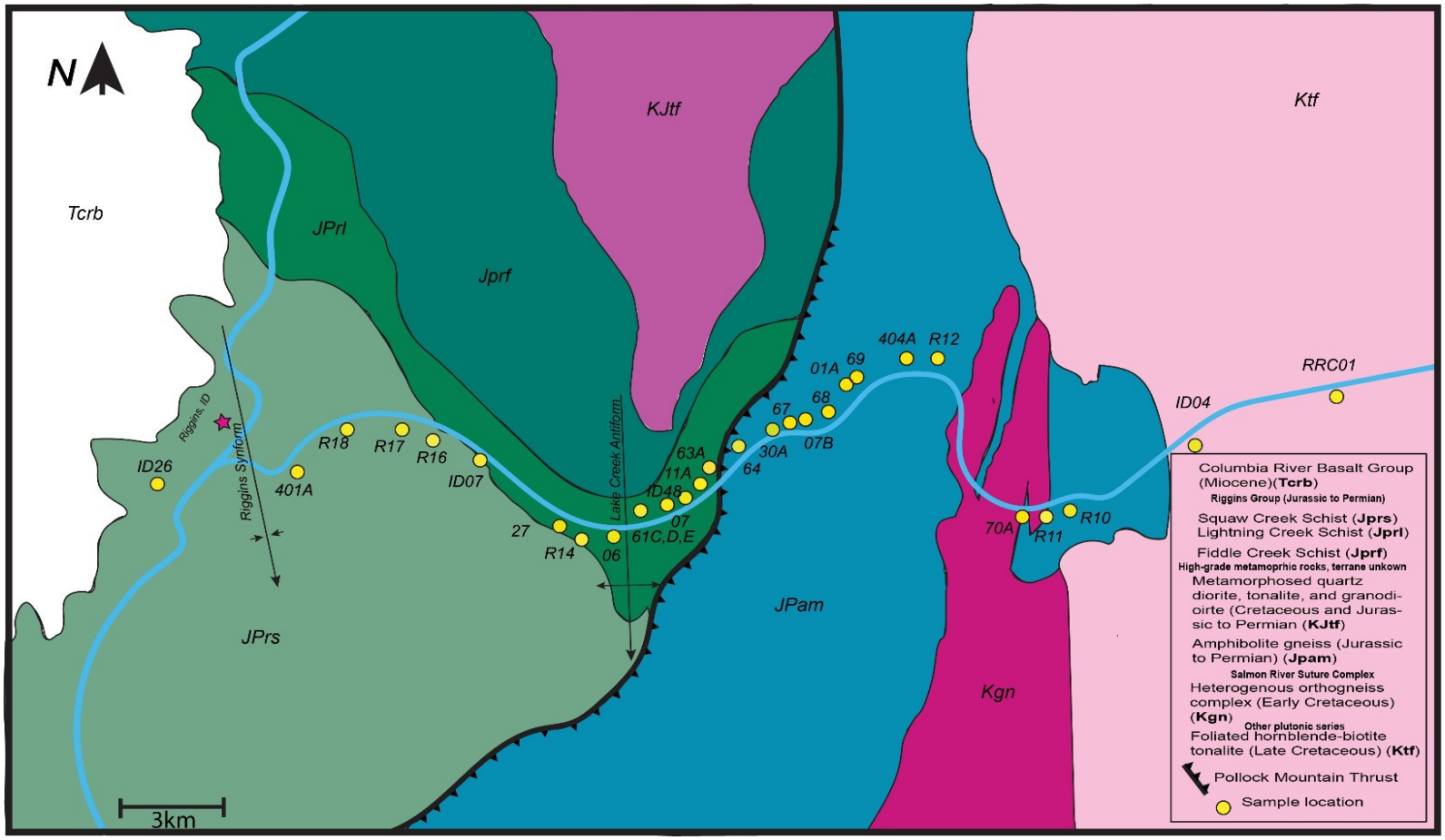

Figure 3. Sample location map along the Salmon River with sample locations collected from Lund and Snee, (1988) and McKay et al., (2017). Map was modified from Lund, (2004). Samples with ID and (RRCO1) are from McKay et al. (2017) and R from Lund and Snee, (2004).

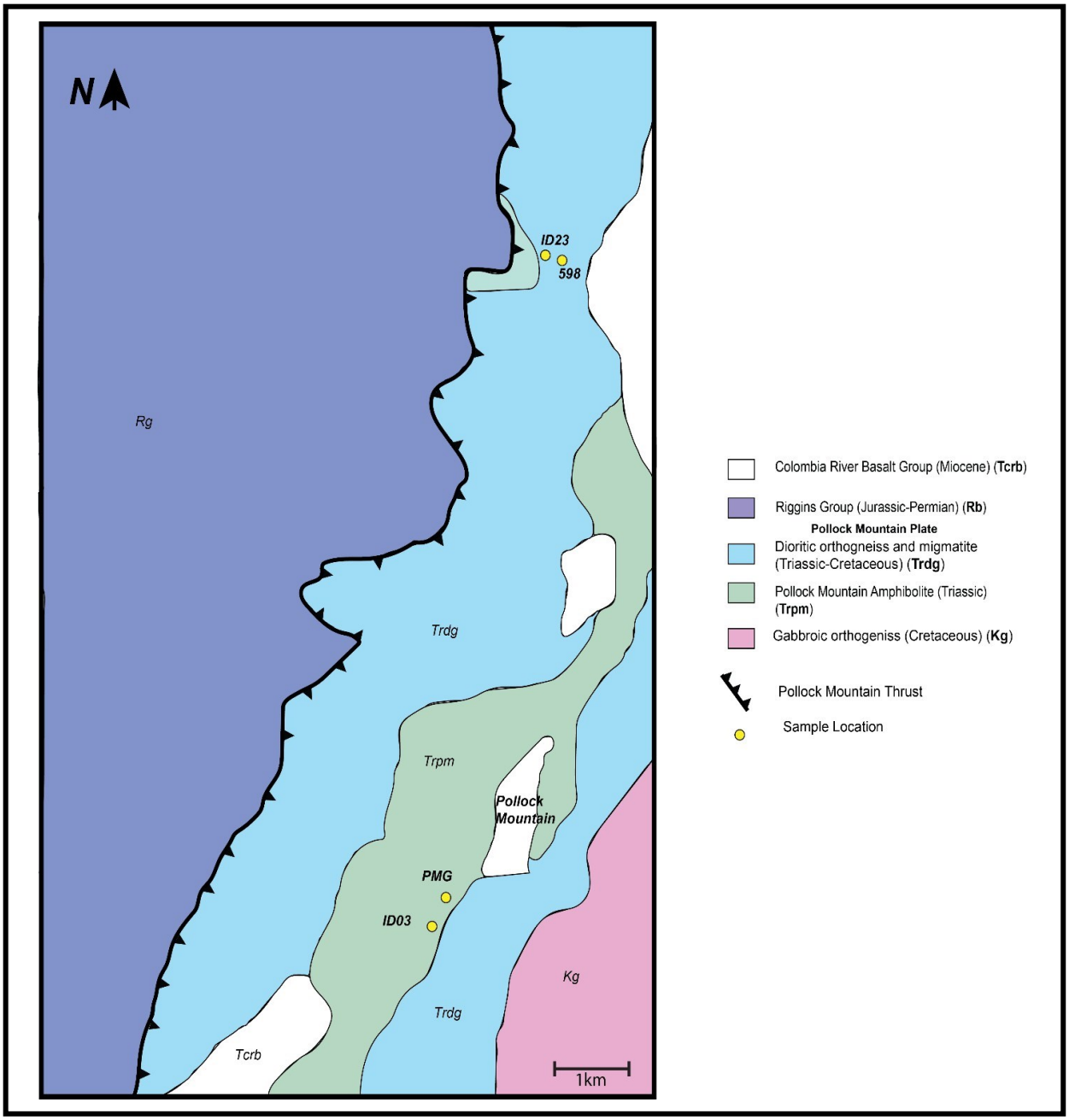

Figure 4. Sample location map showing samples collected on Pollock Mountain along with samples collected from Getty et al. (1993) and McKay et al. (2017). Map was modified by Nandi et al. (2018). Samples indicated with ID are from McKay et al. (2017) and 598 is from Getty et al. (1993).

METHODS

The timing and conditions of peak metamorphism, exhumation-related cooling, and contractional deformation within the three lithotectonic packages were quantified. Temperature- time exhumation paths were created to model peak metamorphic conditions. These paths can be obtained by quantifying U-Pb ages and closure temperatures of metamorphism from apatite, zircon, and rutile, while also using minerals hornblende, muscovite, biotite, and garnet to create a full cooling history of the Salmon River suture zone.

To obtain the cooling and crystallization ages of the rocks along the Salmon River suture zone, 96 hand samples were collected from two field seasons. Samples were collected from igneous intrusions and boudinage intrusions across the Salmon River suture zone. Along with intrusions, the country rock was sampled as well for some of the locations to create a complete cooling history. Based on location and rock type, 41 samples were chosen for further analysis and mineral separation processes. Standard separation techniques were used to separate apatite, zircon, and rutile from the sampled rocks (Strong and Driscoll, 2016). Grains were hand-picked and then placed onto tape mounts. Minerals were analyzed at the University of Arkansas Trace Element and Radiogenic Isotope Laboratory using laser ablation inductively coupled plasma mass spectrometer (LA-ICPMS). Grains were ablated with a 20-25 mm spot using an ESI NWR 193 nm Excimer laser. Samples were reduced in Iolite4 under VizualAge UComPbine. The background crop starts at one second for 16 seconds, and the end is set for zero. For the standards and samples, the start is at 18.5 seconds with a duration

of zero that ends at 10 seconds. The index channel is U238 with the reference material selected for the appropriate mineral. Beam seconds should be selected as gaps between samples with a beam sensitivity of 1000. Under the VizualAge UComPbine section, the common Pb correction will be for Pb 204 with a common Pb composition of Stacey-Kramers.

Apatite is named for being misleading as it can resemble other minerals and shows great chemical and physical variability. Zircon can resemble apatite depending on certain pressure conditions, high pressure zircons form hexagonal sides. Both standards for apatite and zircon were analyzed through the LA-ICPMS at the same time, by being placed on the same tape mount. Analyzing both standards helps identify whether the mineral is zircon or apatite. Using this method, the calcium and zirconium content (in parts per million(ppm)) was recorded for each grain. Apatite has high amounts of calcium and zircon will have high amounts of zirconium. This method can alleviate the error of distinguishing apatite from zircon.

Of the 41 samples, zircon, rutile, and apatite were found in 19 samples, however, not all three mineral phases were found in each sample (See Appendix A for UTM coordinates of samples). Weighted mean age, mean square weighted distance (MSWD), and kernel density estimate (KDE) of each sample were calculated using an online version of IsopltR (Vermeesch, 2018). The weighted mean was plotted using the final U-Pb age versus uncertainty, and the KDE shows the distributions of the ages within the sample. KDE diagrams represented the populations of each sample with the outliers removed to get the most ideal MSWD value and mean age. Outliers for each sample were decided based on the MSWD values. Ages that were much higher or much

lower than the mean age were removed from the analysis.

U-Pb Zircon

U-Pb Zircon Analytical Approach. Eleven of the samples contained zircon, with 104 zircons total. Summary of all the Zircon data that was used can be found in Appendix B. Nine samples were reduced using the Final $^{206}Pb/^{238}U$ age mean. Three of the 11 samples needed to be corrected for common lead. These samples were processed with a Final $^{206}Pb/^{238}U$ mean age for ^{207}Pb. Samples were normalized using standard Pleŝovice (334 ± 5.6 Ma).

U-Pb Rutile

Zr-in-Rutile Thermometry. Zirconium (Zr) in rutile thermometry is a method for determining crystallization temperatures in rutile found in metamorphic and igneous rocks and can be used as a tool for evaluating the temperature conditions before subsequent high- temperature overprinting (Usuki et al., 2017). The Zr concentration in the rutile structure is used to calculate the temperature. This method, however, can only be applied when the SiO_2- ZrO_2- TiO_2 system is in equilibrium with quartz, zircon, and rutile (Zack et al., 2004; Watson et al., 2006; Kotowski et al., 2021). There are multiple calibrations to find crystallization temperature for rutile. Temperatures found by the Zr-in-rutile method range from 430 to 1,100°C (Zack et al., 2004, Watson et al., 2006), and are dependent on Zr concentrations, and the minerals present around the rutile. Collecting rutile from garnet inclusions versus matrix play an important role in how much Zr is present. Rutile found in the matrix gives higher Zr continents (3330-9960 ppm) and

are more scattered compared to rutile inclusions (Usuki et al., 2017). Coarse and elongated rutile in a quartz-rich domain gives a ppm range of 3330-5840 ppm (Usuki et al., 2017). All of the rutiles sampled from the Salmon River suture zone were collected from the rock's matrix from quartz-rich intrusions. Watson et al., (2016) derived an equation for calculating the temperature of zirconium crystallization in rutile:

$$T(°C)_{rutile} = \frac{4470 \pm 120}{(7.36 \pm 0.10) - log_{10}(Zr\ ppm)} - 273 \qquad (1)$$

The uncertainty in temperature estimates from equation (1) will come from the differing level of Zr present in the rutiles (Watson et al., 2006). Equation (1) is based on the Zr concentration in the rutile structure.

U-Pb Rutile Analytical Approach. Four of the samples contained rutile grains, with a total of nine grains. Rutile can contain a large proportion of common lead; therefore, a common lead correction is necessary (Cherniak, 2000). The final mean age was calculated using $^{206}Pb/^{238}U$ with a ^{207}Pb correction. The two rutile standards used were R632 (495 ± 10.5 Ma) and Sugluk-4 (1714 ± 35 Ma). Summary of all rutile data that was used can be found in Appendix C.

U-Pb Apatite

Closure Temperature. For many minerals, the closure temperature, or the temperature at which certain elements are locked into the crystal lattice, does not vary significantly (rutile) or is sufficiently high that the age likely reflects crystallization (zircon). The closure temperature of apatite with respect to U and Pb, however, varies significantly based on the size of the mineral grain, and the cooling rate (Dodson, 1973; Cherniak et al., 1991). Dodson (1973) determined the closure temperature of apatite to

be defined by equation (2)

$$Tc = \frac{E/R}{\ln\left(ART_c^2 D_o/a^2\right)/E\ (dT/dt)} \quad (2)$$

where T_C is the closure temperature recorded in Kelvin, E is the activation energy (54.6 kcal/mol; from Cherniak et al., 1991), R is the Gas constant (0.00199 kcal/K*mol), A is a constant depending on the geometries of the mineral (55 for a sphere or 27 for a prism), D_o is the diffusion coefficient at an infinitely high temperature, a is the effective radius (cm), and lastly, dT/dt is based on estimates from published thermochronology (Dodson, 1973; Cherniak et al., 1991; Faure and Mensing, 2005). To calculate closure temperature, the length and width of each grain were measured in the microscope by each grain's c (long) and a2 (short) crystallographic axes in micrometers. Using cooling rates of 7 °C/m.y. (±1 °C/m.y.), based on cooling estimates from McKay et al., (2017) from the Salmon River suture zone rocks. The resulting closure temperature is reported with the U-Pb age of each grain. The temperatures were recorded with ± 3 °C to add the error for possible broken grains.

U-Pb Apatite Analytical Approach. Fifteen samples contained apatite grains with 312 grains total. The apatite samples were corrected for common lead, with the final mean age calculated using $^{206}Pb/^{238}U$ with a ^{207}Pb correction. The two standards used for apatite were Durango (28 ± 2 Ma) and McClure Mountain (523 ± 10 Ma). Summary of all Apatite data used can be found in Appendix D

RESULTS

U-Pb Zircon

Uranium Thorium (U/Th) ratios in zircons provide details on igneous and metamorphic crystallization activity. Zircon with high U/Th ratios that are greater than 10 and are likely to be metamorphic, whereas low U/Th ratios that are below ~10 are more likely to reflect igneous zircon crystallization (Rubatto, 2002; Gatewood and Stowell, 2012; Yakymchuk et al., 2018). Zircon tends to be produced with wider ranges of U/Th ratios when there is magmatism origin with extensional tectonism (McKay et al., 2018) These ratios are good indicators of the crystallization timing of these rocks. Low U/Th ratios are expected to occur late in the cooling and crystallization history near the solidus and in the presence of the mineral monazite (Yakymcuk et al., 2018). If these ratios decrease, it could show that collisional and continental arc magmas are representing lower temperature conditions. Opposingly, if these ratios were higher, it would show extensional magma and tectonics with hotter temperature conditions (McKay et al., 2018). U-Pb zircon ages range from 171 to 100 across the Salmon River suture zone. U/Th values range in both igneous and metamorphic crystallization.

Below Pollock Mountain Thrust Fault. Samples found in the footwall of the Pollock Mountain thrust that contained zircons were located within the Lightning Creek schist. Six total zircon grains were collected from three samples. Moving west to east along the Salmon River, the samples are 06, 61C, and 63A.

Sample 06 (Fig. 5, Fig. 6A) was located on the Lake Creek antiform and was sampled from an intrusion that was composed of biotite and garnets from the Lightning Creek schist that contained two zircon grains with a weighted mean age of 104.92 ±

5.96 Ma (MSWD =10.9). Both of these grains had a U/Th ratio that was greater than 20.

Sample 61C (Fig. 5, Fig. 6B) was sampled from the Lightning Creek schist and was a granitic intrusion that had three grains yielding a ^{207}Pb corrected age for $^{206}Pb/^{238}U$ of 100.58 ± 7.96 Ma (MSWD= 1.51). Two of the grains are just below the ratio of 10 for U/Th with one grain above it.

Sample 63A was an intrusion sampled from the Pollock Mountain amphibolite. The intrusion was parallel to the foliation of the rocks. It is the closest to the Pollock Mountain thrust yielding a mean age of 142.4 ± 9.2 Ma for one grain with a U/Th ratio value of 8.33.

Above Pollock Mountain Thrust Fault. Samples found in the hanging wall of the Pollock Mountain thrust fault that contained zircon were located in the Pollock Mountain Amphibolite gneiss rock unit. A total of 99 zircon grains were collected from eight samples. The samples moving west to east along the Salmon River are 64, 30A, 67, 07B, 68, 404A, and 70A. Sample PMG is to the south on Pollock Mountain.

Sample 64 (Fig. 5, Fig. 6C) was from an intrusion composed of quartz and a little biotite with two zircon grains yielding a mean age of 137.65 ± 8.22 Ma (MSWD = 1.14). The grains from sample 64 had a high lead content, so they were reduced using a ^{207}Pb correction. The U/Th ratio of these grains was all greater than 10. One grain of zircon was reduced without a lead correction and yielded an age of 103.07 ± 2.4 Ma with a U/Th ratio value of 49.

Sample 30A (Fig. 5, Fig. 6D) was from a biotite quartz intrusion with a total of 10 grains that yielded a mean age of 103.07 ± 1.89 Ma (MSWD = 2.32). The zircon grains are metamorphic with high U/Th values that are greater than 20. They have a trend of

the older the grains are the higher the U/Th ratio.

Sample 67 (Fig. 5, Fig. 6E,) was not sampled from an intrusion, but from the country rock with five zircon grains and three outliers. These grains yielded a weighted mean age of 171.60 ± 6.20 Ma (MSWD =0.43). The outliers had an average age of 129.65 ± 3.5 Ma. One grain was below a U/Th ratio of 10, while the rest were fairly high with ratios greater than 20. There is a trend of the older the grains are the more of a concentration of U/Th that is present in the zircon grain.

Sample 07B (Fig. 5, Fig. 6F) was a pegmatite boudinage intrusion with biotite and quartz containing seven zircon grains. The mean age of the grains is 124.34 ± 8.06 Ma (MSWD = 4.04). The U/Th ratio range for four grains is between eight and nine. Three of the grains are in a ratio range of 22 to 25.

Sample 68 (Fig. 5, Fig. 6G) was micaceous tonalite with two grains of zircon that gave a mean age of 147.84 ± 3.04 Ma (MSWD = 4.68). These grains had a high lead content, so they were reduced using a ^{207}Pb correction. Both of these grains had a U/Th ratio that was less than 10 indicating igneous activity.

Sample 404A (Fig. 5, Fig. 6H) was sampled from a boudinage intrusion that was composed of quartz and biotite containing 50 zircon grains with three outliers. The mean age of 123.76 ± 1.64 Ma (MSWD = 5.22) was calculated for 47 grains. Two populations for the U/Th ratios were recorded, a population above and below 10. With activity above 10, this indicates metamorphic activity. Four of these grains lie above 10, and the rest are below, decreasing in ratios as the grains are older.

Sample 70A (Fig. 5, Fig. 6I) is from the Pollock Mountain amphibolite gneiss and has been metamorphosed containing 11 zircon grains with four outliers. The weighted

mean calculated age is 134.72 ± 7.73 Ma (MSWD = 3.29). Much of the population of U/Th ratios are greater than 100 with two that are less than 10.

Sample PMG (Fig. 5, Fig. 6J,) contained seven zircons with two outliers. The average mean age of these grains is 171.65 ± 11.92 Ma (MSWD = 1.46). There are two populations for the U/Th ratios, above and below 10. Three of the grains are above 10 with one grain above 100.

U-Pb Rutile

The ages of rutile decrease moving west to east along the Salmon River. The age of sample 401A is 166 Ma, 27 is 143, 07 is 92 Ma and 01A is 89Ma. The concentration of Zr in rutile was around 4200ppm (parts per million) with one sample above 4300ppm.

Below Pollock Mountain Thrust Fault. Samples 401A, 27, and 07 were found in the footwall of the Pollock Mountain thrust fault. Sample 401A was located closest to the town of Riggins and is a quartz boudinage intrusion located in the Squaw Creek schist formation. While only containing one grain, it yielded an age of 166 ± 5.6 Ma. The Zr in rutile concentration for sample 401A was calculated at 928 ± 20 °C. Sample 27 was found in the Lightning Creek schist formation and was sampled from a quartz intrusion with one grain an age of 143.5 ± 2.2 Ma was calculated. Its Zr in rutile concentration was calculated at 926 ± 20 °C. Sample 07 was composed of garnets and biotite and contained six rutile grains, while located in the Lightning Creek schist. The weighted mean age of the grains was 92.3 ± 8.37 Ma (MSWD = 1.25). Its Zr- in-rutile concentration was averaged at 925 ± 20 °C.

Above Pollock Mountain Thrust Fault. Sample 01A contained some potassium feldspar in a boudinage intrusion and was found above the Pollock Mountain thrust fault in the hanging wall in the Amphibolite gneiss formation. Contains only one rutile grain with a mean age of 89.6± 5.29 Ma. Its Zr-in-rutile concentration was calculated at 925 ± 20 °C.

U-Pb Apatite

Apatite U-Pb ages record either (1) crystallization of apatite in rocks below ~450°C or (2) cooling of rocks through the 350-500°C cooling window. Since the Salmon River suture zone rocks are documented to have experienced temperatures greater than 650°C, the U-Pb apatite ages from the rocks within the suture zone can be assumed to reflect cooling, providing an age for the post-metamorphic thermal history of the Salmon River suture zone (Selverstone et al., 1992; Getty et al., 1993; Snee et al., 1995; Kirkland, et al., 2018). Generally, the bigger the apatite grains are, the higher the closure temperature will be, meaning that the system has a larger area for it to cool and crystallize (Fig. 7). The range of ages of apatite found along the Salmon River are from ~114-70 Ma, with temperatures ranging from ~427 to 475 °C and cooling rates less than 5 °C/m.y. The average grain size ranges between one to four micrometers. Apatite samples collected in the Salmon River suture zone were found in the Lightning Creek Schist and the Pollock Mountain amphibolite.

Below Pollock Mountain Thrust Fault. Samples found in the footwall of the Pollock Mountain thrust fault that contained apatite were located within the Lightning Creek schist. A total of 156 apatite grains were collected from seven samples. Samples

moving west to east along the Salmon River are 27, 06, 61C, 61D, 61E, 07, and 11A.

Sample 27 (Fig. 7, Fig. 8, Fig. 9A) was sampled from a quartz intrusion in the schist country rock. The sample contained six apatite grains that were analyzed for U-Pb ages. With a weighted mean age of 85.53 ± 3.44 Ma (MSWD= 0.75). The average closure temperature is about 447 °C. The sample was split into two populations to create a cooling rate between the highest to lowest closure temperature. Population one at 92.10 ± 4.4 Ma with a closure temperature of 473 °C and population two at 82.63 ± 5.7 Ma with a closure temperature of 442°C, with a cooling rate of 3.18 °C/m.y.

Sample 06 (Fig.7, Fig. 8, Fig. 9B) was located on the Lake Creek antiform and was sampled from an intrusion that was composed of biotite and garnets. The sample contained 23 apatite grains, with a weighted mean age of 82.96 ± 3.07 Ma (MSWD =2.56) for 14 of those grains. Two outlier populations of nine grains with an age of 71.62 ± 2.3 Ma (three grains) and 104.09 ± 6.0 Ma (six grains) were excluded from further analysis. The average closure temperature for the grains from sample 06 is about 460 °C.

Samples 61C, 61D, and 61E (Fig. 7, Fig. 8, Fig. 9C, D, E) were all sampled from the same location. Each sample was collected from differing granitic intrusions located in the Lightning Creek schist. Sample 61C contained 21 apatite grains with six outliers. The 15 apatite grains yielded a mean age of 97.41 ± 3.64 Ma (MSWD = 1.10), and the average closure temperature of 61C was 467 °C. Sample 61D was sampled from a boudinage intrusion that contained 16 apatite grains with seven outliers with a mean age of 94.16 ± 4.19 Ma (MSWD = 2.74). The average closure temperature of sample 61D was 449 °C. Sample 61E contained 64 apatite grains with a mean age of 93.97 ±

2.86 Ma (MSWD = 2.10) for 41 grains, with two outlier populations of 70.56 ± 4.5 Ma (13 grains) and 131. 91 ± 19.5 Ma (10 grains). The average closure temperature of 61E was 448 °C.

Sample 07 (Fig. 7, Fig. 8, Fig. 9F) was collected from the schist facies of the Lightning Creek schist, which is composed of garnet and biotite, and was not collected from an intrusion, but country rock. Fifteen apatite grains were found with seven outliers that were excluded. The weighted mean age of the eight grains was 115.52 ± 5.99 Ma (MSWD = 3.15). The two outlier populations were at 95.56 ± 3.2 Ma (three grains) and 155.22 ± 11.3 Ma (four grains). Sample 07 yielded an average closure temperature of 424 °C.

Sample 11A (Fig. 7, Fig. 8, Fig. 9G) is a quartz biotite intrusion in the Lightning Creek schist that is interpreted to have intruded country rock before mid-crustal deformation. Sample 11A was collected from rocks that have been interpreted to lie in both the footwall (Blake et al., 2009) and hanging wall (Lund, 2004) of the Pollock Mountain thrust fault, but for this paper, it will be placed in the footwall. Sample 11A yielded 11 apatite grains with a weighted mean age of 92.20 ± 2.71 Ma (MSWD = 2.58). Two of the grains with an age of 133.82 ± 6.3 Ma was considered an outlier and excluded from further analyses. Sample 11A had an average closure temperature of 445 °C.

Above Pollock Mountain Thrust Fault. Samples found in the hanging wall of the Pollock Mountain thrust fault that contained apatite were located in the Pollock Mountain Amphibolite gneiss rock unit. A total of 156 apatite grains were collected from eight samples. Samples moving west to east along the Salmon River are 64, 30A, 67,

68, 69, 404A, 70A, and PMG. Sample PMG is to the south on Pollock Mountain.

Sample 64 (Fig. 7, Fig. 8, Fig. 9H) was from a boudinage intrusion with quartz and a little biotite. Twenty-one apatite grains yielded a weighted mean age calculated at 84.34 ± 3.59 Ma (MSWD = 2.50) for 14 grains. Seven of the grains from sample 64 were considered outliers, with an age of 162.12 ± 22.2 Ma. The average closure temperature of these grains is about 464°C.

Sample 30A (Fig. 7, Fig. 8, Fig. 9I) was sampled from a biotite quartz intrusion within the Pollock Mountain amphibolite. It contained eight apatite grains with a weighted mean age of 114.34 ± 2.32 Ma (MSWD = 2.68). Sample 30A had an average closure temperature of 452°C.

Sample 67 (Fig. 7, Fig. 8, Fig. 9J) was sampled from the gneiss country rock near Riggins Hot Springs. It consisted of 13 apatite grains with five outliers. Apatite yielded a weighted mean age of 96.92 ± 6.63 Ma (MSWD = 3.38) for eight grains. The average closure temperature for sample 67 is 456 °C. The sample was split into two populations to create a cooling rate between the highest to lowest closure temperature. Population one at 123.44 ± 14.7 Ma with a closure temperature of 456 °C and population two at 98.90 ± 5.19 Ma with a closure temperature of 452 °C, with a cooling rate of 0.19 °C/m.y.,

Sample 68 (Fig. 7, Fig. 8, Fig. 9K) was micaceous tonalite consisting of 23 grains with a weighted mean age of 97.32 ± 5.29 Ma (MSWD = 3.56) for 11 grains. The sample had two populations of outliers, population one at 76.91 ± 4.0 Ma (five grains) and population two at 156.36 ± 32 Ma (seven grains). The average closure temperature for sample 68 was 449 °C.

Sample 69 (Fig. 7, Fig. 8, Fig. 9L) is an intrusion with large potassium feldspar crystals within the schist country rock. Consisting of 51 apatite grains with seven outliers. Apatite yielded a weighted mean age of 84.24 ± 2.87 Ma (MSWD = 3.90) for 42 grains. The seven outliers had an average age of 171.39 ± 20.6 Ma. The sample was split into three populations to create a cooling rate between the highest to lowest closure temperature. Population one at 148.92 ± 29.57 Ma (four grains) with a closure temperature of 468 °C, population two at 113.23 ± 13.6 Ma (14 grains) with a closure temperature of 462 °C, and population 3 at 83.71 ± 5.14 Ma (25 grains) with a closure temperature of 470 °C. The cooling rate between populations one and two is calculated at 0.18 °C/m.y., and the rate between populations two and three was 0.29 °C/m.y. The overall cooling rate for sample 69 is 0.029 °C/m.y.

Sample 404A (Fig. 7, Fig. 8, Fig. 9M) was an intrusion consisting of mostly quartz and biotite with 11 apatite grains and four outliers with a weighted mean age of 71.45 ± 3.61 Ma (MSWD = 0.57) for six grains. An average closure temperature of 455 °C was calculated. The sample was split into two populations to create a cooling rate between the highest to lowest closure temperature. Population one at 84.53 ± 5.09 Ma with a closure temperature of 478 °C and population two at 72.34 ± 4.66 Ma with a closure temperature of 446 °C, with a cooling rate of 2.61 °C/m.y.

Sample 70A (Fig. 7, Fig. 8, Fig. 9N) is from the Pollock Mountain amphibolite gneiss unit and has been metamorphosed that is consisting of three apatite grains with a mean age of 90.33 ± 5.88 Ma (MSWD = 3.06). The average closure temperature for sample 70A was 475°C.

Sample PMG (Fig. 7, Fig. 8, Fig. 9O) was collected on Pollock Mountain and

contained 26 apatite grains with three outliers. It yielded a mean age of 110.34 ± 2.48 Ma (MSWD = 1.04), with the three outliers having an age of 175.2 ± 12.1 Ma. The average closure temperature was 465 °C. The sample was split into two populations to create a cooling rate between the highest to lowest closure temperature. Two age populations, one at 124.26 ± 3.59 Ma (four grains) with a closure temperature of 502 °C, and 108.37 ± 2.65 Ma (19 grains) with an average closure temperature of 457 °C. Between the two populations, there was a cooling rate of 5.41 °C/ m.y.

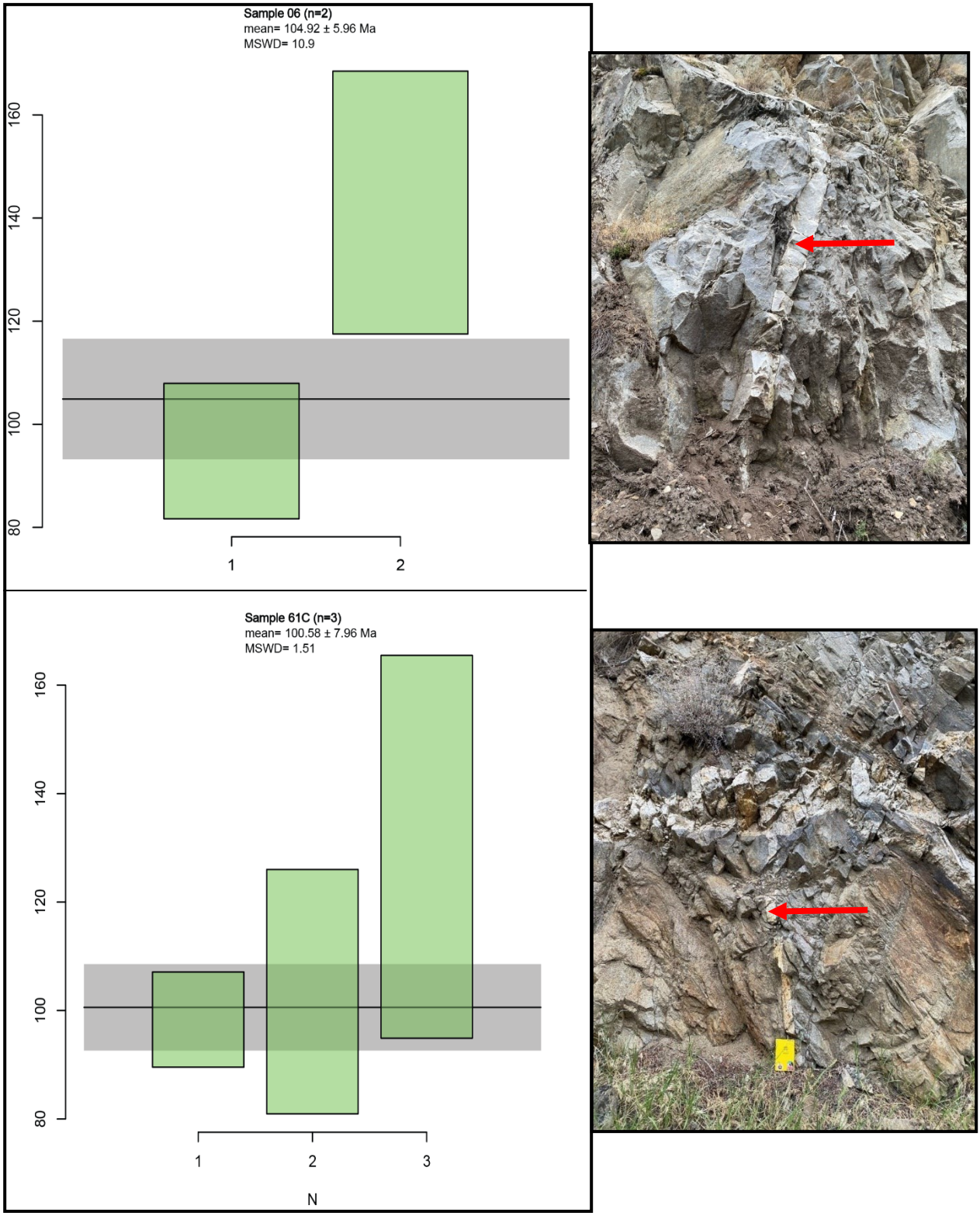

Figure 5. Weighted mean ages for U-Pb zircon and sample location photos. Error is recorded to sigma 3.

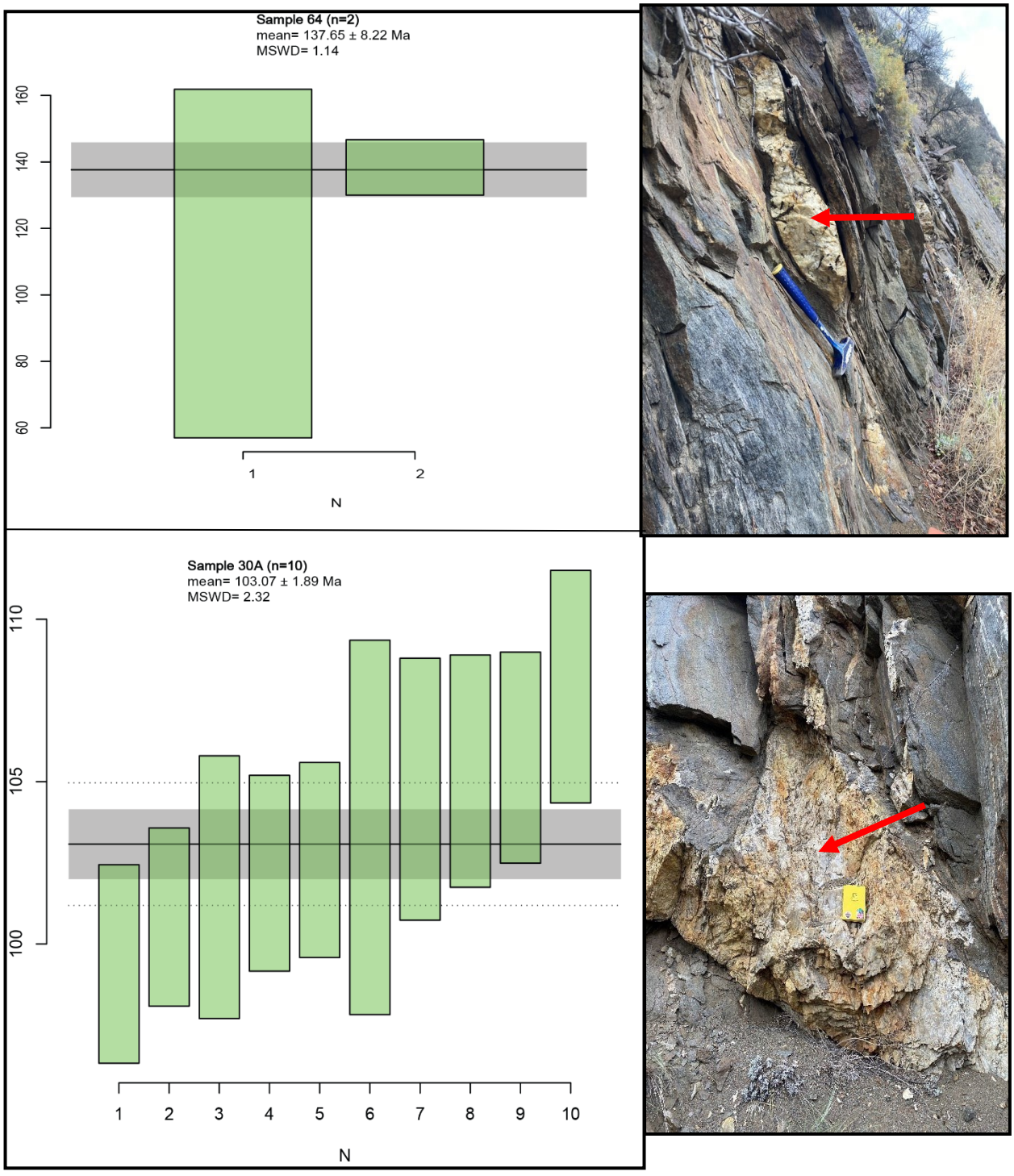

Figure 5 continued. Weighted mean ages for U-Pb zircon and sample location photos. Error is recorded to sigma 3.

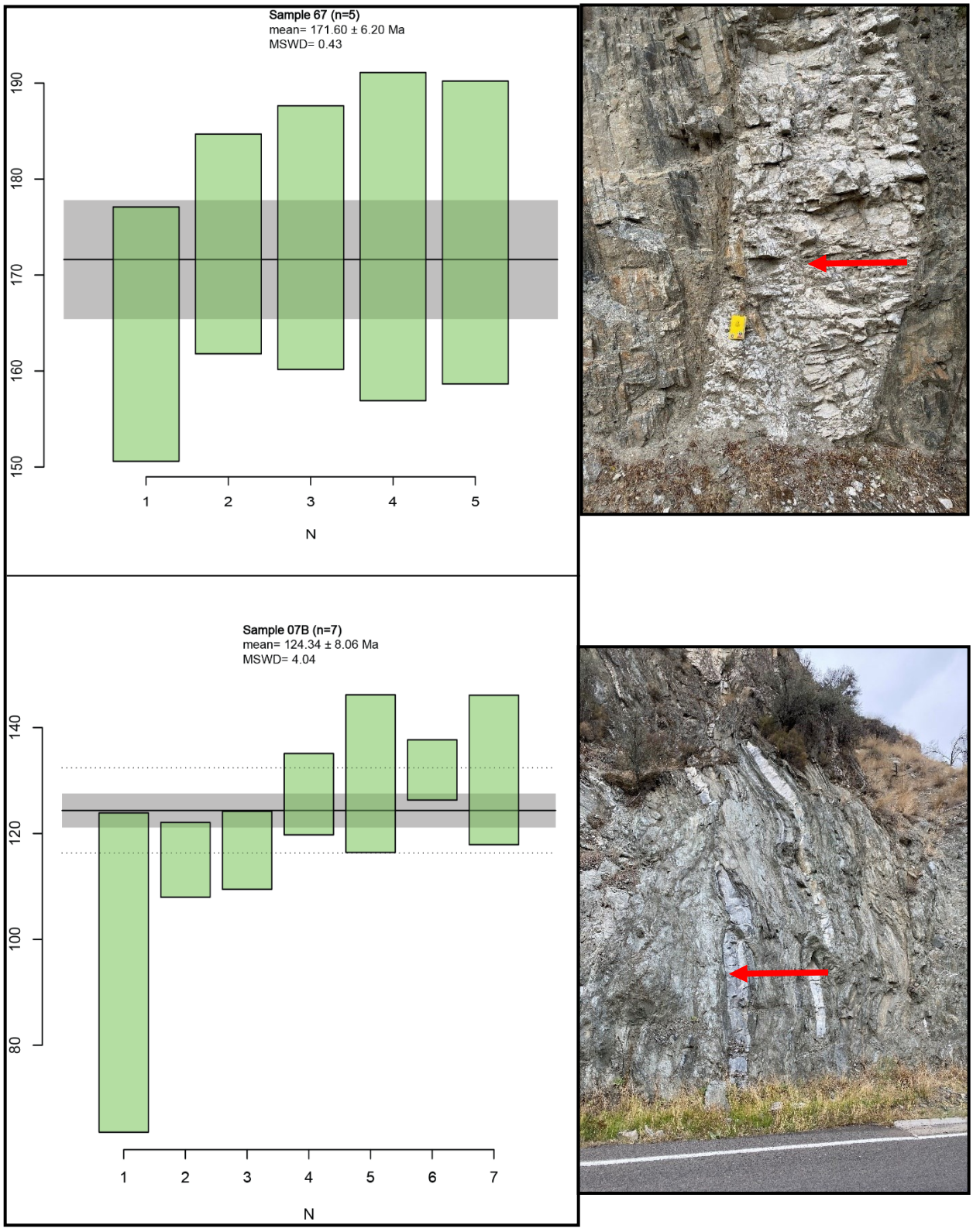

Figure 5 continued. Weighted mean ages for U-Pb zircon and sample location photos. Error is recorded to sigma 3.

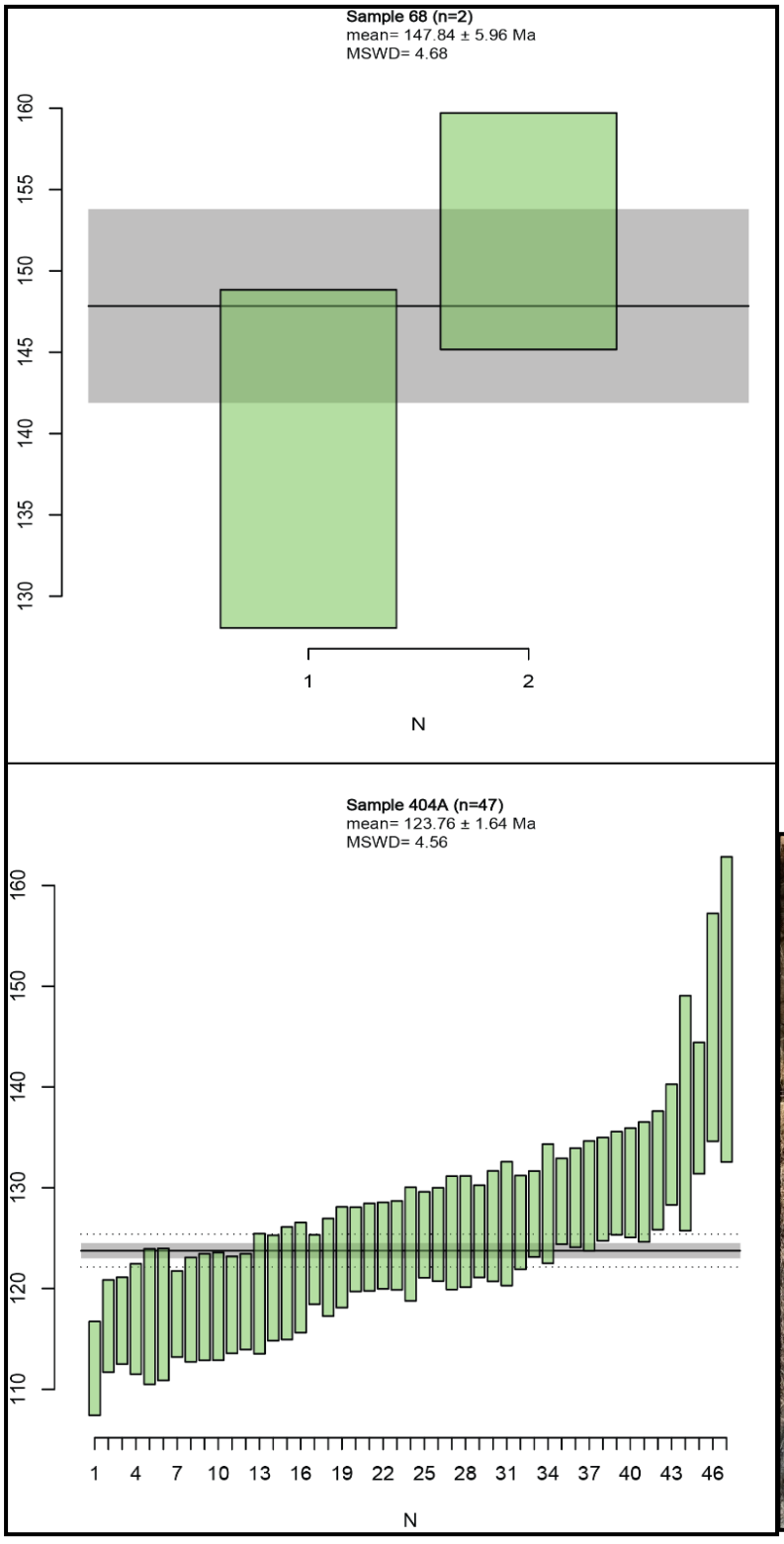

Figure 5 continued. Weighted mean ages for U-Pb zircon and sample location photos. Error is recorded to sigma 3.

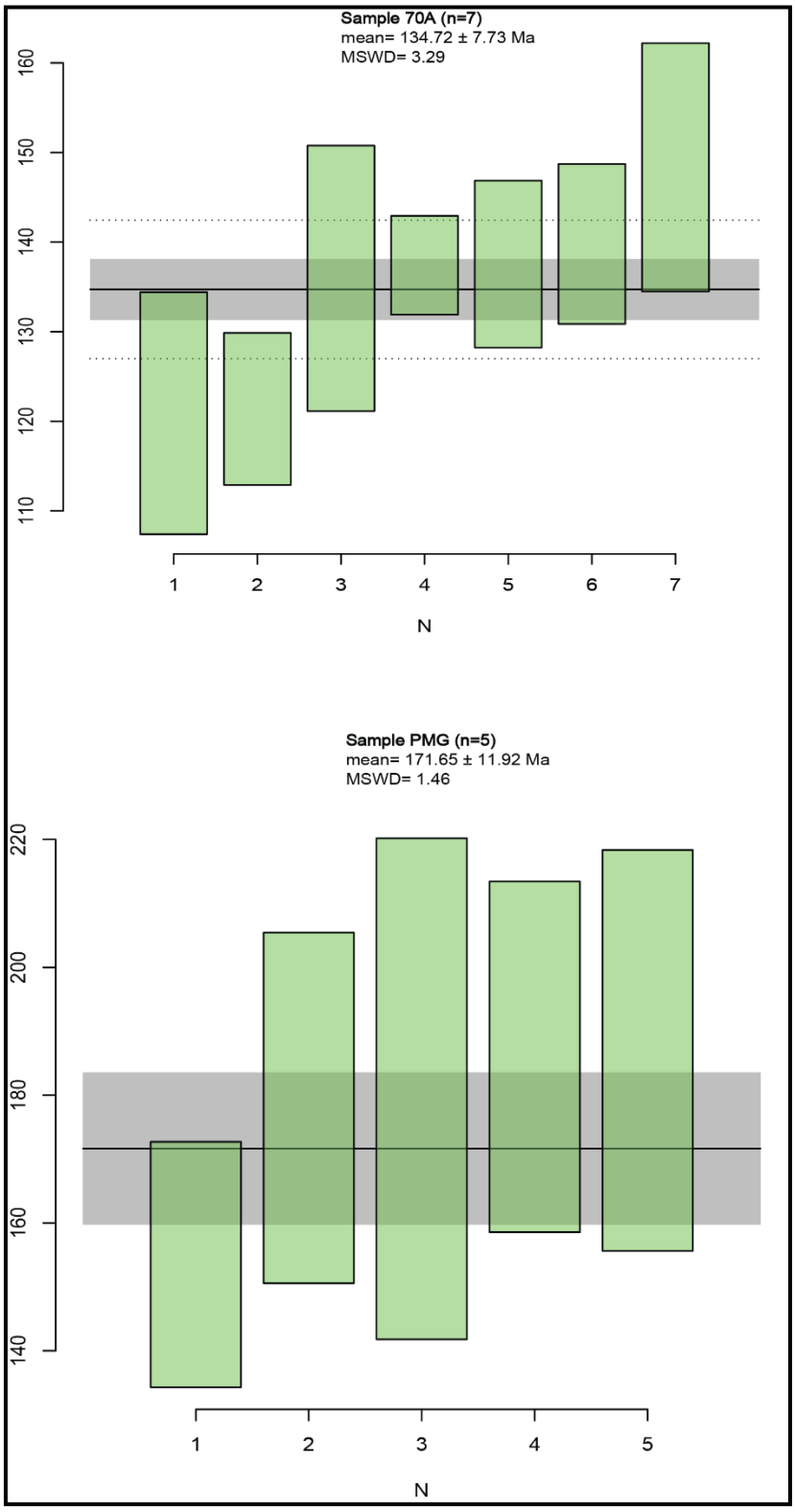

Figure 5 continued. Weighted mean ages for U-Pb zircon and sample location photos. Error is recorded to sigma 3.

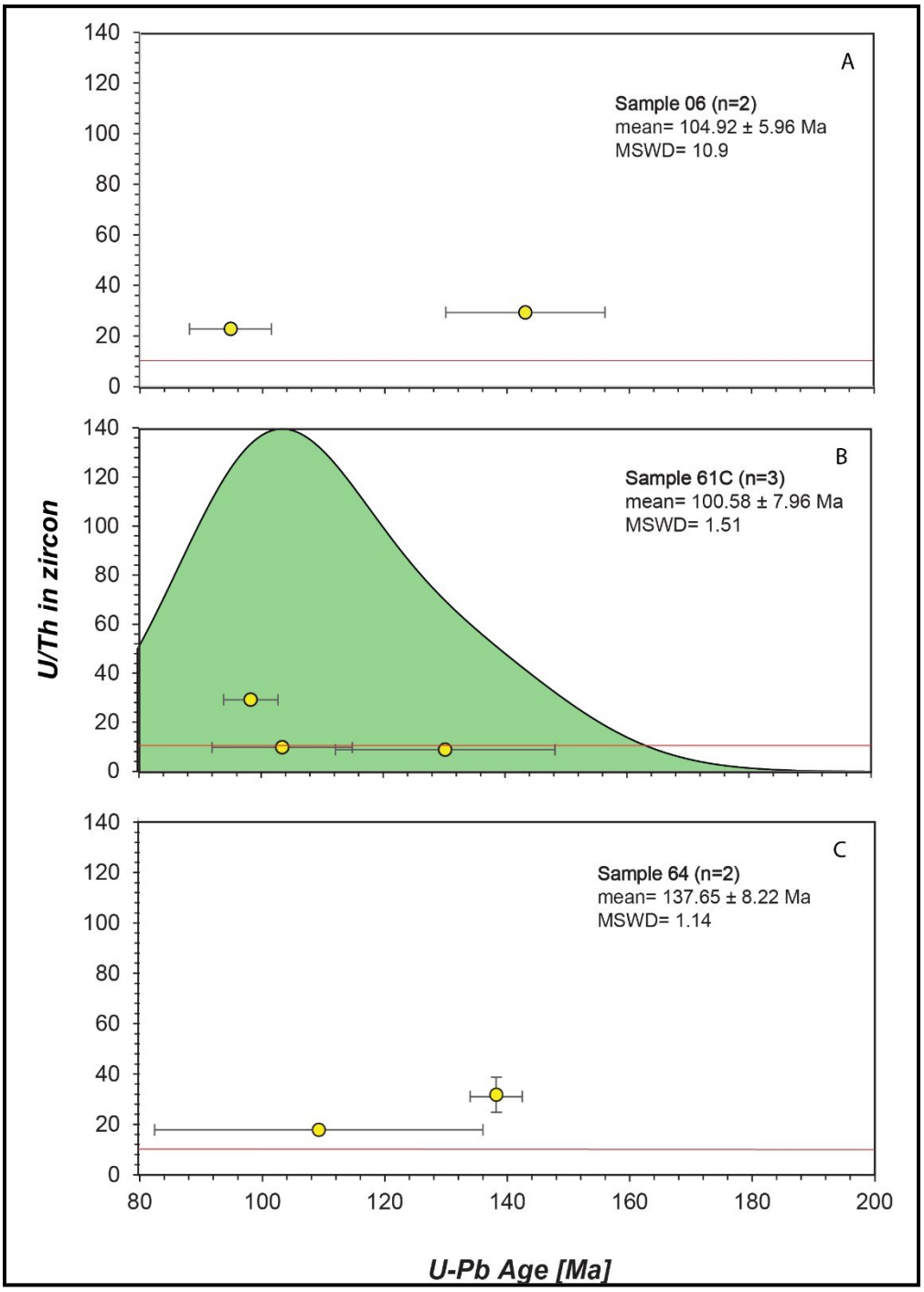

Figure 6. Zircon crystallization age vs U/Th ratios in zircon with an age population represented by a kernel density estimate (KDE). Ages are plotted from $^{206}Pb/^{238}U$ final age with a ^{207}Pb correction.

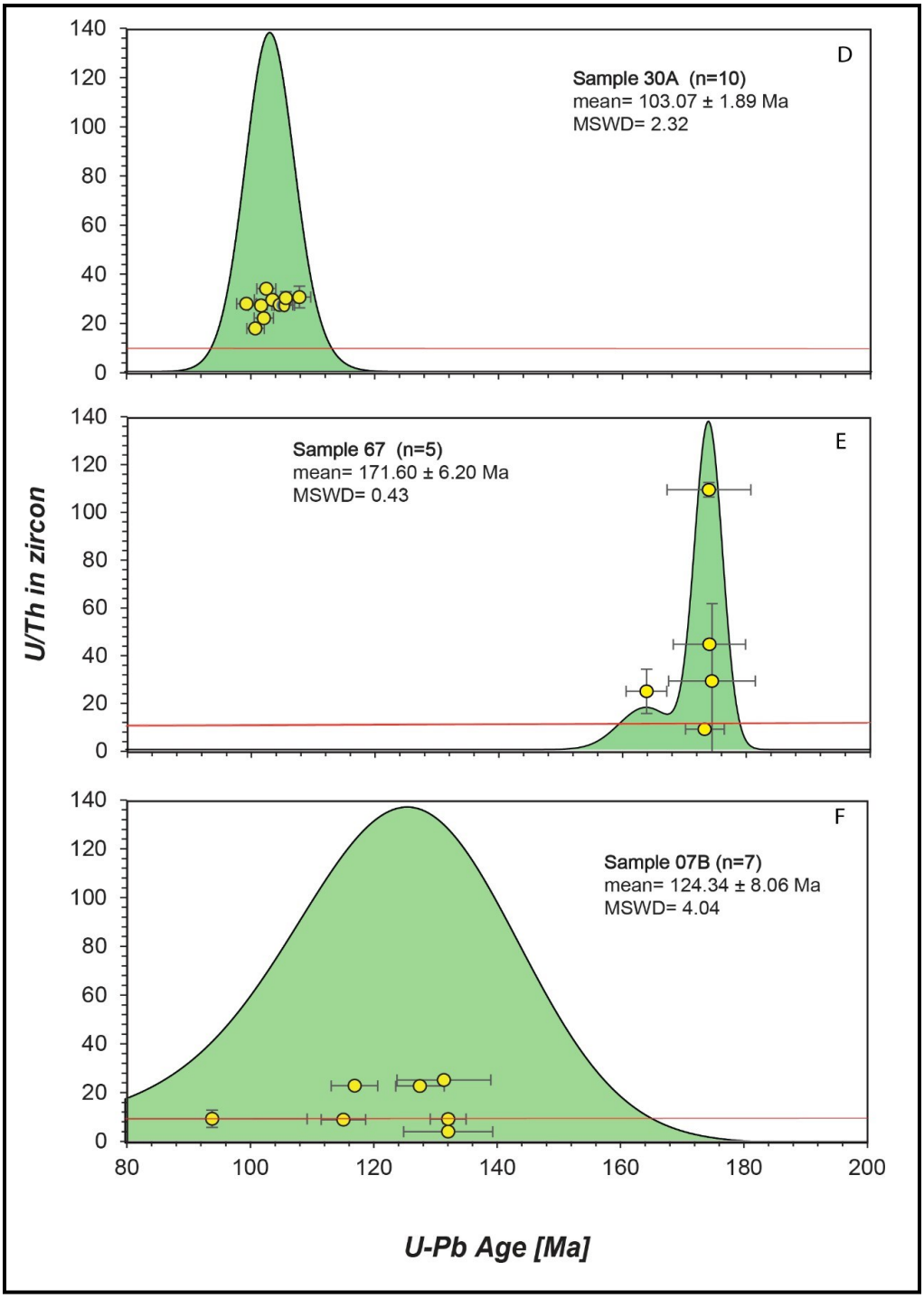

Figure 6 continued. Zircon crystallization age vs U/Th ratios in zircon with an age population represented by a kernel density estimate (KDE). Ages are plotted from $^{206}Pb/^{238}U$ final age with a ^{207}Pb correction.

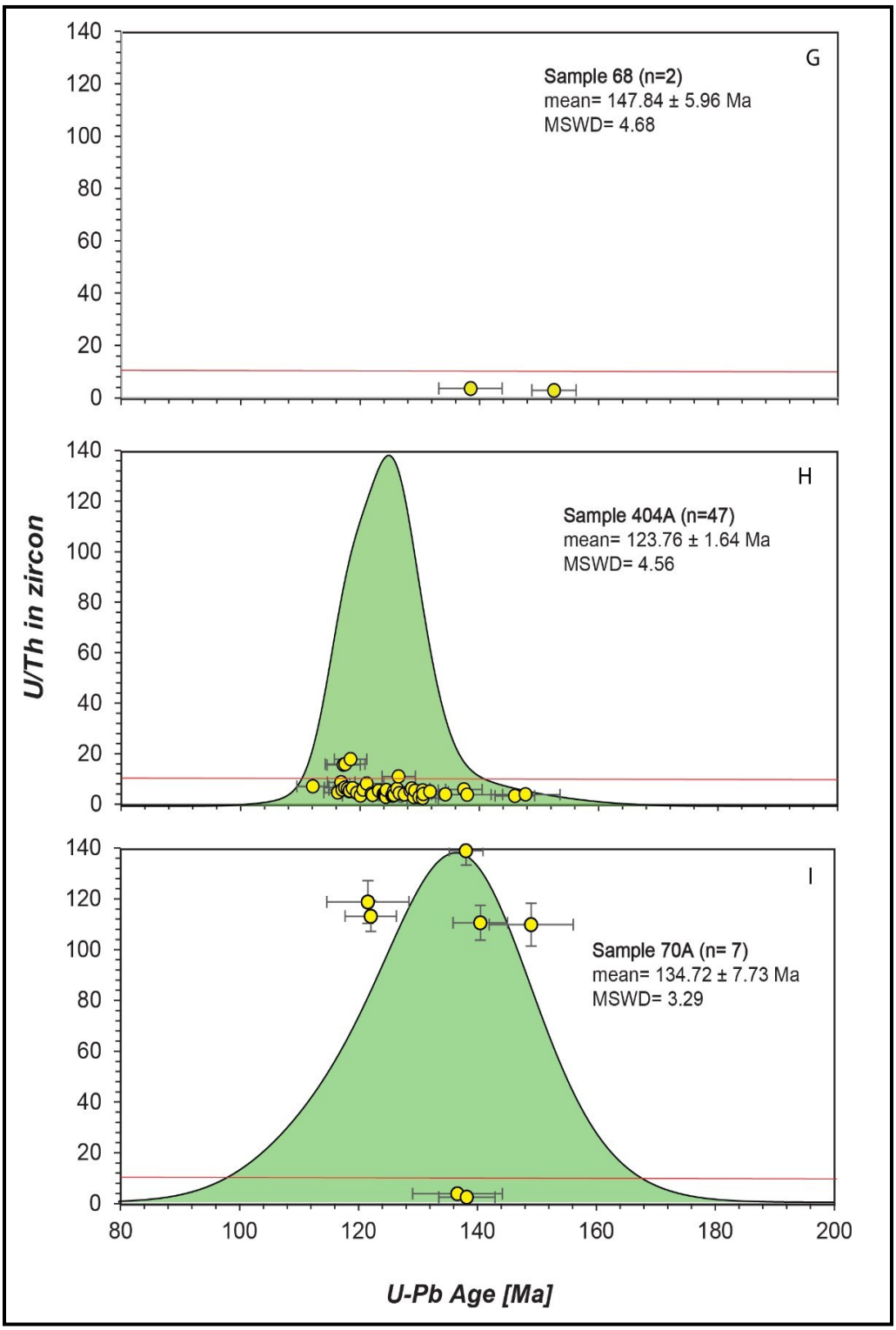

Figure 6 continued. Zircon crystallization age vs U/Th ratios in zircon with an age population represented by a kernel density estimate (KDE). Ages are plotted from $^{206}Pb/^{238}U$ final age with a ^{207}Pb correction.

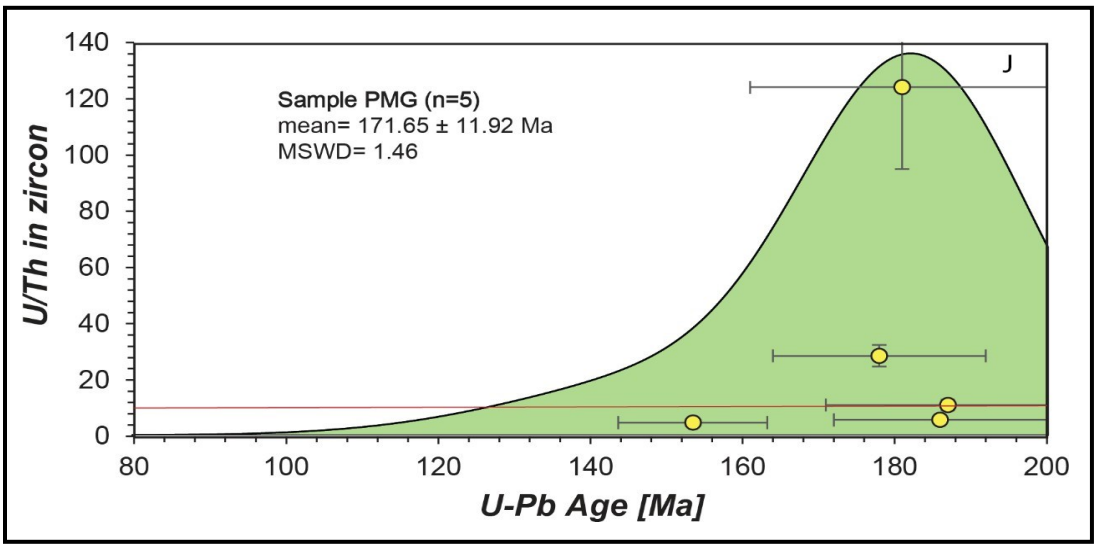

Figure 6 continued. Zircon crystallization age vs U/Th ratios in zircon with an age population represented by a kernel density estimate (KDE). Ages are plotted from $^{206}Pb/^{238}U$ final age with a ^{207}Pb correction.

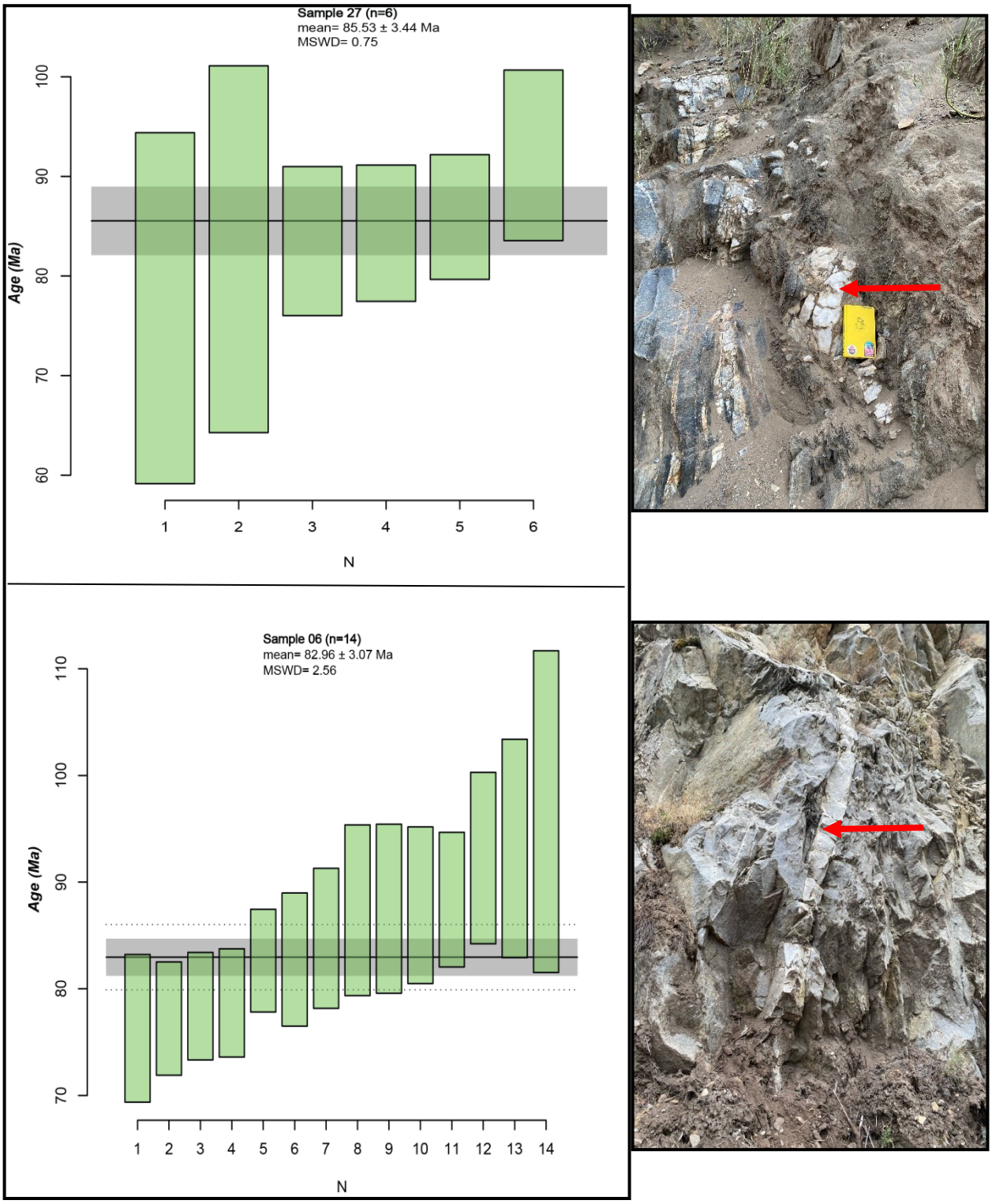

Figure 7. Weighted mean ages for U-Pb apatite and sample location photos. Error is recorded to sigma 3

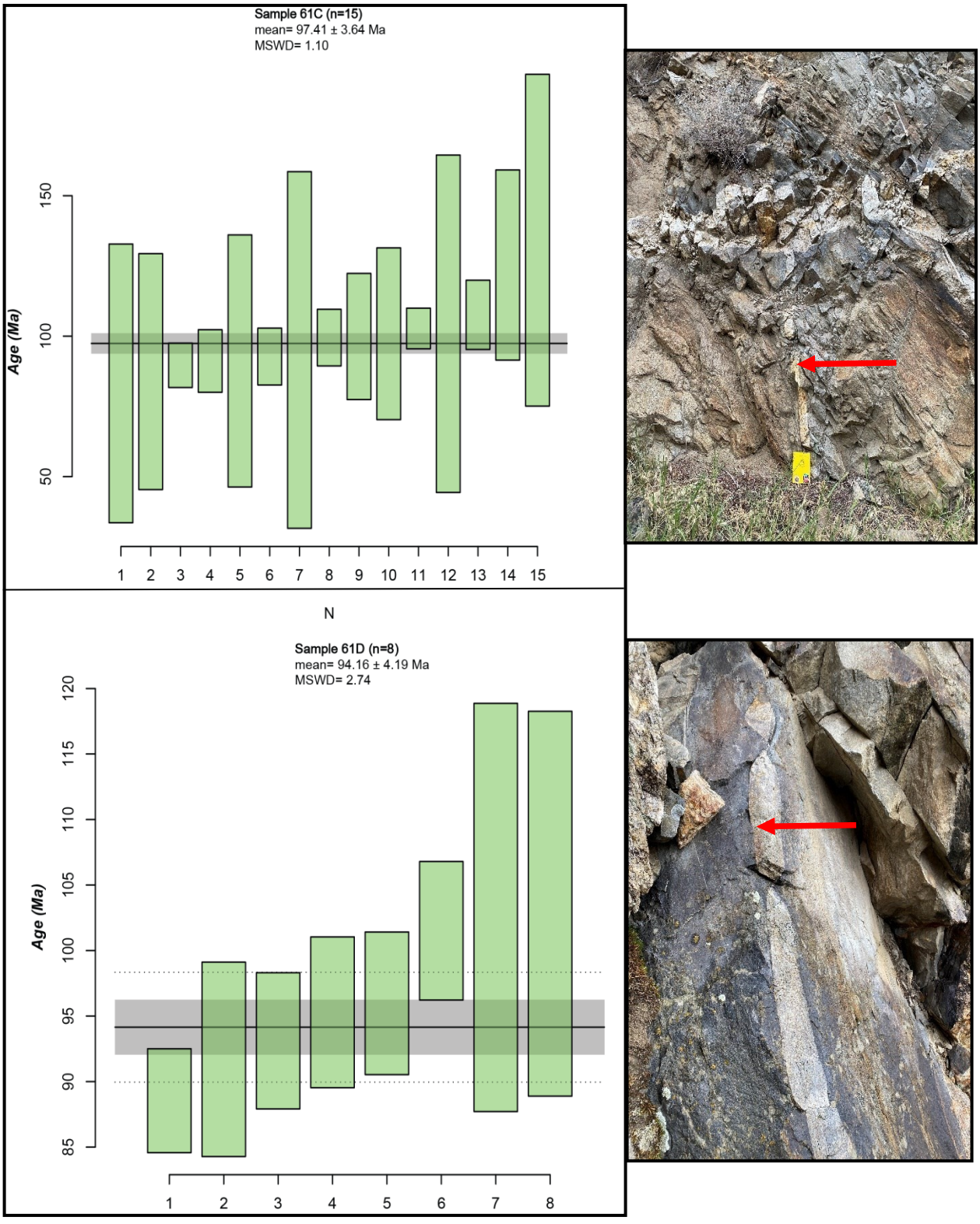

Figure 7 continued. Weighted mean ages for U-Pb apatite and sample location photos. Error is recorded to sigma 3

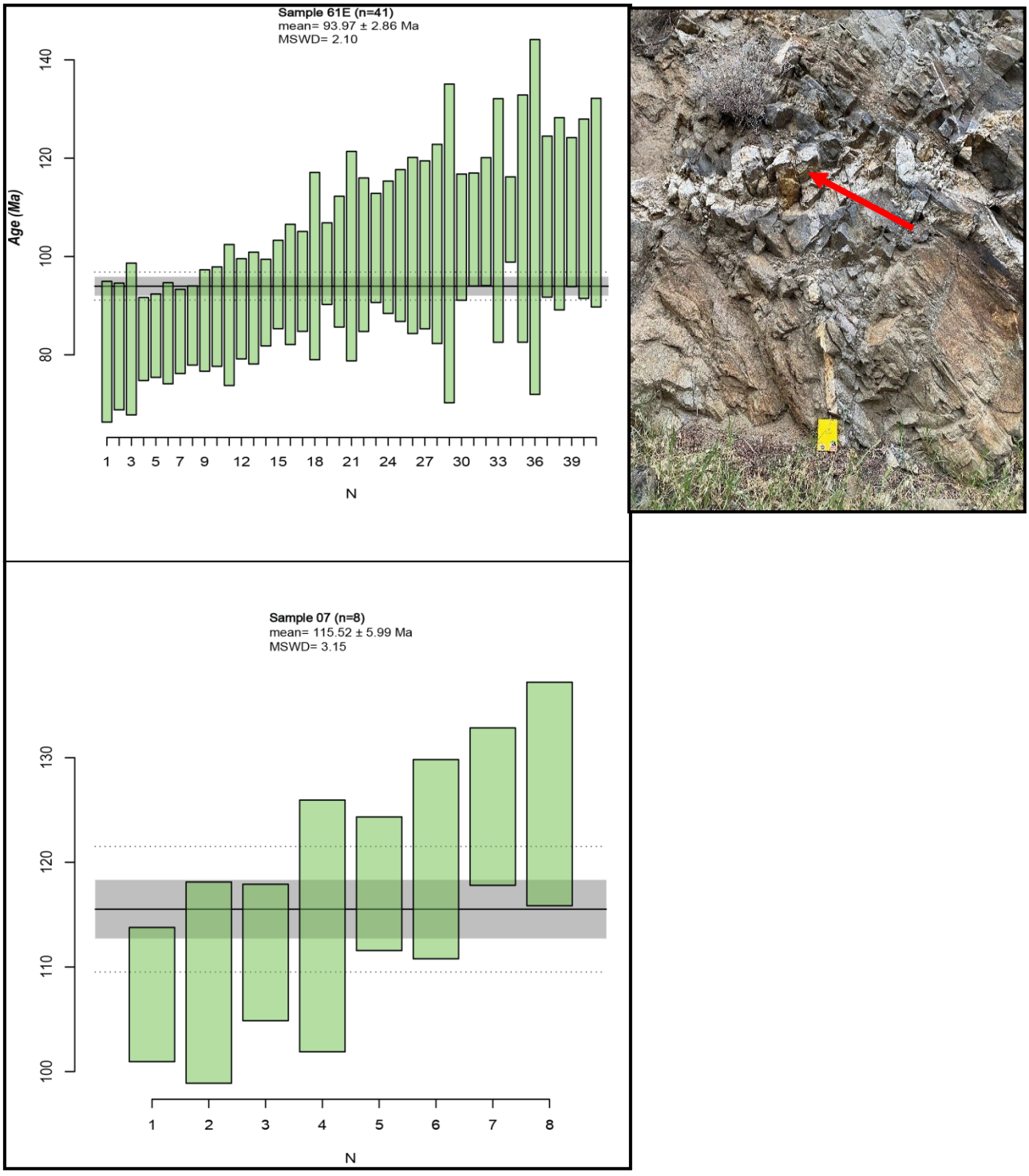

Figure 7 continued. Weighted mean ages for U-Pb apatite and sample location photos. Error is recorded to sigma 3

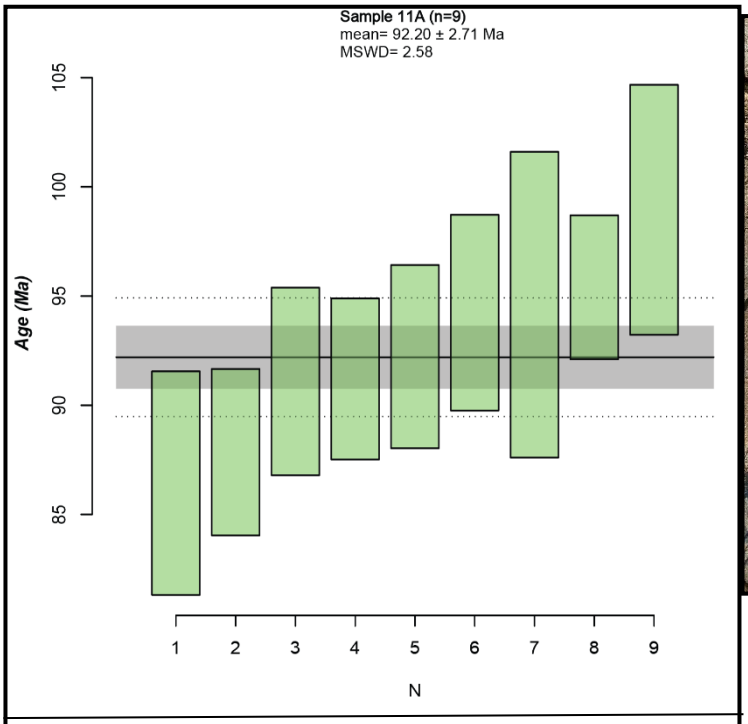

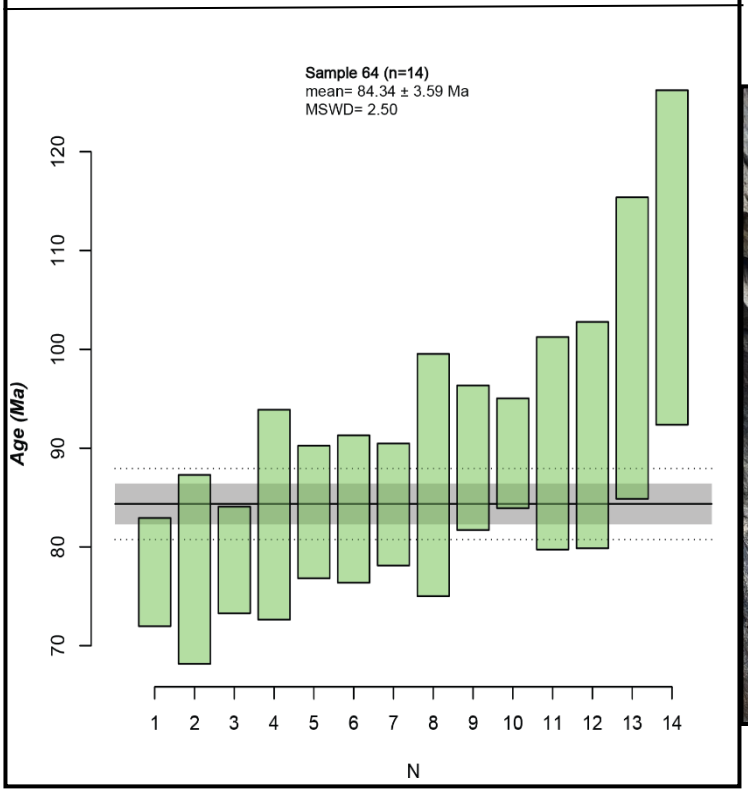

Figure 7 continued. Weighted mean ages for U-Pb apatite and sample location photos. Error is recorded to sigma 3

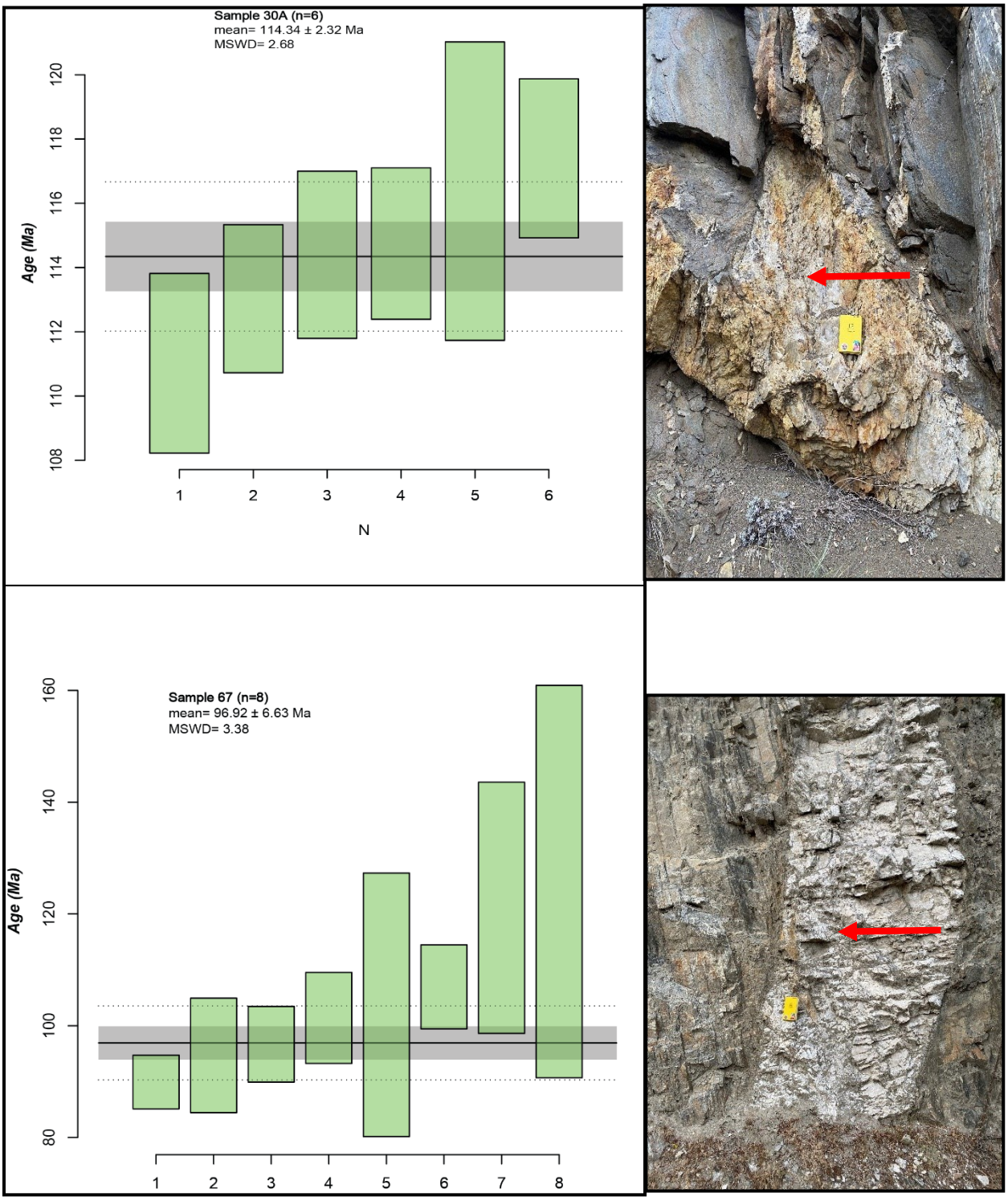

Figure 7 continued. Weighted mean ages for U-Pb apatite and sample location photos. Error is recorded to sigma 3

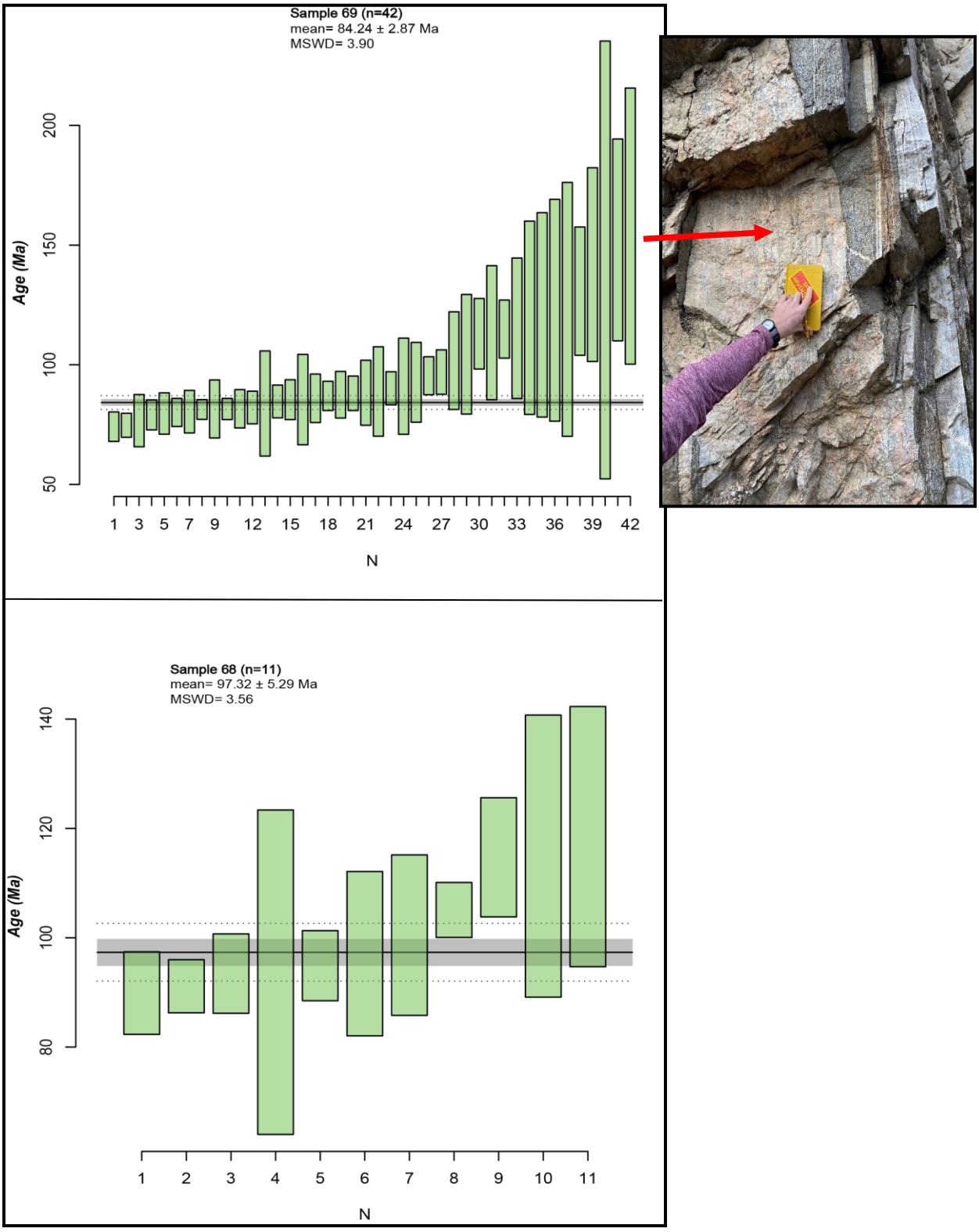

Figure 7 continued. Weighted mean ages for U-Pb apatite and sample location photos. Error is recorded to sigma 3

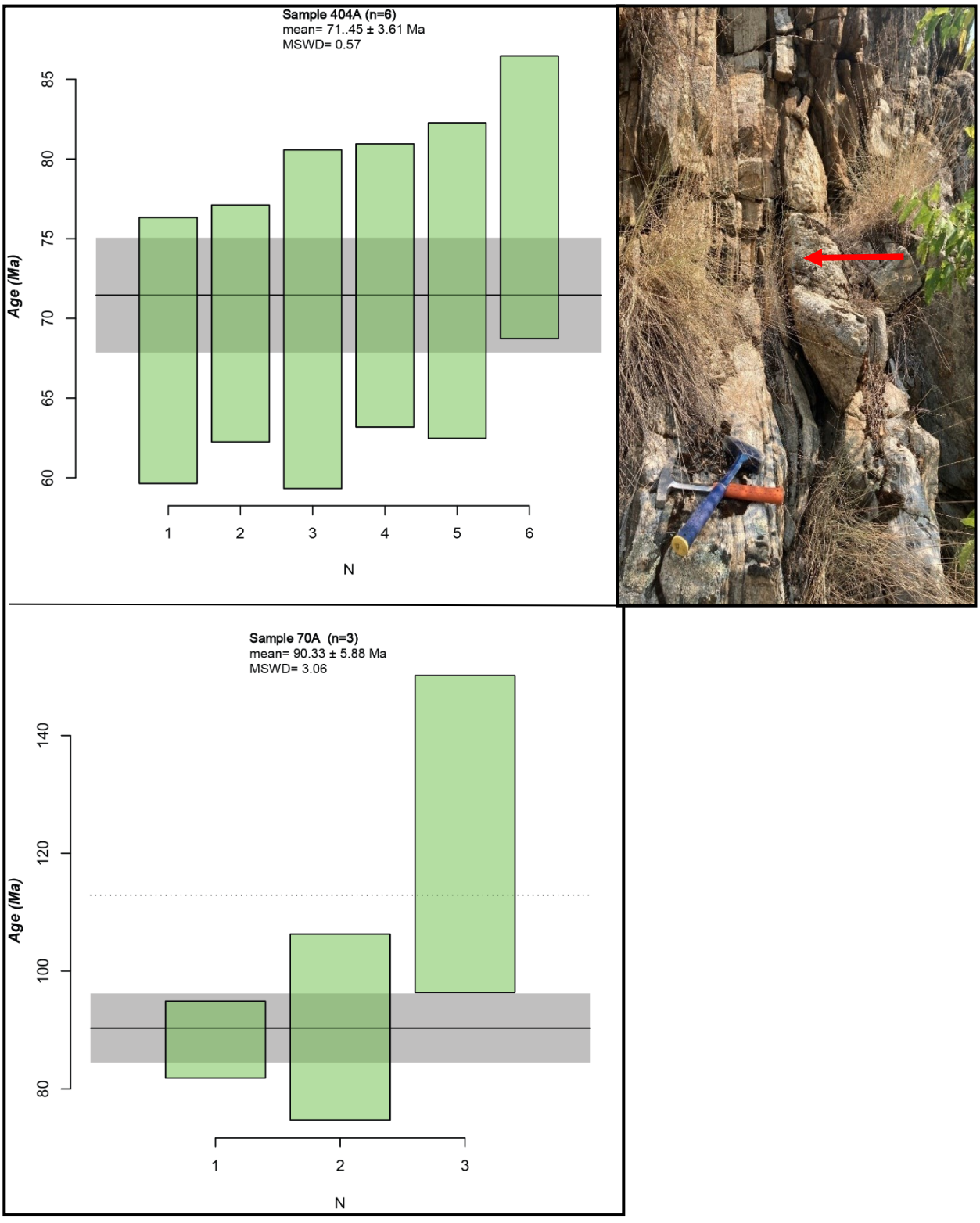

Figure 7 continued. Weighted mean ages for U-Pb apatite and sample location photos. Error is recorded to sigma 3

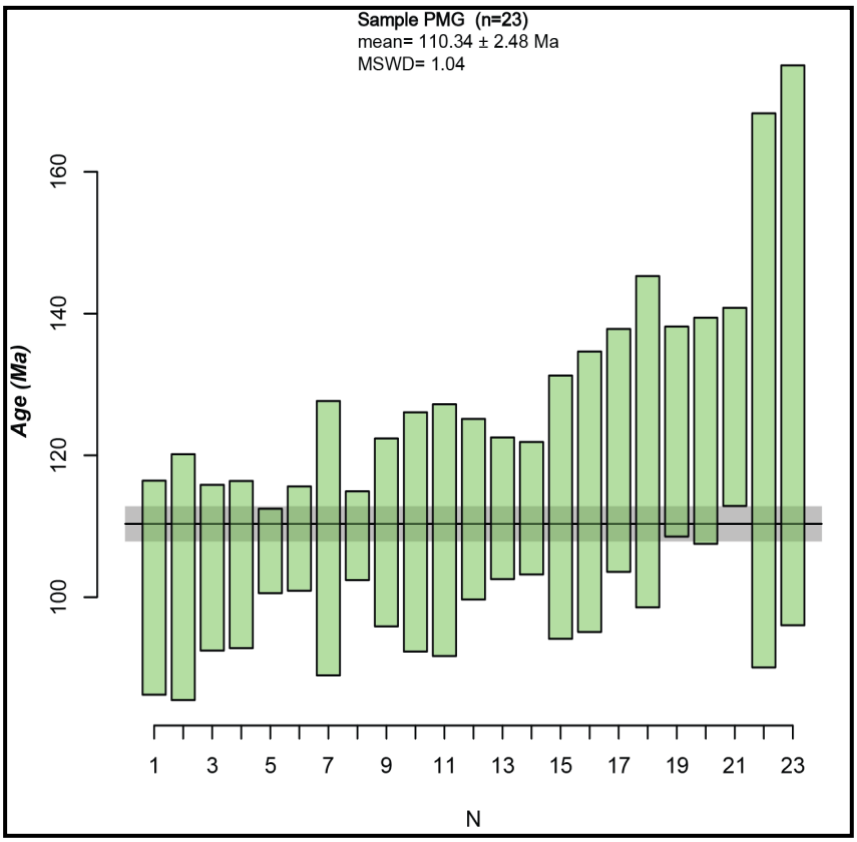

Figure 7 continued. Weighted mean ages for U-Pb apatite and sample location photos. Error is recorded to sigma 3

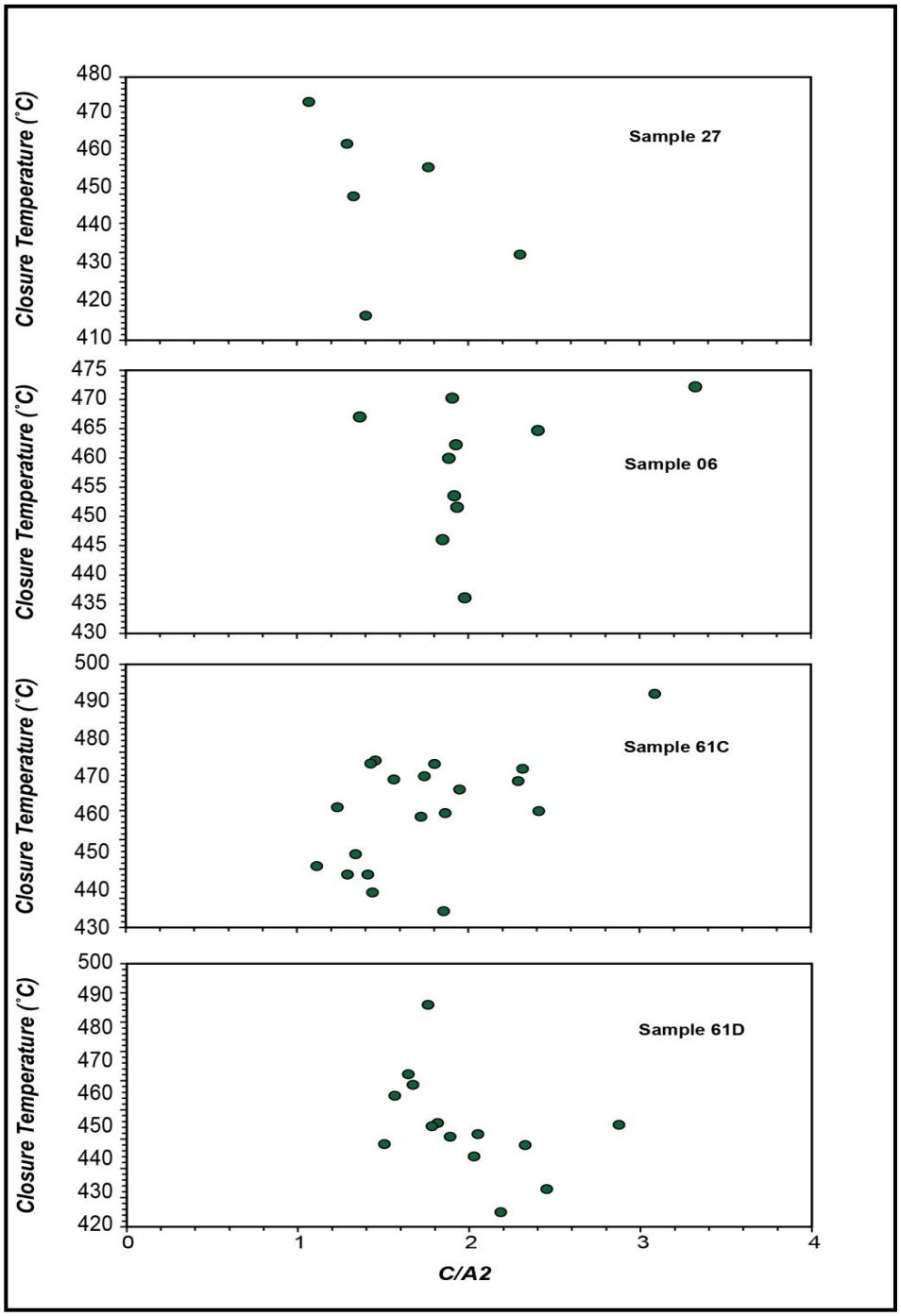

Figure 8. Grain size vs closure temperature for each apatite sample of the rocks found within the Salmon River suture zone. The c/a2 axis was found by measuring the long and short side of each apatite grain. The y-axis is plotting the closure temperature that was calculated for each sample using the Dodson (1973) equation listed above (equation 2). The x-axis is the average grain size of each grain, which was calculated by measuring the c (long) and a2 (short) axes of each grain and then dividing them, recorded in micrometers.

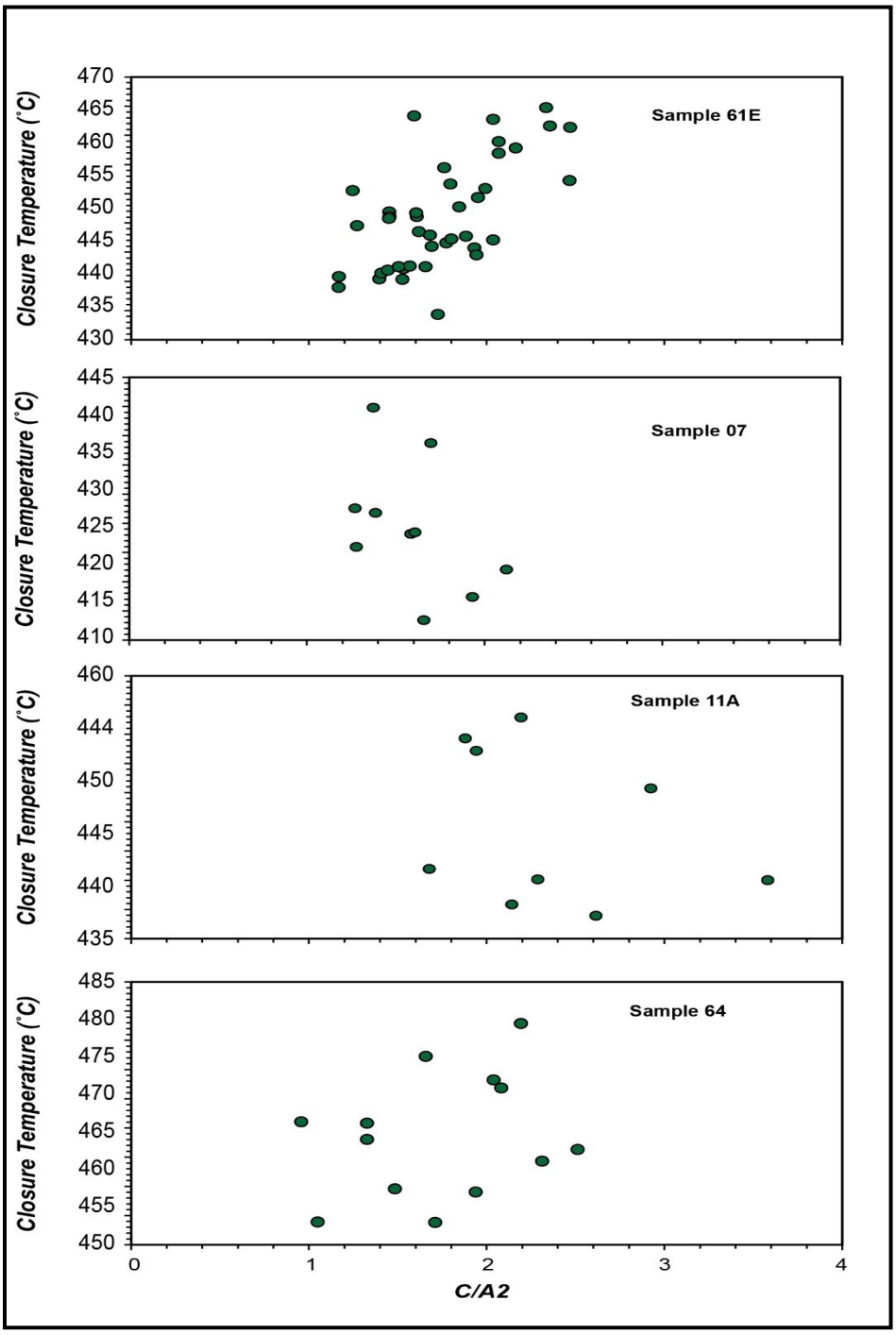

Figure 8 continued. Grain size vs closure temperature for each apatite sample of the rocks found within the Salmon River suture zone. The c/a2 axis was found by measuring the long and short side of each apatite grain. The y-axis is plotting the closure temperature that was calculated for each sample using the Dodson (1973) equation listed above (equation 2). The x-axis is the average grain size of each grain, which was calculated by measuring the c (long) and a2 (short) axes of each grain and then dividing them, recorded in micrometers.

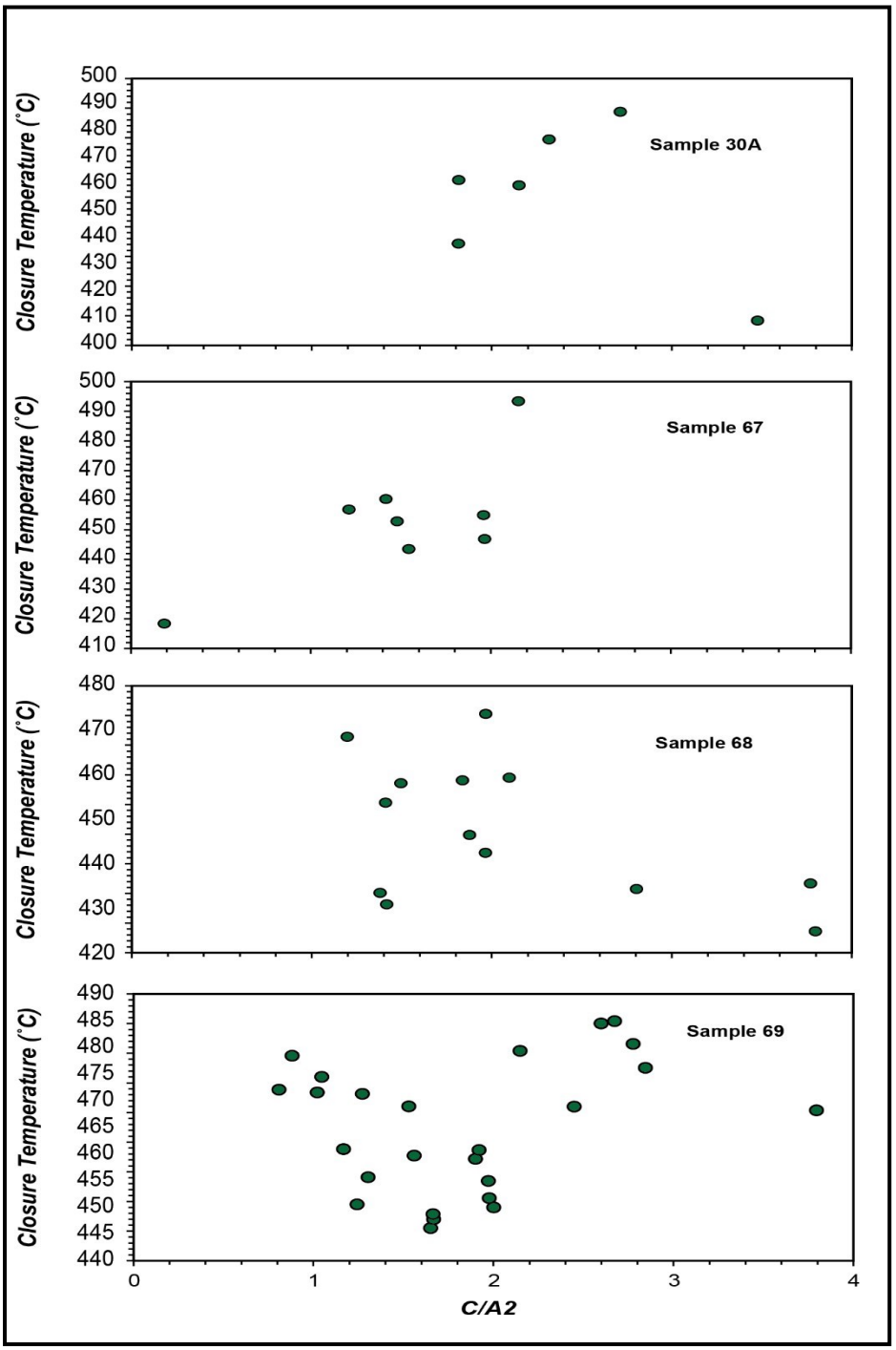

Figure 8 continued. Grain size vs closure temperature for each apatite sample of the rocks found within the Salmon River suture zone. The c/a2 axis was found by measuring the long and short side of each apatite grain. The y-axis is plotting the closure temperature that was calculated for each sample using the Dodson (1973) equation listed above (equation 2). The x-axis is the average grain size of each grain, which was calculated by measuring the c (long) and a2 (short) axes of each grain and then dividing them, recorded in micrometers.

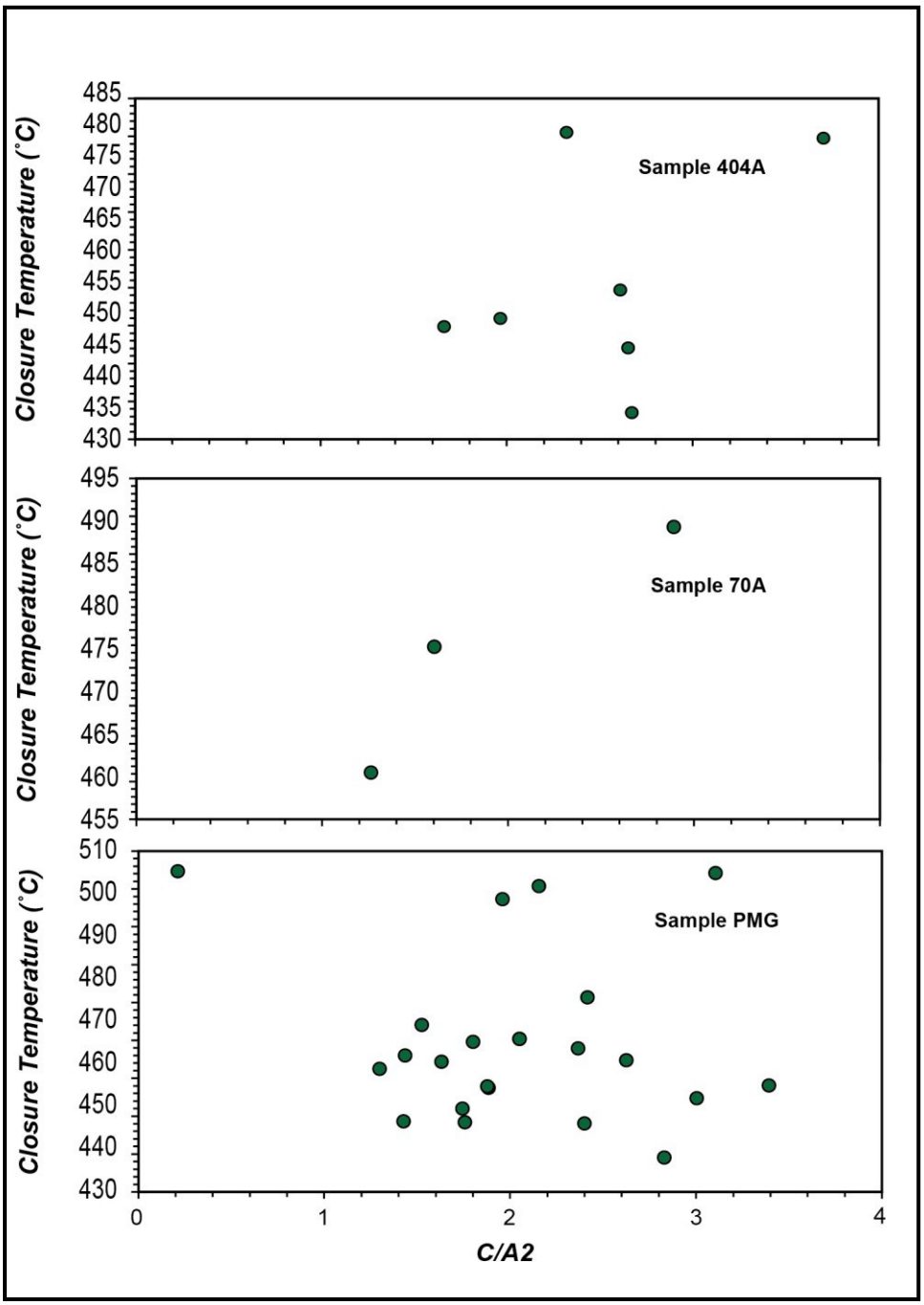

Figure 8 continued. Grain size vs closure temperature for each apatite sample of the rocks found within the Salmon River suture zone. The c/a2 axis was found by measuring the long and short side of each apatite grain. The y-axis is plotting the closure temperature that was calculated for each sample using the Dodson (1973) equation listed above (equation 2). The x-axis is the average grain size of each grain, which was calculated by measuring the c (long) and a2 (short) axes of each grain and then dividing them, recorded in micrometers.

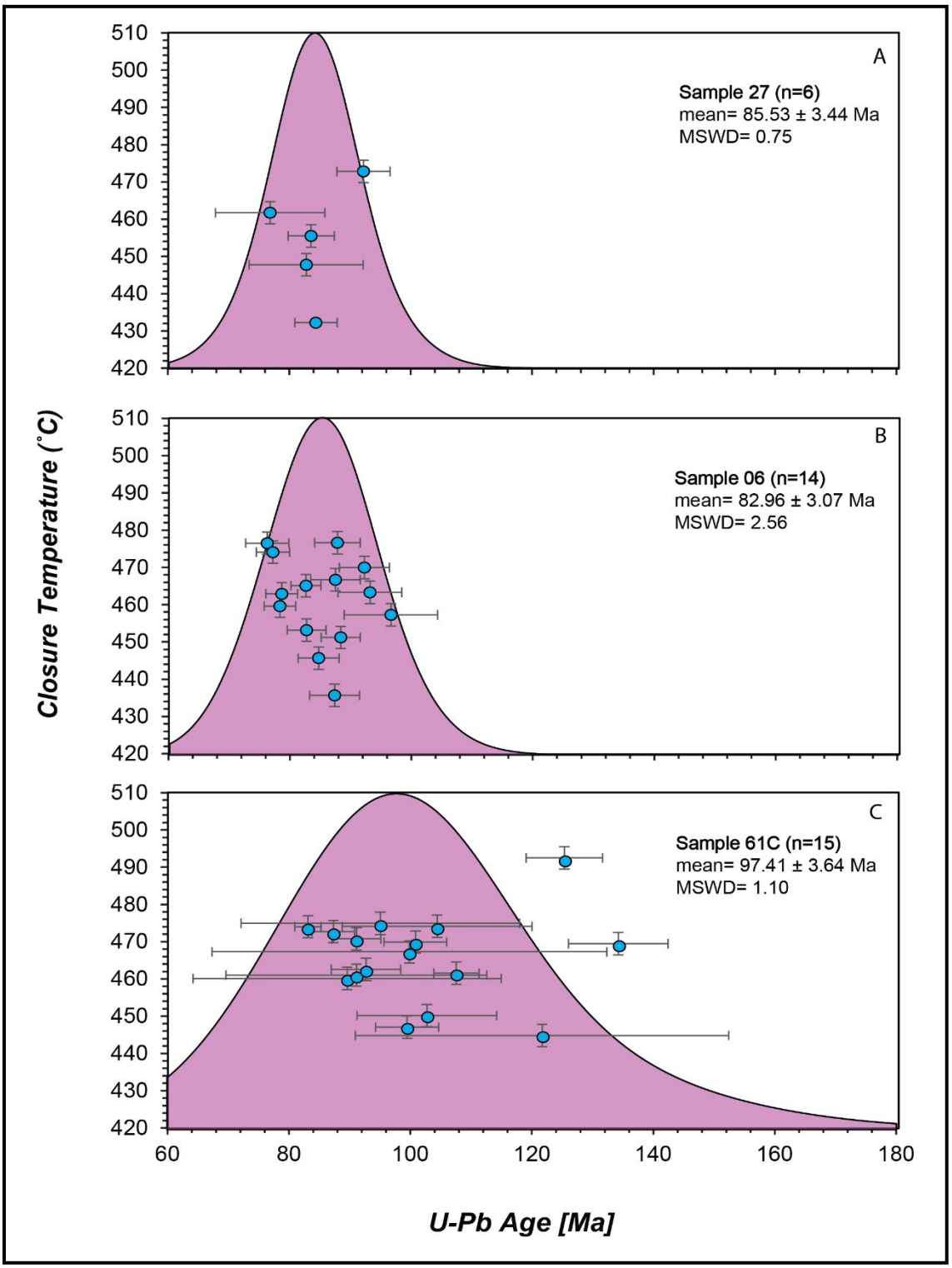

Figure 9. Kernel density estimates (KDE) age plot and closure temperature for all apatite samples from the Salmon River Suture zone, showing the distribution of $^{206}Pb/^{238}U$ final age with a ^{207}Pb correction vs closure temperature.

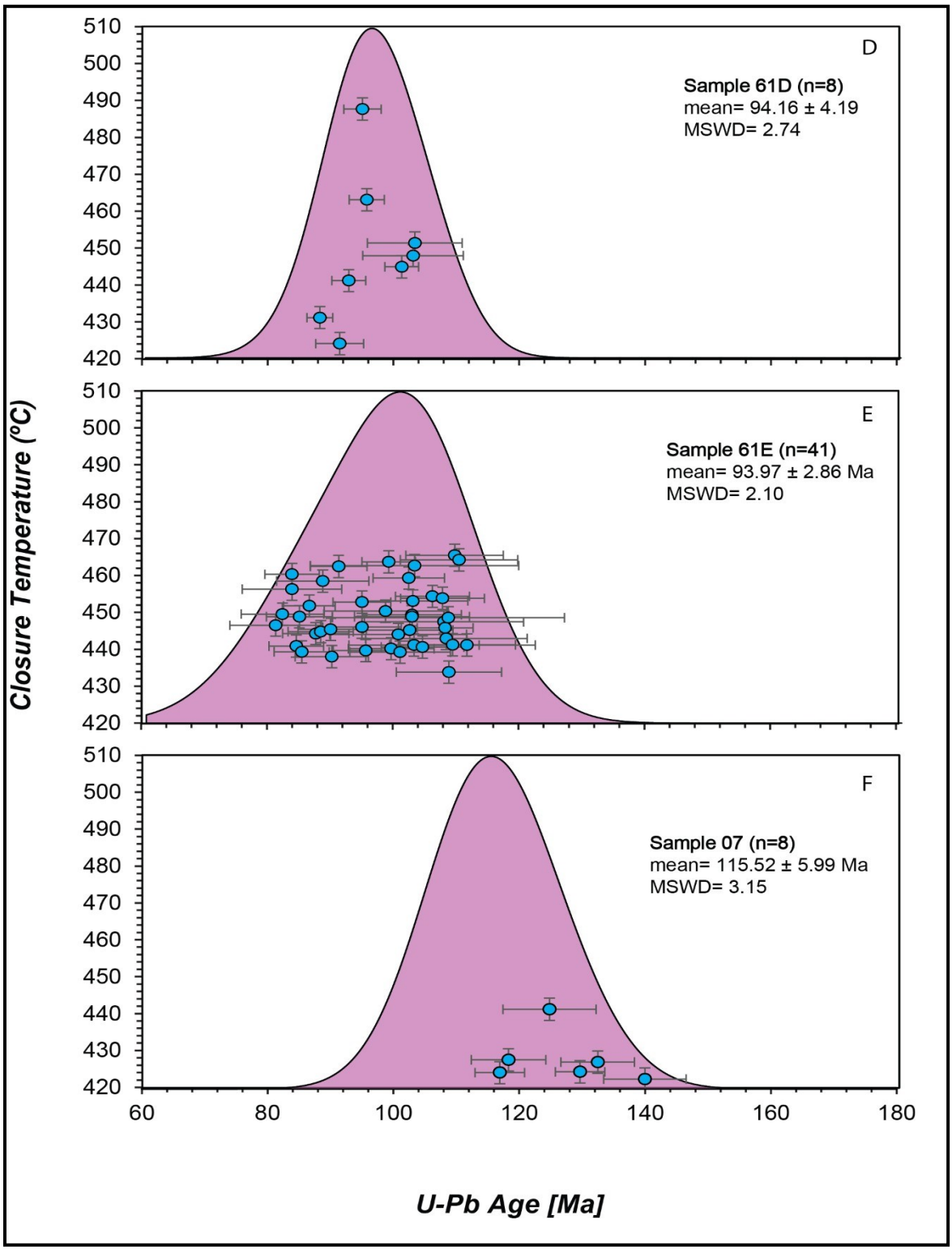

Figure 9 continued. Kernel density estimates (KDE) age plot and closure temperature for all apatite samples from the Salmon River Suture zone, showing the distribution of $^{206}Pb/^{238}U$ final age with a ^{207}Pb correction vs closure temperature.

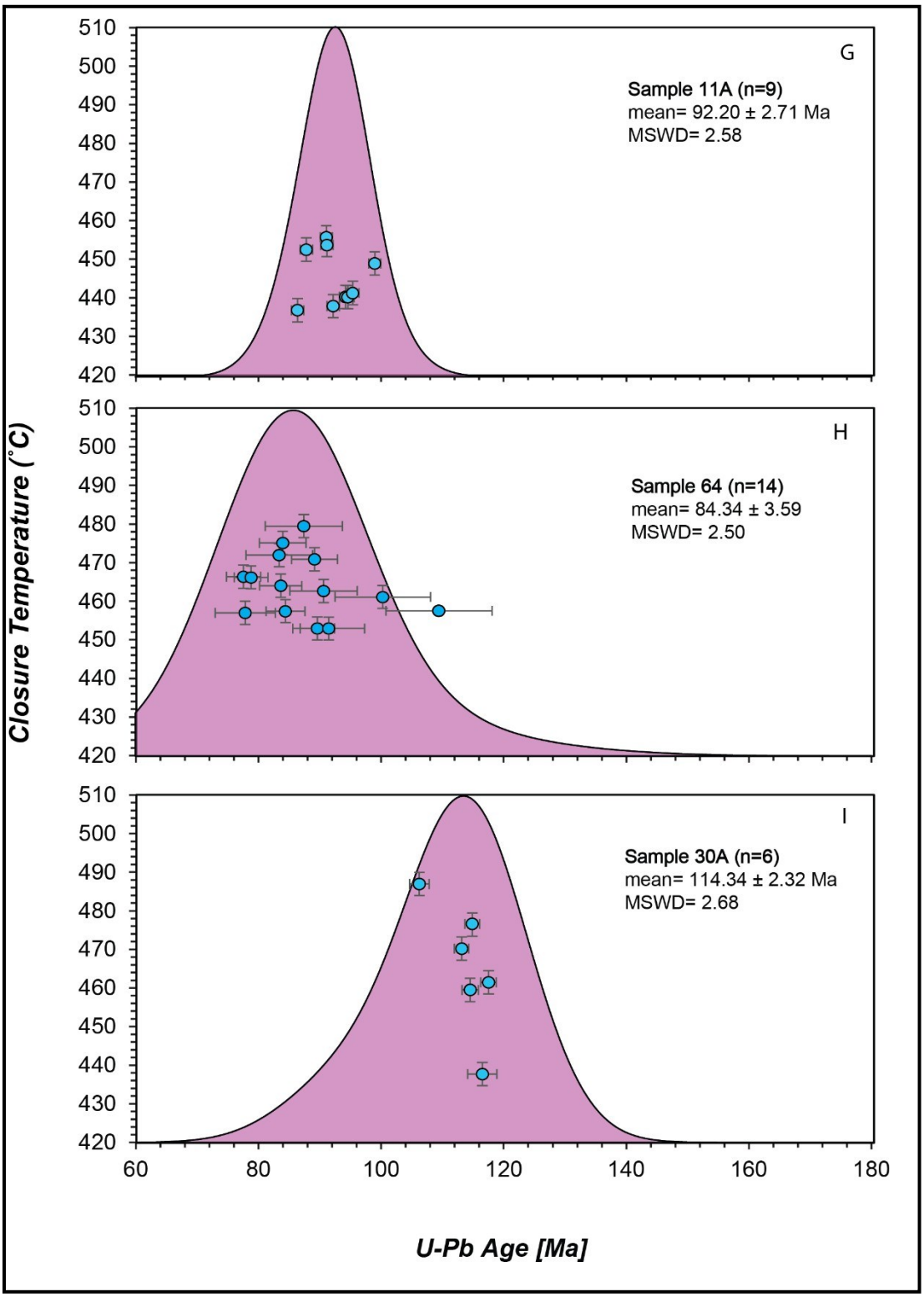

Figure 9 continued. Kernel density estimates (KDE) age plot and closure temperature for all apatite samples from the Salmon River Suture zone, showing the distribution of $^{206}Pb/^{238}U$ final age with a ^{207}Pb correction vs closure temperature.

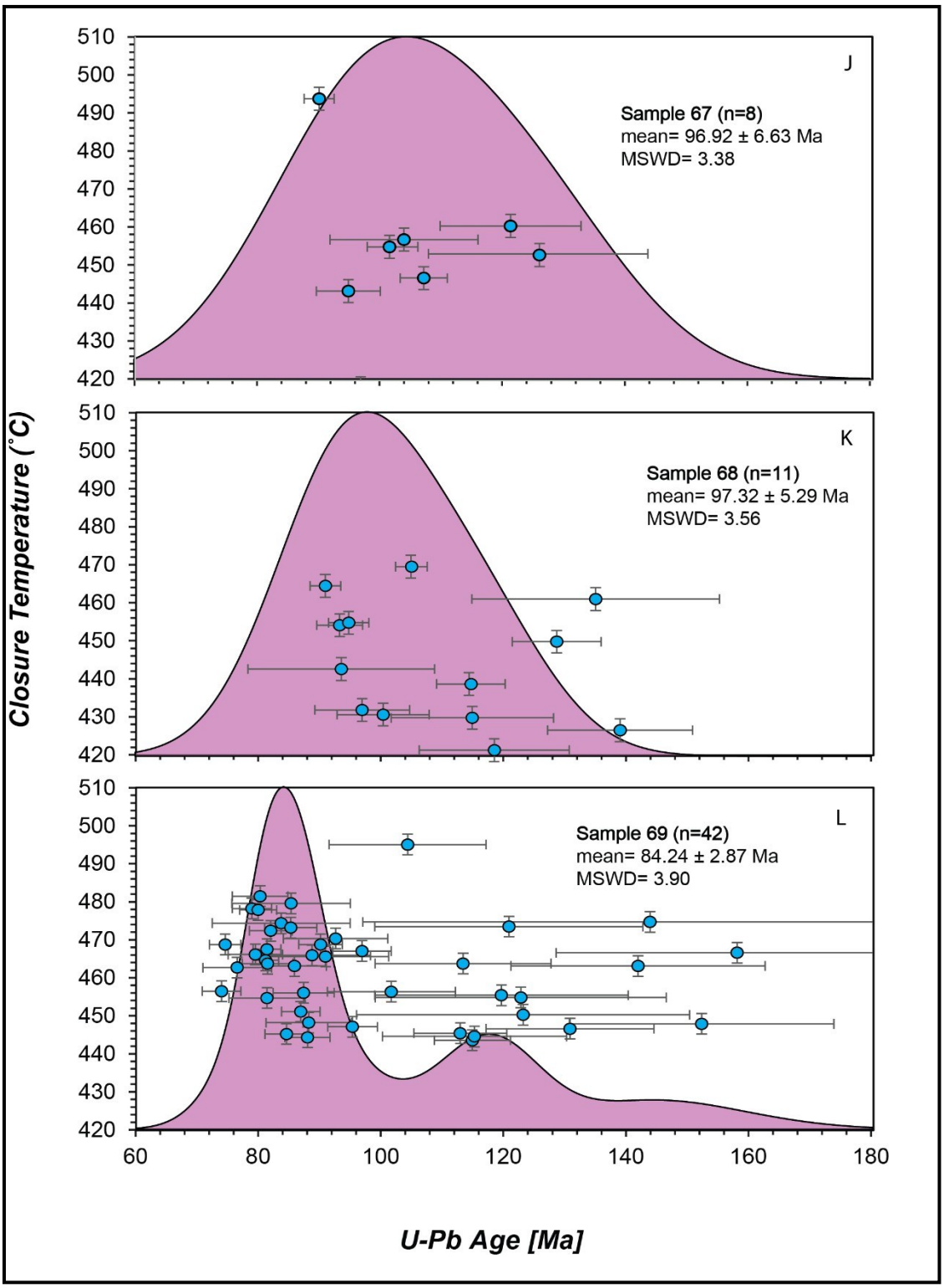

Figure 9 continued. Kernel density estimates (KDE) age plot and closure temperature for all apatite samples from the Salmon River Suture zone, showing the distribution of $^{206}Pb/^{238}U$ final age with a ^{207}Pb correction vs closure temperature.

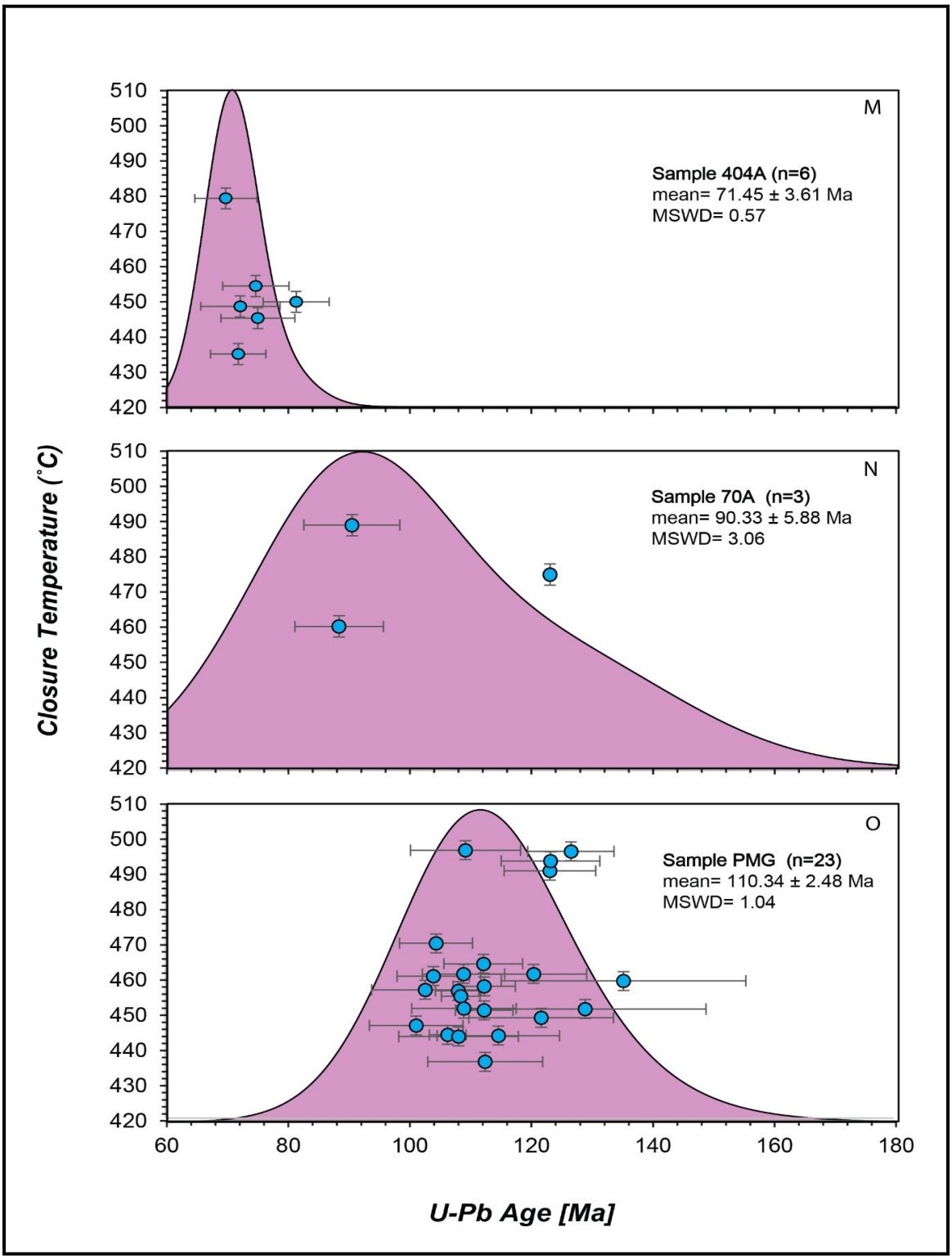

Figure 9 continued. Kernel density estimates (KDE) age plot and closure temperature for all apatite samples from the Salmon River Suture zone, showing the distribution of $^{206}Pb/^{238}U$ final age with a ^{207}Pb correction vs closure temperature.

DISCUSSION

Metamorphic History of Zircon

The ages of zircons found in the Salmon River suture zone range from 171 to 100 Ma. When removing the samples that had only a few grains, that gave high ages, the trend moving west to east along the river shows the ages becoming older as the sample locations move closer to the Idaho Batholith moving east. The samples throughout the Salmon River suture zone record both metamorphic and igneous activity according to their respective U/Th values contained in zircon. Metamorphism began at 141 Ma and persisted to about 124 Ma (McKay et al. 2017). Igneous activity occurred with intrusions from 147 to 116 Ma. The earliest ages of metamorphism in the Salmon River suture zone are derived from the Pollock Mountain plate (McKay et al., 2017). The youngest metamorphic ages are found in the footwall of the Pollock Mountain thrust fault.

Early studies suggest that metamorphism in the suture zone (Hamilton, 1963: Onasch, 1977) was related to the intrusion of the 100-54 Ma Idaho batholith to the east of the Salmon River suture zone (Gaschnig et al., 2010). Sm-Nd garnet geochronology done by Getty et al., (1993), and McKay et al., (2017) have proposed that island arc amalgamation and subsequent accretion were recorded by distinct metamorphic events that occurred from 144 Ma to 128 Ma (Sleverstone et al., 1992; Getty et al., 1993; McKay et al., 2017). With U-Pb zircon data, this range can be pushed back to include metamorphism from 171 Ma to 100 Ma for the Salmon River suture zone.

Below Pollock Mountain Thrust Fault. In the footwall of the Pollock Mountain thrust, the ages for zircons are around 100 Ma. Both sample locations contained

igneous and metamorphic activity. Igneous activity intruded at 116 Ma with metamorphism occurring around 104 Ma for the footwall. Comparing garnet ages from McKay et al. (2017) to the zircon ages are similar. Garnet found in the Rapid River plate analyzed by McKay et al. (2017) recorded metamorphism that began around the late stage of Pollock Mountain metamorphism at 126 Ma (ID26) and continued to 113 Ma (ID07). P-T estimates from McKay et al. (2017) suggest that the Rapid River plate records Cretaceous isothermal loading of 3 kbar for 124- 113 Ma at 600-700°C. The Hazard Creek Complex intruded metamorphic rocks in the Rapid River plate between 118 and 113 Ma (U-Pb zircon; Manduca et al., 1993; Unruh et al., 2008).

Above Pollock Mountain Thrust Fault. In the hanging wall, the ages range from 171 Ma to 103 Ma. The Pollock Mountain plate contained both igneous and metamorphic activity for the zircons. Igneous activity intruded from 147 to about 120 Ma, with metamorphism occurring from 171- 103 Ma. Garnet ages from McKay et al. (2017) can be used to compare the zircon ages found in the hanging wall of the Pollock Mountain thrust fault. Ages from Sm-Nd garnet geochronology are likely derived from garnets with a significant age range, meaning that different ages may represent averages of different proportions of age-zoned garnet, being interpreted as distinct metamorphic events (McKay et al., 2017). It was interpreted by McKay et al., (2017) that garnet growth in the Pollock Mountain plate could have resulted from a long- lived tectonthermal event beginning between 141 and 137 Ma and continuing until 124 Ma, based on overlapping Sm-Nd garnet ages from the two sample localities (ID03, ID23); (McKay et al., 2017). Getty et al. (1993) used Sm-Nd garnet geochronology and $^{40}Ar/^{39}Ar$ thermochronology to date metamorphism and cooling in the Pollock Mountain

plate. They inferred that the pre- 144 Ma metamorphism corresponded to the collision of the Olds Ferry and Wallowa magmatic arcs, and the 128 Ma metamorphism dated docking of the Blue Mountains Province to the Laurentian margin (McKay et al., 2017). The pre-144 metamorphism is compatible with 159-154 Ma age constraints derived from Late Jurassic deformed sedimentary rocks within the Baker terrane (Schwartz et al., 2011; McKay et al., 2017). Peak metamorphic conditions in the Pollock Mountain plate are estimated as 8-11 kbar at 600-625 °C (Selverstone et al., 1992), and are inferred to have predated emplacement of the Hazard Creek Complex (Manduca et al., 1993; Fleck and Criss, 2004). A hornblende $^{40}Ar/^{39}Ar$ age of 119 Ma from the Pollock Mountain amphibolite (Getty et al. 1993) indicates that the thrust sheet cooled below the closure temperature of Ar in hornblende (~525 °C) during emplacement of the Hazard Creek Complex (McKay et al., 2017).

Zr-in-Rutile Thermochronology

Rutile most often crystallizes under conditions of medium and high-grade metamorphism, and much less frequently in low-pressure hydrothermal quartz veins and igneous rocks with crystallization temperatures ranging from approximately 430°C to over 1100°C (Kotowski, 2021). Zirconium concentrations in rutile from metamorphic rocks can vary from several ppm to 11,000ppm. Zr-in-rutile geothermometry is a relatively new method and is mainly used for determining crystallization temperatures of rutile in various metamorphic and igneous rocks (Kotowski, 2021). Zr (ppm) shows an inverse correlation with grain length. The rutile grains that were sampled along the Salmon River samples were elongated compared to the apatite (hexagonal) and

zircons (tetrahedral), which is consistent with the average Zr content of 4276 ppm for all of the rutile grains from the Salmon River suture zone. The crystallization temperature for the samples of rutile was about 926 °C, with peak metamorphic activity in the Salmon River suture zone occurring at 650 °C, this indicates that the rutile grains are igneous.

Spatial Cooling Trends in the Salmon River Suture Zone

Many “hot orogens” are characterized by high geothermal gradients that are greater than or equal to 30°C/km in the middle to lower crust (Collins, 2002; Morisset et al., 2009; Vauchez et al., 2019). A characteristic of “hot orogens” is to have been cooled very slowly, with rates estimated at less than 10 °C/m.y. (Morisset et al., 2009; Guergouz et al., 2018; Vauchez et al., 2019). This is characteristic of the Araçuaí-Ribeira belt in southeast Brazil, where there is slow cooling in the middle crust (3-5 °C/m.y.) with a peak temperature (~800 °C at 600 Ma) that is followed by faster cooling (>10 °C/m.y.) after the final amalgamation of Western Gondwana (Vauchez et al., 2019). Cooling rates can be used to constrain the evolution of the exhumed continental crust. These cooling rates in active orogens can be as high as 100-350 °C/m.y. (Zeck et al., 1992). Where cooling rates in ancient tectonically inactive orogens are much lower (Busch et al., 1996; Dunlap, 2000), it occurs when there is the exhumation of metamorphic and igneous rocks that formed in the middle to lower crust. An explanation for slow cooling estimates could reflect partial resetting in the upper crust during long near-isothermal periods of many years (Dunlap, 2000).

Tectonic plates consist of positively buoyant crustal and negatively buoyant lithospheric mantle layers (Boonma et al., 2019). This plays an important role in driving

plate tectonics and affects the pattern of upper mantle convection (Ueda, et al., 2012). Three processes can occur to decrease the cooling rates in a “hot orogeny”. First, high temperatures (>1000 °C) in the middle crust decrease its thermal conductivity. This can cause a heat reservoir to form in the middle to lower crust (Michaut et al., 2007; Whittington et al., 2009; Nabelek et al., 2010). Second, high temperatures in the middle to lower crust can trigger a widespread partial melting and the generation of large volumes of magmas that were emplaced in the middle crust (Michaut et al., 2007). Finally, the viscosity of hot and partially molten middle crust is too low to sustain high topography (Vauchez et al., 2019).

Apatite records the cooling history of the rocks in the Salmon River suture zone. The U- Pb age of apatite records the time at which the mineral began to cool, this value can be calculated and is the closure temperature. Cooling rates in the Salmon River area from apatite vary from less than 3 °C/m.y. (27, 67,69, 404A) to approximately 5 °C/m.y. (PMG). For the minerals found in the Salmon River suture zone, at higher closure temperatures (600-530 °C), there is slow cooling occurring (8.8 °C/m.y. in footwall) and faster cooling (18 °C/m.y. in hanging wall) that becomes slightly more rapid (12 °C/m.y. in the footwall and 35 °C/m.y. in hanging wall) as it falls below 530-460 °C, which is the closure temperature of apatite. Pollock Mountain records a slower cooling rate with 6.2 °C/m.y. (at 625-465 °C) and 11°C/m.y. for (530-465 °C). Cooling rates in the Salmon River suture zone are characteristic of cooling rates in eastern Tibet with slow cooling of 3 °C/m.y. (27 Ma to 12 Ma) increasing to ~12-25 °C/m.y. (12 Ma and 3 Ma), with rates increasing to 29-63 °C/m.y. (3 Ma to present) (Tan et al., 2017).

Below Pollock Mountain Thrust Fault. Rocks found in the footwall of the

Pollock Mountain thrust fault cooled at lower temperatures compared to the hanging wall. The closure temperatures range from 427 °C to 460 °C (± 3 °C). Ages below the thrust fault range from 92- 85 Ma for the country-rock of the Lightning Creek schist and Pollock Mountain Amphibolite, and 97- 82 Ma for the intrusions recording the cooling history. The rocks with apatite are relatively younger in the footwall of the Pollock Mountain thrust fault as opposed to the hanging wall.

Above Pollock Mountain Thrust Fault. Rocks found in the hanging wall of the Pollock Mountain thrust fault are hotter as the system began to cool at higher closure temperatures compared to the footwall. The range of closure temperatures went from 448 °C to 475 °C (± 3 °C). Rocks found here record older and hotter apatite cooling ages and compared to the footwall, with a range of 97-96 Ma for the country rock and the intrusions, 114 to 71 Ma. Most of the grains found in the hanging wall were larger than the footwall indicating the correlation between higher temperatures for cooling of the mineral.

Multi-mineral Temperature-time Paths from the Salmon River Suture Zone

Garnet, hornblende, biotite, and muscovite ages from Lund and Snee (1988) and McKay et al. (2017) were used to create a multi-mineral temperature-time path from the Salmon River suture zone. Four garnet ages were used from McKay et al., (2017) using Sm-Nd isochron ages and two U-Pb zircon ages. Lund and Snee (1988) calculated $^{40}Ar/^{39}Ar$ data for the mineral's hornblende, muscovite, and biotite. All minerals and their ages were collected along the Salmon River. $^{40}Ar/^{39}Ar$ dating of minerals hornblende, biotite, and muscovite is the best method for determining the thermal history and age of

complex metamorphic terranes (Lund and Snee, 1988). The closure temperature for hornblende is between 580-480°C (Harrison, 1981), 325- 270°C for muscovite (Snee et al., 1988), and 300-260°C for biotite (Harrison and McDougall, 1980; Snee, 2007).

Sample locations (ID48, ID07, ID26, ID03) from McKay et al. (2017); and are the Sm-Nd Garnet ages. ID48 is below the Pollock Mountain thrust, within the Rapid River plate. Sample ID48 contains anhedral to subhedral garnet with hornblende, biotite, chlorite, kyanite, staurolite, rutile, plagioclase, and quartz. The mean age of ID48 is 112.5 ± 1.5 Ma (McKay et al., 2017). ID07 is within the Rapid River plate and very close to the location of ID48. Sample ID07 is on the Lake Creek antiform and is composed of amphibolite that contains garnet, hornblende, zoisite, clinozoisite, plagioclase, quartz, ilmenite, and rutile. ID07 yielded a mean age of 113 ± 35 Ma (McKay et al. 2017). ID26 was sampled from the Squaw Creek Schist that is slight to the south of Riggins containing garnet, hornblende, biotite, titanite, ilmenite, plagioclase, and quartz. Its mean age is 124.3 ± 5.8 Ma (McKay et al., 2017). ID03 was sampled on Pollock Mountain from the Pollock Mountain plate. Sample ID03 is an amphibolite containing garnet, hornblende, biotite, plagioclase, quartz, ilmenite, and rutile. Garnet from sample ID03 yielded a mean age of 139 ± 2 Ma (McKay et al., 2017).

Samples RRC01 and ID04 are the two U-Pb zircon samples that were collected by McKay et al., (2017). These two samples were collected from the pluton to provide a comparison with garnet ages to evaluate the possible contributions to heating during metamorphism, the timing of deformation, and the age of metamorphism (McKay et al., 2017). RRC01 is an undeformed biotite-hornblende tonalite that had a mean age of 90.4 ± 0.8 Ma. ID04 is a moderately deformed orthogneiss with a mean age of 108.1 ± 1.8

Ma (McKay et al., 2017).

Seven sample locations were chosen by Lund and Snee (1988); for hornblende, muscovite, and biotite data. Samples from the Riggins Group included R18, R17, R16, R14, and R12. R11 is from deformed tonalite and R10 is from a pegmatite in tonalite. Sample R18 gave a plateau age for hornblende as 106.5 ± 1.4 m.y. R17 had Ar-loss with an age of 107-105 m.y. R16 had a Ar loss age of 100.5 -93 m.y. for hornblende, and for biotite had a plateau age of 88.2 ± 0.5m. y. R12 had an Ar loss age for hornblende of 93.5-88 m.y. R11 had a plateau age of 85.1 ± 0.4 m.y. R10 gave a plateau age for muscovite of 76.7 ± 0.5 m.y. (Lund and Snee, 1988). One $^{40}Ar/^{39}Ar$ hornblende collected from Getty et al., (1993) was used (sample 598) to get a hornblende age of 119 ± 2 Ma on Pollock Mountain. Hornblende $^{40}Ar/^{39}Ar$ age of 119 ± 2 Ma from the Pollock Mountain amphibolite indicates that the thrust sheet cooled below the closure temperature of Ar in hornblende at about 525 °C, which was at the emplacement of the Hazard Creek Complex (Getty et al., 1993; McKay et al. 2017).

All of the minerals from Mckay et al., (2017) and Lund and Snee (1988) were plotted (Fig. 10) with the apatite and rutile ages to create a cooling trend from all the minerals. Since zircon has a closure temperature of >900 °C (DiPietro, 2013), it was removed from the graph to show a more ideal age/cooling trend. Using thermochronology (U-Pb apatite, rutile) and metamorphic geochronology estimates (Sm-Nd garnet and $^{40}Ar/^{39}Ar$ hornblende, biotite, muscovite), temperature-time paths were constructed (T-t) for rocks both in the hanging wall and footwall of the Pollock Mountain thrust fault. Cooling age estimates based on closure temperature calculations and U-Pb ages of apatite are within error of $^{40}Ar/^{39}Ar$ ages of hornblende, garnet, biotite,

and muscovite.

Below Pollock Mountain Thrust Fault. Minerals found in the footwall have different cooling histories than the minerals in the hanging wall. Between garnet and rutile, there is a cooling rate of 2.7 °C/m.y. Rutile and hornblende cool at 8.8 °C/m.y. Hornblende to apatite cools at a rate of 12 °C/m.y. Lastly, apatite to biotite cools more rapidly at 90 °C/m.y. Overall, the cooling rate for the footwall from the minerals garnet to biotite is 14 °C/m.y. Rapid cooling (90 °C/m.y.) occurs at about 90 Ma which indicates that this is when the entire rock cooled together, meaning that from rutile down to biotite, must have all cooled relatively around the same time as they are all around the same age.

Above Pollock Mountain Thrust Fault. Minerals found in the hanging wall cool faster than those in the footwall. Two cooling histories are found in the hanging wall of the Pollock Mountain thrust fault, along the Salmon River and Pollock Mountain. The cooling history along the Salmon River record an overall cooling of 35 °C/m.y. from rutile to biotite. Between rutile and hornblende, the cooling rate is 18 °C/m.y. Hornblende to apatite cool at a rate of 35 °C/m.y. Lastly, apatite to biotite and muscovite cools rapidly at a rate of 90 °C/m.y. The cooling history within Pollock Mountain records a history between the minerals garnet and apatite with a rate of 6.2 °C/m.y. Between garnet and hornblende, the cooling rate is 4.75 °C/m.y. Lastly, the rate of cooling between hornblende to apatite is 11 °C/m.y. Cooling rates for Pollock Mountain indicate slower cooling compared to the Salmon River, indicating they have separate cooling histories within the Salmon River suture zone. Faster cooling rates in the hanging wall are characteristic of thrust faults as the rocks are being exhumed from a greater

distance compared to the footwall. The overall cooling rate in the hanging wall from rutile to biotite is 35 °C/m.y., this is higher than the overall cooling rate in the footwall (14 °C/m.y.). There are two different cooling rates between the Salmon River and Pollock Mountain indicating that the salmon river rocks are deeper with Pollock Mountain cooling occurring first.

While the hanging wall shows a faster cooling (35 °C/m.y.) rate than the footwall (14°C/m.y.), the overall cooling of the Salmon River suture zone is relatively slow cooling for both the footwall and the hanging wall. The age at which each mineral phase starts to cool, corresponds to the opposing fault block. A rate of 90 °C/m.y. for apatite to biotite was calculated for both the footwall and hanging wall. This means that there is very little to no change in cooling rates between both temperature-time models. There is, however, change within the mineral phases that are hotter than 550 °C in both the footwall and hanging wall, where the ages are older. Once the rock hits the age of 90 Ma they are now together and cooled. The rocks of the Salmon River suture zone were possibly buried for a long period of time and then simultaneously brought to the surface.

There are four possible events that are occurring during the cooling of the rocks in the Salmon River suture zone. These events are based on the T-t model that was created for the mineral phases found within the Salmon River suture zone. 1) Episodic cooling, the minerals are cooling rapidly then slow down into a stair step fashion that can be caused by possible faulting that could be occurring. This could explain why between some mineral phases there are fast cooling and then slow cooling between others. 2) Partial retention could explain that the minerals are holding onto their ratios and taking a long time to cool as they are holding onto their initial heat. 3) Broken

apatite grains, since the closure temperature of apatite is reliant on the grain size, there is an error that can be dependent on if the grain is broken or not. Each apatite grain is width dependent, so if the grain was broken it would only change the temperature by ± 2 °C (Fig. 11). Grains are more likely to break in length instead of width. 4) Closure temperature not working, the closure temperature found for apatite is compatible with previous closure temperature estimates found in the Salmon River suture zone. This data fits in with the previously dated garnet, hornblende, muscovite, and rutile to create a full cooling path history.

Delamination

Lithosphere delamination is believed to play a major role in mountain building (Li et al., 2016). The concept of lithosphere delamination was introduced by Bird (1978), who proposed that a dense lithospheric mantle could sink into the underlying asthenosphere from the crust (Bird, 1978; Kay and Kay, 1993; Li et al., 2016). This occurs when there is detachment and sinking of the lithospheric mantle. Delamination can happen with or without a certain portion of the lower crust from the tectonic plate (England and Molnar, 1990; Molnar et al., 1993; Li et al., 2016). With the sinking of the lithospheric mantle, the removal can induce a rapid uplift response that can result in a regional increase in surface elevation, causing rapid erosion to occur (Molnar et al., 1993; Garzione et al., 2008). Since the Salmon River suture zone is a collisional orogen, lithosphere delamination can occur in either the overriding plate or the subducting plate (England and Molnar, 1990; Molnar et al., 1993; Li et al., 2016). Lithospheric roots have been proposed to form beneath Cordilleran magmatic arcs and

result in phase changes that were associated with crustal thickening (Kay and Kay, 1993; Saleeby et al., 2003; Garzione et al., 2006; Ren and Shen, 2008; Li, et al., 2016).

With the delamination model, rocks within the Salmon River suture zone should be cooling rapidly (>100 °C/m.y.) (Dunlap, 2000) from the rapid buoyancy-driven uplift of the overlying rocks (Selverstone et al., 1992). Lithosphere delamination that occurs during continental collision generally results in a wide and flat mountain belt or plateau. In collisional orogens without major delamination develop steep mountain belts (Li, et al., 2016), this is characteristic of the Salmon River suture zone. The cooling rates of the apatite samples are < 5 °C/m.y. If the lithosphere delamination model were true, there would not be a significant change between cooling rates on each side of the Pollock Mountain thrust fault. However, cooling rates occur faster in the hanging wall of this fault with rates of 8.8 °C/m.y. in the footwall between rutile and hornblende and 18 °C/m.y. in the hanging wall between the same minerals. Slow cooling rates within the apatite samples (<3 °C/m.y.) are incompatible with fast exhumation rates indicating that the delamination model cannot be correct meaning that there is rapid cooling with delamination. With the delamination model, Selverstone et al. (1992) noted that garnet should be rapidly exhuming. Garnets found in the footwall are buried for about 20 Ma before they are cooled (2.7 °C/m.y.) and at about 40 Ma in the hanging wall, indicating slow cooling (6.2°C/m.y.). Here, the T-t paths show that the minerals are all brought to the surface together and possibly related to the Western Idaho shear zone that was initiated after 104 Ma that is constrained by weakly deformed granites that are interpreted as shear zone deformation (Braudy et al., 2017). Deformation was active in the Western Idaho shear zone until around 90 Ma (Giorgis et al., 2008; Braudy et al.,

2017).

Thrust Propagation

A thrust fault occurs when the older rocks that are below are pushed above younger rocks. It was interpreted by McKay et al. (2017) that isothermal loading within the Salmon River suture zone was controlled by thrust stacking that drove metamorphism in structural sheets that are underlying the Pollock Mountain plate that is similar to the northern and central Appalachians (Spear et al., 1990; Bosbyshell et al., 2016; McKay et al., 2017). Within the Salmon River suture zone, crustal thickening that is from thrust loading was diachronous, with westward fault propagation occurring through the duration of Jurassic-Cretaceous tectonism along the western Laurentia margin (McKay et al. 2017). With this model, magmatic heating is not required to drive metamorphism. Pressure, temperature, and time histories from adjacent lithotectonic packages in the Salmon River suture zone show evidence for westward younging of structural burial and metamorphism (McKay et al., 2017). Peak burial in the eastern part of the Salmon River suture zone between 140-125 Ma is followed by structural burial of the rocks to the west at 125-115 Ma (McKay et al., 2017). Similar exhumation sequences can be seen in other forward-breaking fold-thrust belts (McClelland and Oldow, 2004), suggesting a westward- propagating thrust fault system in the middle crust during Salmon River suture deformation and metamorphism. The hanging wall is exhumed and subsequently cooled by transport along the underlying thrust fault, and the footwall is buried beneath the higher temperature hanging wall (McKay et al., 2017).

The series of west-vergent thrust shear zones and thrust faults that are to the

west in the Salmon River suture zone is representative of the thrust propagation hypothesis that drove the high magnitude exhumation by the forward propagation of a west-vergent thrust belt. (Lund and Snee, 1988; Blake et al., 2009; Gray et al., 2012; Gray, 2013). The metamorphic and cooling ages of the rocks in the Salmon River suture zone are increasing from west to east and this is driven by the Pollock Mountain thrust fault indicating thrust propagation. The rocks are younger in the footwall of this indicating thrusting as a major component of exhumation rates and magnitudes of the Salmon River suture zone. With this thrusting model, it records the rocks in the hanging wall to be hotter (~448 °C for footwall and ~460 °C for hanging wall) and slightly older (90-80 Ma for footwall and 110-85 Ma for hanging wall) as they were once buried deep within the crust and exhumed at (35 °C/m.y.) than the footwall (14 °C/m.y.) of the thrust fault. Since the minerals found within the rocks in the Salmon River suture zone all cooled around 90 Ma at the same time in the footwall and hanging wall, the Pollock Mountain thrust fault must have occurred first before the exhumation of the rocks meaning the fault is older than 90 Ma, after 90 Ma rocks are together at the surface.

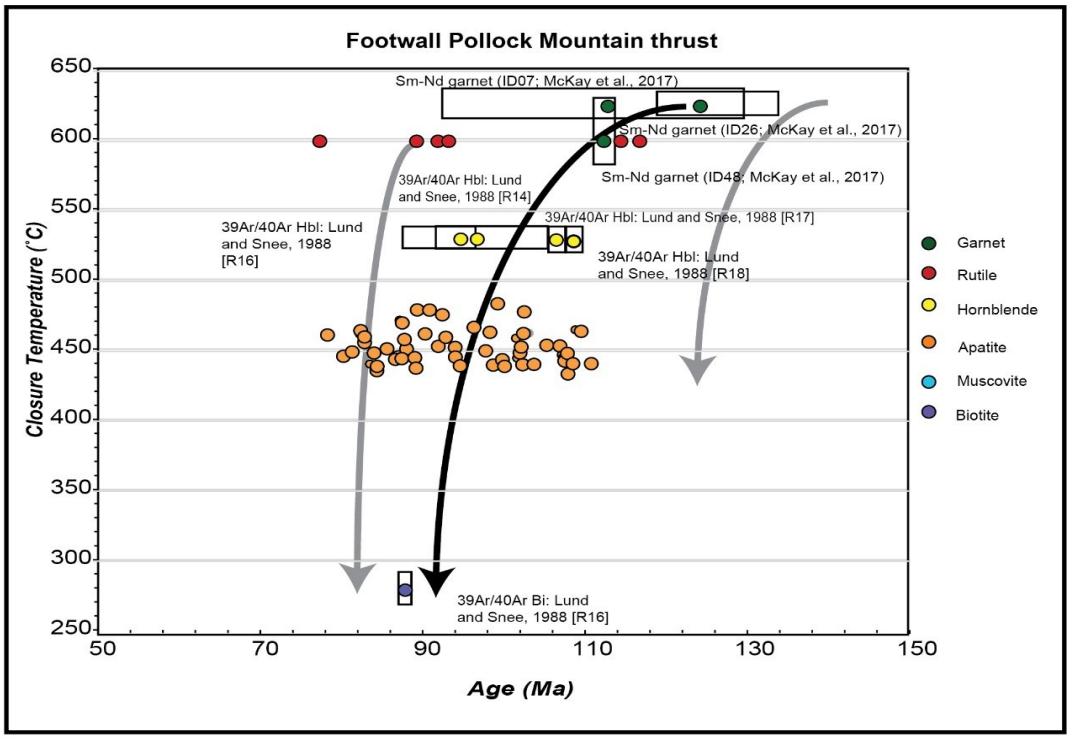

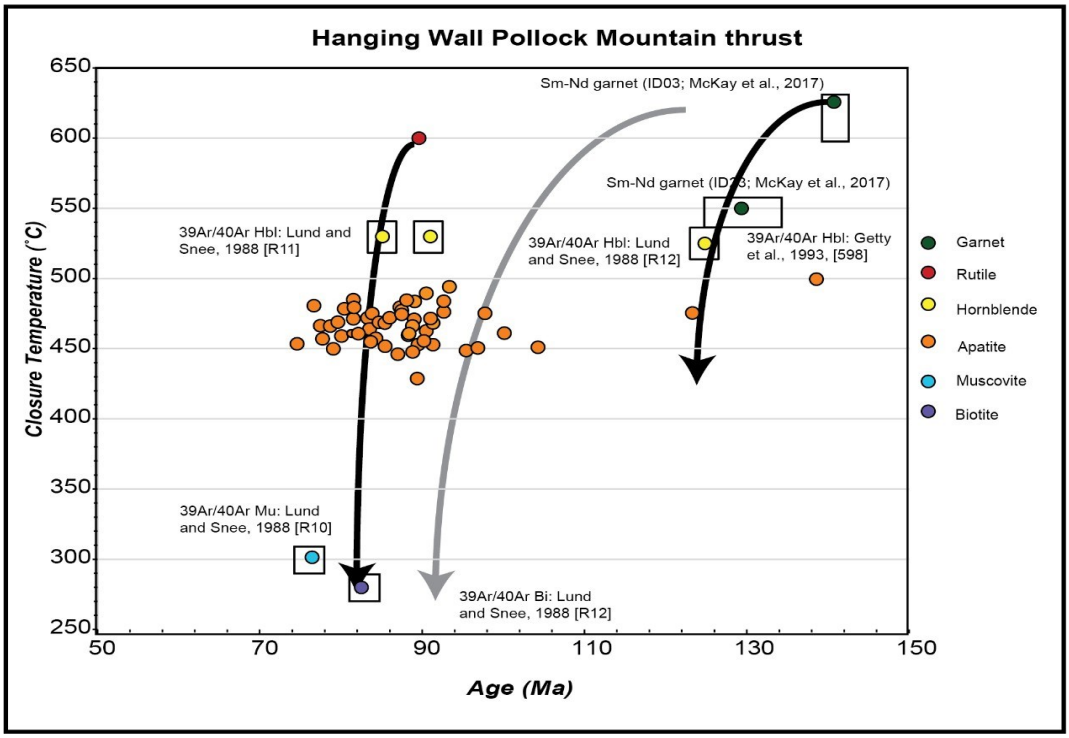

Figure 10. Temperature-time paths using the minerals: apatite, rutile, garnet, muscovite, biotite, and hornblende. The black arrows are showing the cooling path on each side of the Pollock Mountain Thrust fault. The gray arrow is showing the cooling path in the opposing side.

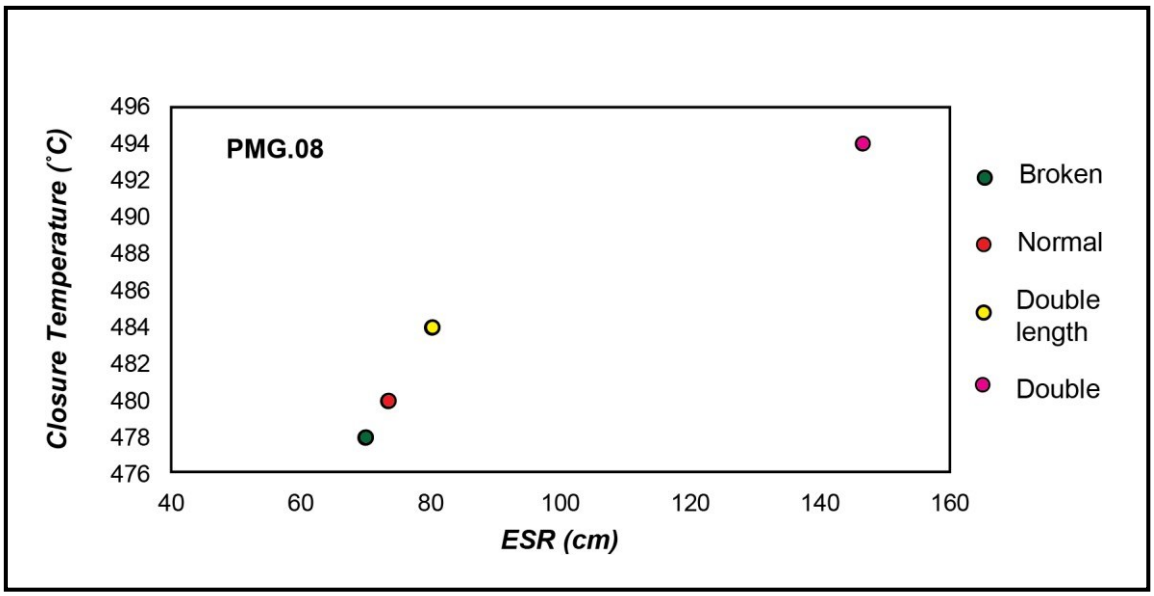

Figure 11. Graph from one grain from sample PMG indicating how different lengths of the mineral can affect the closure temperature. The broken grain just had the length cut in half, double length was where the length was doubled, the double grain was both length and width doubled.

CONCLUSION

The Salmon River suture zone is representative of processes that operates in suture zones globally. It experienced Jurassic-Cretaceous deformation with the collision of a volcanic arc terrane with the western edge of North America. Here, rocks record burial and exhumation that are used to investigate the processes that drive high-magnitude exhumation within the Salmon River suture zone. U-Pb geochronological data was collected from the rocks along the Salmon River and Pollock Mountain to constrain the processes that helped drive exhumation. The minerals apatite, zircon, and rutile were used to constrain the age and temperature data to create a temperature-time cooling path. For the rocks found within the Salmon River suture zone, apatite yielded a weighted mean age range of 95-80 Ma, zircon ages, 140-100 Ma, and rutile 166-89 Ma. The overall apatite ages of the rocks in the Salmon River are within error in the range of 80 to 90 Ma, so there, however, is not a clear direction if the ages are decreasing in a certain direction. The closure temperature of apatite was constrained from the previous temperature window of 350-500 °C to 450-475°C, which falls in a temperature range that had missing information from previous studies completed by Lund and Snee (1988) and McKay et al., (2017). Rocks found along the Salmon River and Pollock Mountain have different cooling histories, regional cooling within the Salmon River suture zone may be occurring as rocks are buried deep for a long period of time and then brought to the surface together. The footwall and hanging wall of the Pollock Mountain thrust record different cooling histories. There is moderate cooling from peak metamorphism to ~< 500 °C, thrust sheets may then slow down when cooling through ~450 °C. At

about 425 °C there is an increased cooling rate through 90 Ma. Cooling rates are significantly less than predicted for the lithosphere delamination model. The T-t model for the Salmon River suture zone is compatible with the thrust-driven exhumation hypothesis, with slow cooling rates (<5 °C/m.y. for apatite) across the region, but faster exhumation overall with 14 °C/m.y. in the footwall and hanging wall rates of 35 °C/m.y. for Salmon River, and 6.2 °C/m.y. for Pollock Mountain.

REFERENCES CITED

Alberti, E.A., 1988, A structural, petrologic, and isotopic study of the Rapid river area and selected mafic complexes in the northwestern US: Implications for the evolution of an abrupt island arc-continent boundary [Ph.D thesis]: Cambridge, Massachusetts, Harvard University, p. 160.

Armstrong, R.L., Taubeneck, W.H., and Hales, P.O., 1977, Rb-Sr and K-Ar geochronology of Mesozoic granitic rocks and their Sr isotopic composition, Oregon, Washington, and Idaho: Geological Society of America Bulletin, v. 88, p. 397–411.

Avé Lallemant, H.G., 1995, Pre-Cretaceous tectonic evolution of the Blue Mountains province, northeastern Oregon, in Vallier, T.L., and Brooks, H.C., eds., Geology of the Blue Mountains region of Oregon, Idaho, and Washington; petrology and tectonic evolution of pre-Tertiary rocks of the Blue Mountains region: U.S. Geological Survey Professional Paper 1438, p. 359–414.

Blake, D.E., Gray, K.D., Giorgis, S., and Tikoff, B., 2009, A tectonic transect through the Salmon River suture zone along the Salmon River canyon in the Riggins region of west- central Idaho: The Geological Society of America, p. 345- 372.

Blake, D.E., Bruce, M.L, and Reed, D.N., 2016, Geologic Map of the Riggins Hot Springs Quadrangle and Adjacent Areas, Idaho County, Idaho: Idaho Geological Survey, scale 1:24,000.

Bird, P., 1978, Initiation of intracontinental subduction in the Himalaya: J. Geophys. Res., v. 83, p. 4975-4987.

Boonma, K., Kumar, A., Garcia-Castellanos, D., Jimenez-Munt, I., and Fernandez, M., 2019, Lithospheric mantle buoyancy: the role of tectonic convergence and mantle composition: Scientific Reports, v. 9.

Bosbyshell, H., Srogi, L., and Blackmer, G.C., 2016, Monazite age constraints on the tectonothermal evolution of the central Appalachian Piedmont: American Mineralogist, v. 101, p. 1820-1838.

Braudy, N., Gaschnig, R.M., Wilford, D., Vervoort, J.D., Nelson, C.L., Davidson, C., Kahn, M.J., and Tikoff, B., 2017, Timing and deformation conditions of the western Idaho shear zone, West Mountain, west-central Idaho: The Geological Society of America, v. 9, p.157-183.

Brooks, H.C., 1979, Geologic map of the Huntington and part of the Olds Ferry quadrangle, Baker and Malheur counties, Oregon: Oregon Department of

Geology and Mineral Industries Geologic Map Series, GMS-13, scale 1:62,500.

Brooks, H.C., and Vallier, T.L., 1978, Mesozoic rocks and tectonic evolution of eastern Oregon and western Idaho: Pacific Coast Paleogeography Symposium, p. 133-145.

Burke, K., Ashwal, L.D., and Webb, S.J., 2003. New way to map old structures using deformed alkaline rocks and carbonatites: Geology, v. 31, p. 391-394.

Busch, J.P., van der Pluijm, B.A., Hall, C.M., and Essene, E.J., 1996, Listric normal faulting during postorogenic extension revealed by $^{40}Ar/^{39}Ar$ thermochronology near the Roberson Lake shear zone, Grenville orogen, Canada: Tectonics, v. 15, p. 387-402.

Busch, J.P., Mezger, K., and van der Pluijm, B.A., 1997, Suturing and extensional reactivation in the Grenville orogen, Canada: Geology, v. 25, no.6, p. 507-510.

Carpenter, P.S. and Walker, N.W., 1992, Origin and tectonic significance of the Aldrich Mountains serpentinite matrix mélange, northeast Oregon: Tectonics, v. 11, p. 690-708.

Cawood, P.A., Kroner, A., Collins, W.J., Kusky, T.M., Mooney, W.D., and Windley, B.F., 2009, Accretionary orogens through Earth history: The Geological Society, London, Special Publications, v. 318, p. 1-36.

Collins, W.J., 2002, Hot Orogens, tectonic switching, and creation of continental crust: Geology. 30, p. 535-538.

Coney, P.L., Jones, D.L., and Monger, J.W.H., 1980, Cordilleran suspect terranes, Nature, v.288, p. 329-333.

Coleman, R.G., Manning, C.E., Mortimer, N., Donato, M.M., and Hill, L.B., 1988, Tectonic and regional metamorphic framework of the Klamath Mountains and adjacent Coast Ranges, California, and Oregon: in Ernst, W.G., ed., Metamorphism and Crustal Evolution of Western United States, v. 7, p. 1059-1097.

Cherniak, D.J., 1991, Lead diffusion in apatite and zircon using ion implantation and Rutherford backscattering techniques: Geochemica et Cosmochimica Acta, v. 55, p. 1663-1673.

Cherniak, D.J., 2000, Pb diffusion in rutile: Contributions to Mineralogy and Petrology, v. 139, p. 198-207.

Coward, R.I., 1983, Structure, Stratigraphy, and Petrology of the Elkhorn Ridge Argillite, Sumpter Area, Northeastern Oregon [Ph.D. dissertation]: Houston, Texas, Rice

University, p. 144.

Criss, R.E., and Fleck, R.J., 1987, Petrogenesis, geochronology and hydrothermal systems of the northern Idaho batholith and adjacent areas based on $^{18}O/^{16}O$, D/H, $^{87}Sr/^{86}Sr$, K-Ar and $^{40}Ar/^{39}Ar$ studies: U.S Geological Survey Professional Paper, 1436, p. 95-137.

Dewey, J.F., 1977, Suture Zone Complexities: A Review: Tectonphysics, v. 40, p. 53-67.

Dickinson, W.R., 2004, Evolution of the North American Cordillera: Annu. Rev. Earth Planet Sci. v.32, p. 13-45.

Dickinson, W.R., and Vigrass, L.W., 1965, Pre-Cenozoic history of Supplee-Izee District, Oregon: implications for geosynclinal theory: Geological Society of America Bulletin, v. 75, p. 1037-1044.

Dickinson, W.R., and Thayer, T.P., 1978, Paleographic and paleotectonic implications of Mesozoic stratigraphy and structure in the John Day inlier of central Oregon, in Howell, D.G., and McDougall, K.A., eds., Mesozoic Paleogeography of Western United States: Los Angeles, California, Pacific Section, society of Economic Paleontologists and Mineralogists, p. 147-161.

Dickinson, W.R., 1979, Mesozoic fore-arc basin in central Oregon: Geology, v. 7, p. 166-170.

DiPietro, J.A., 2013, Chapter 20- Keys to the Interpretation of Geological History: Landscape Evolution in the United States, p. 327-344.

Dodson, M.H., 1973, Closure Temperature in Cooling Geochronological and Petrological Systems: Contributions Mineral and Petrology, v. 40, p. 259-274.

Dorsey, R.J., and LaMaskin, T.A., 2006, Basinal Response to Triassic-Jurassic Collisional Tectonics in the Blue Mountains Province, Northeastern Oregon: American Journal of Science.

Dunlap, W.J., 2000, Nature's diffusion experiment: The cooling-rate cooling-age correlation: Geology, v. 28, no. 2, p. 139-142.

Engebretson, D.C., Cox, A., and Gordon, R.G., 1985, Relative plate motions between oceanic and continental plates in the Pacific Basin: Geological Society of America Special Paper 206.

England, P., and Molnar, P., 1990, Surface uplift, uplift of rocks, and exhumation of rocks: Geology, v. 18, p. 1173-1177.

Evenchick, C.A., McMechan, M.E., McNicoll, V.J., and Carr, S.D., 2007, A synthesis of

the Jurassic-Cretaceous tectonic evolution of the central and southeastern Canadian Cordillera: Exploring links across the orogen, The Geological Society of America Special Paper, p. 117-145.

Faure, G., and Mensing, T.M., 2005, Isotopes Principles and Applications: John Wiley & Sons, Inc., Hoboken, New Jersey.

Ferns. M.L., and Brooks, H.C., 1995, the Bourne and Greenhorn subterranes of the Baker terrane, north-eastern Oregon: implications for the evolution of the island-arc system, in Vallier, T.L., and Brooks, H.C., eds., Idaho and Washington: Petrology and Tectonic Evolution of Pre-Tertiary Rocks of the Blue Mountains Region: U.S. Geologic Survey Professional Paper 1438, p. 331-358.

Fleck, R.J., and Criss, R.E., 1985, Strontium and oxygen isotopic variations in Mesozoic and Tertiary plutons of central Idaho: Contributions to Mineralogy and Petrology, v. 90, p. 291-308.

Fleck, R.J., and Criss, R.E., 2004, Location, age, and tectonic significance of the western Idaho suture zone (WISZ): U.S. Geological Survey Open-File Report 2004-1039.

Garzione, C.N., Molnar, P., Libarkin, J.C., and MacFadden, 2006, Rapid late Miocene rise of the Bolivian Altiplano: Evidence for removal of mantle lithosphere: Earth and Planetary Science Letters, v. 241, p. 543-556.

Garzione, C.N., Hoke, G.D., Libarkin, J.C., Withers, S., MacFadden, B., Eiler, J., Ghosh, P., and Mulch, A., 2008, Rise of the Andes: Science, v. 320.

Gaschnig, R.M., Vervoort, J.D., Lewis, R.S., and McClelland, 2010, Migrating magmatism in the northern US Cordillera: in situ U-Pb geochronology of the Idaho batholith: Contributions to Mineralogy and Petrology, v. 159, pg. 863-883.

Gatewood, M.P., and Stowell, H.H., 2012, Linking zircon U-Pb and garnet Sm-Nd ages to date loading and metamorphism in the lower curst of a Cretaceous magmatic arc, Swakana Geniss, WA, USA: Lithosphere.

Getty, S.R., Selverstone, J., Wernicke, B.P., Jacobsen, S.B., Aliberti, E., and Lux, D.R., 1993, Sm-Nd dating of multiple garnet growth events in an arc-continent collision zone, north-western U.S. Cordillera: Contributions to Mineralogy and Petrology, v. 115, p. 45-57, doi: 10.1007/BF00712977.

Giorgis, S., McCllelland, W., Fayon, A., Singer, B., and Tickoff, B., 2008, Timing of deformation and exhumation in the western Idaho shear zone, McCall, Idaho: Geological Society of America Bulletin, v. 120, p. 1119-1133, doi:10.1130/B26291.1.

Gray, K.D., and Oldow, J.S., 2005, Contrasting structural histories of the Salmon River Belt and Wallowa Terrane; implications for terrane accretion in northeastern Oregon and west- central Idaho, Geological Society of America Bulletin, v. 117, p. 687-706, doi:10.1130/B25411.1.

Gray, K.D., Watkinson, A.J., Gaschnig, R.M., and Isakson, V.H., 2012, Age and structure of the Crevice pluton: overlapping orogens in west-central Idaho?: Can. J. Earth Sci., v. 49.

Gray, K.D., 2013, Structure of the arc-continent transition in the Riggins region of west-central Idaho [Ph.D. Thesis]: Washington State University, Pullman.

Guergouz, C., Martin, L., Vanderhaeghe, O., Thebaud, N., and Fiorentini, M., 2018, Zircon and monazite petrochronologic record of prolonged amphibolite to granulite facies metamorphism in the Ivrea-Verbano and Strona-Ceneri Zones, NW Italy: Lithos, v. 308- 309, p. 1-18.

Hacker, B.R., Donato, M.M., Barnes, C.G., McWilliams, M.O., and Ernst, W.G., 1995, Timescales of orogeny; Jurassic construction of the Klamath Mountains: Tectonics, v. 14, p. 677-703.

Hamilton, W., 1963, Metamorphism in the Riggins Region Western Idaho: Geological Survey Professional Paper 436.

Hamilton, W., 1969, Reconnaissance geologic map of the Riggins quadrangle, west-central Idaho: U.S. Geological Survey Miscellaneous Geologic Investigations Map I–579, scale 1:125,000.

Harrison, T.M., and McDougall, I., 1980, Investigations of an intrusive contact, northwest Nelson, New Zealand- I. Thermal, chronological, and isotopic constraints: Geochim. Cosmochim. Acta, v. 44, p. 1985-2003.

Harrison, T.M., 1981, Diffusion of ^{40}Ar in hornblende: Contributions in Mineralogy Petrology, v. 78, p. 324-331.

Kay, R.W., and Kay, S.M., 1993, Delamination and delamination magmatism: Tectonophysics, v. 219, p. 177-189.

Kays, M.A., Stimac, J.P., and Goebel, P.M., 2006, Permian-Jurassic growth and amalgamation of the Wallowa composite terrane, northeastern Oregon: Geological Studies in the Klamath Mountains Province, California and Oregon-A Volume in Honor of William P. Irwin: Geological Society of America Special Paper 410, p. 465-494.

Kirkland, C.L., Yakymchuk, C., Szilas, K., Evans, N., Hollis, J., McDonald, B. and Gardiner, N.H., 2018, Apatite: a U-Pb thermochronometer or geochronometer?

Lithos, p. 143-157.

Kotowski, J., 2021, Rutile Mineral Chemistry and Zr-in-Rutile Thermometry in Provenance Study of Albian (Uppermost Lower Cretaceous Terrigenous Quartz Sands and Sandstones in Southern Extra-Carpahtian Poland: minerals, no. 11, v. 55.

Kuntz, M.A., and Snee, L.W., 2007, Geological studies of the Salmon River suture zone and adjoining areas, west-central Idaho and eastern Oregon: U.S. Geological Survey Professional Paper 1738.

LaMaskin, T.A., Dorsey, R.J., Vervoort, J.D. Schmitz, M.D., Tumpane, K.P., and Moore, N.O., 2015, Westward Growth of Laurentia by Pre-Late Jurassic Terrane Accretion, Eastern Oregon and Western Idaho, United States: The Journal of Geology, v. 123, no. 3, p. 233- 267.

Li, Z., Liu, M., and Gerya, T., 2016, Lithosphere delamination in continental collisional orogens: A systematic numerical study: Journal of Geophysical Research: Solid Earth, v. 121, p.5186-5211.

Lund, K., 1984, Tectonic history of a continent-island arc boundary, west-central Idaho [Ph.D. thesis]: University Park, Pennsylvania State University, p 210.

Lund, 2004, Geologic Map of the Western Part of the Payette National Forest, West-Central Idaho: U.S Geological Survey, scale 1:100,000.

Lund, K., and Snee, L.W., 1988, Metamorphism, Structural Development, and Age of the Continent Island Arc Juncture in West-central Idaho: U.S Geological Survey.

Lund, K., McCollough, W.F., and Price, E.H., 1993, Geologic map of the Slate Creek-John Day Creek area, Idaho County, Idaho: U.S. Geologic Survey Miscellaneous Investigation Map 1- 2299, scale 1:50,000.

Manduca, C.A., 1988, Geology and Geochemistry of the Oceanic Arc-Continent Boundary in the Western Idaho Batholith near McCall: Dissertation (Ph.D.) California Institute of Technology.

Manduca, C.A., Kuntz, M.A., and Silver, L.T., 1993, Emplacement and deformation history of the western margin of the Idaho batholith near McCall, Idaho: Influence of a major terrane boundary: Geological Society of America Bulletin, v. 105, p. 749-765, doi:10.1130/0016- 7606.

McClelland, W.C., Tikoff, B., and Manduca, C.A., 2000, Two-phase evolution of accretionary margins: Examples from the North American Cordillera, in Housen, B., et al., eds., Advances in paleomagnetism and tectonics of active margins, in honor of the retirement of Myrl E. Beck, Jr.: Teconophysics, v. 326, p. 37-55,

doi:10.1016/S0040.

McClelland, W.C., and Oldow, J.S., 2004, Displacement transfer between thick-and thin- skinned decollement systems in the central North American Cordillera, vertical coupling and decoupling in the lithosphere: Geological Society, London Special Publication 227, p. 177- 195.

McKay, M.P., Bollen, E.M., Gray, K.M., Stowell, H.H., and Schwartz, J.J., 2017, Prolonged metamorphism during long-lived terrane accretion: Sm-Nd garnet and U-Pb zircon geochronology and pressure-temperature paths from the Salmon River suture zone, west- central Idaho, USA: Lithosphere, doi:10.1130/L642.1.

McKay, M. P., Jackson, W.T., and Hessler, A.M., 2018, Tectonic stress regime recorded by zircon Th/U: Gondwana Research.

Michaut, C., Jaupart, C., and Bell, D., 2007, Transient geotherms in Archean continental lithosphere: New constraints on thickness and heat production of the subcontinental lithospheric mantle: Journal of Geophysical Research, v. 112.

Molnar, P., England, P., and Martinod, J., 1993, Mantle dynamics, uplift of the Tibetan plateau, and the Indian Monsoon: Rev. Geophys., v. 31, p. 357-396.

Moores, E.M., 1981, Ancient Suture Zones within Continents: Science, v. 213, no. 4503, p. 41- 46.

Morisset, C.E., Scoates, J.S., Weis, D., Friedman, R.M., 2009, U-Pb and $^{40}Ar/^{39}Ar$ geochronology of the Saint-Urbain and Lac Allard (Havre-Saint-Pierre) anorthosite and their associated Fe-Ti oxide ores, Quebec: evidence for emplacement and slow cooling during the collisional Ottawan orogeny in the Grenville Province: Precambrian Research, v. 174, p. 95-116.

Nabelek, P.I., Whittington, A.G., and Hofmeister, A.M., 2010, Strain heating as a mechanism for partial melting and ultrahigh temperature metamorphism in convergent orogens: Implications of temperature-dependent thermal diffusivity and rheology: Journal of Geophysical Research, v. 115.

Nandi, S.K, Brown, M.B, DeYoung, S., McKay, M.P., Muttel, S., and Spurgeon, 2018, Geologic Map and Cross Sections of the Pollock Mountain 7.5- Minute Quadrangle, Idaho and Adams Counties, Idaho: USGS EDMAP unpublished report.

Nestell, M.K., 1983, Permian foraminiferal faunas of central and eastern Oregon: Geological Society of America Abstracts with Programs, v. 15, no.5, p. 371.

Oldow, J.S., Bally, A.W., Ave Lallemant, H.G., and Leeman, W.P., 1989, Phanerozic evolution of the North American Cordillera: United States and Canada, in Bally,

A.W., and Palmer, A.R., eds., The Geology of North America- An Overview: Boulder, Colorado, Geological Society of America, Geology of North America, v. A, p. 139-232, doi:10.1130/DNAG- GNA-A.139.

Onasch, C.M., 1977, Structural evolution of the western margin of the Idaho Batholith in the Riggins, Idaho area [Ph.D. thesis]: University Park, Pennsylvania State University, p.196.

Ren, Y., and Shen, Y., 2008, Finite frequency tomography in southeastern Tibet: Evidence for the causal relationship between mantle lithosphere delamination and the north-south trending rifts: J. Geophys. Res., v. 113.

Rubatto, D., 2002, Zircon trace element geochemistry: Partitioning with garnet and the link between U-Pb ages and metamorphism: Chemical Geology, v. 184, p. 123-138, doi:10.1016S0009-2541(01)00355-2.

Saleeby, J. Ducea, M., and Clemens0Knott, D., 2003, Production and loss of high-density batholitic root, southern Sierra Nevada, California: Tectonics, v. 22, no. 6.

Schwartz, J.J., Snoke, A.W., Frost, C.D., Barnes, C.G., Gromet, L.P., and Johnson, K., 2010, Analysis of the Wallowa-Baker terrane boundary: Implications for the tectonic accretion

Schwartz, J.J., Snoke, A.W., Cordley, F., Johnson, K., Frost, C.D., Barnes, C.G., LaMaskin, T.A., and Wooden, J.L., 2011, Late Jurassic magmatism, metamorphism, and deformation in the Blue Mountains Province, northeastern Oregon: Geological Society of America Bulletin, v. 123, p. 2083–2111, doi:10.1130/B30327.1.

Selverstone, J., Wernicke, B.P., and Alberti, E.A., 1992, Intracontinental subduction and hinged unroofing along the Salmon River suture zone, west central Idaho: Tectonics, v. 11, no.1, p. 124-144.

Silberling, N.J., Jones, D.L., Blake, M.C., Jr., and Howell, D.G., 1987, Lithotectonic Terranes of the Western Conterminous United States: U.S Geological Survey Map MF-1874-C, scale 1:2,500,000, 1 sheet with 20 p. pamphlet.

Snee, L., Sutter, J.F., and Kelly, W.C., in press,1988, Thermochronology of economic mineral deposits- Dating the stages of mineralization at Panasquierea, Portugal by high precision $^{40}Ar/^{39}Ar$ age-spectrum techniques on muscovite: Economic Geology.

Snee, L., Lund, K., Sutter, J.F., Balcer, D.E., and Evans, K.V., 1995, An 40Ar/39Ar chronicle of the tectonic development of the Salmon River suture zone, western Idaho, in Vallier, T.L., and Brooks, H.C., eds., Geology of the Blue Mountains region of Oregon, Idaho, and Washington; petrology and tectonic evolution of

pre-Tertiary rocks of the Blue Mountains region: U.S Geological Survey Professional Paper 1438, p. 359-414.

Snee, L.W., 2007, Geological studies of the Salmon River suture zone and adjoining areas, west-central Idaho and eastern Oregon: U.S Geological Survey.

Spear, F.S., Hickmott, D.D., and Selverstone, J., 1990, Metamorphic consequences of thrust emplacement, Fall Mountain, New Hampshire: Geological Society of America Bulletin, v. 102, p. 1344-1360.

Stanciu, A.C., Russo, R.M., Mocanu, V.I., Bremner, P.M., Hongsresawat, S., Torpey, M.E., BanDecar, J.C., Foster, D.A., and Hole, J.A., 2016, Crustal structure beneath the Blue Mountains terranes and cratonic North America, eastern Oregon, and Idaho, from teleseismic receiver functions: Journal of geophysical Research: Solid Earth, v. 121, p. 5049-5067.

Strong, T.R., and Driscoll, R.L., 2016, A process for reducing rocks and concentrating heavy minerals: U.S. Geological Survey Open-file Report 2016-1022, p. 1-16.

Sutter, J.F., Snee, L.W., and Lund, K., 1984, Metamorphic, plutonic, and uplift history of a continental-island arc suture zone, west-central Idaho: Geologic Society of America Abstracts with Programs, v. 16, p. 670.

Tan, X., Lee, Y., Xu, X., and Cook, K.L., 2017, Cenezoic exhumation of the Danba antiform, eastern Tibet: Evidence from low-temperature thermochronology: Lithosphere, v. 9, no. 4, p. 534-544.

Tikoff, B., Kelso, P., Manduca, C., Markley, M.J., Gillaspy, J., 2001, Lithospheric and crustal reactivation of an ancient plate boundary: the assembly and disassembly of the Salmon River suture zone, Idaho, USA: The Nature and Tectonic Significance of Fault Zone Weakening, Geological Society, London, Special Publications, v. 186, p. 213-231.

Tumpane, K., Crowley, J., Schmitz, M., and Northrup, C.J., 2008, New geochronological constraints on the deposition of the Huntington Formation, Olds Ferry terrane and implications for the evolution of the Blue Mountains Province: Geological Society of America Abstracts with Programs, v. 40, no. 1, p.47.

Tumpane, K.P., and Schmitz, M.D., 2009, New geochronological constraints on the timing of deposition in the Coon Hollow and Weatherby Formations, and correlations between the Wallowa and Olds Ferry terranes, Blue Mountains Province, northern U.S Cordillera: Geological Society of America Abstracts with Programs, v. 41, no. 7, p. 182.

Ueda, K., Gerya, T.V., Burg, J.P., 2012, Delamination in collisional orogens: Thermomechanical modeling: Journal of Geophysical Research, v. 117.

Unruh, D.M., Lund, L., Kuntz, M.A., and Snee, S.W., 2008, Uranium-lead zircon ages and Sr, Nd, and Pb isotope geochemistry of selected plutonic rocks from western Idaho: U.S. Geological Survey Open-file Report 2008-1142, p. 24.

Usuki, T., Iizuka, Y., Hirajima, T., Svojtka, M., Lee, H., and Jahn, B., 2017, Significance of Zr- in Rutile Thermometry for Deducing the Decompression P-TPath of a Garnet- Clinopyroxene Granulite in the Moldanbian Zone of the Bohemian Massif: Journal of Petrology, v. 58, no. 6, p. 1173-1198.

Vallier, T.L., 1977, The Permian and Triassic Seven Devils Group, western Idaho and northeastern Oregon: U.S., Geological Survey Bulletin 1437, p. 1-58.

Vallier, T.L., 1995, Petrology of pre-Tertiary igneous rocks in the Blue Mountains region of Oregon, Idaho, and Washington: Implications for the geologic evolution of a complex island arc, in Vallier, T.L., and Brooks, H.C., eds., Geology of the Blue Mountains region of Oregon, Idaho, and Washington: U.S. Geological Survey Professional Paper 1438, p. 125-209.

Valier, T.L., and Batiza, R., 1978, Petrogenesis of spilite and keratophyre from a Permian and Triassic volcanic-arc terrane, eastern Oregon and western Idaho: Canadian Journal of Earth Sciences, v. 15, p. 1356-1369.

Vauchez, A., Hollanda, B.M., Monie, P., Mondou, M., Egydio-Silva, M., 2019, Slow cooling and crystallization of the roots of the Neoproterozoic Aracuai hot orogen (SE Brazil): implications for rheology, strain distribution, and deformation analysis: Tectonophysics, v. 766, p. 500-518.

Vermeesch, P., 2018, IsoplotR: a free and open toolbox for geochronology: Geoscience Frontiers, v. 9, p. 1479-1493.

Walker, N.W., 1986, U/Pb Geochronologic and Petrologic Studies in the Blue Mountains Terrane, Northeastern Orogen and Westernmost-Central Idaho: Implications for Pre- Tertiary Tectonic Evolution [Ph.D. dissertation]: Santa Barbara, University of California, p. 224.

Walker, N.W., 1995, Tectonic implications of U-Pb zircon ages of the Canyon Mountain complex, Sparta complex, and related metaplutonic rocks of the Baker terrane, northeastern Oregon, in Vallier, T.L., and Brooks, H.C., eds, Geology of the Blue Mountains Region of Oregon, Idaho, and Washington: Petrology and Tectonic Evolution of Pre-Tertiary Rocks of the Blue Mountains Region: U.S. Geological Survey Professional Paper 1438, p. 247-269.

Watson, E.B., Wark, D.A., Thomas, J.B., 2006, Crystallization thermometers for zircon and rutile: Contributions to Mineralogy and Petrology, v. 151, pg. 413-433.

Whittington, A.G., Hofmeister, A.M., and Nabelek, P.I., 2009, Temperature-dependent thermal diffusivity of the Earth's crust and implications for magmatism: Nature, v. 458, no. 7236, p. 319-321.

Wright, J.E., and Fahan, M.R., 1988, An expanded view of Jurassic orogenesis in the western United States Cordillera; Middle Jurassic (pre-Nevadan) regional metamorphism and thrust faulting within an active arc environment, Klamath Mountains, California: Geological Society of America Bulletin, v. 100, p. 859-876.

Yakymchuk, C., Kirkland, C., and Clark, C., 2018, Th/U ratios in metamorphic zircon: Journal of Metamorphic Geology, v. 36, p. 715-737, doi:10.1111/jmg.12307.

Yonkee, W.A., and Weil, A.B., 2015, Tectonic evolution of the Sevier and Laramide belts within the North American Cordillera orogenic system, Earth Science Reviews, v. 150, p. 531- 593.

Zack, T., Moraes, R., and Kronz, A., 2004, Temperature dependence of Zr in rutile: empirical calibration of a rutile thermometer: Contributions to Mineralogy and Petrology. V. 148, p. 471-488.

Zak, J., Verner, K., Johnson, K., and Schwartz, J.J., 2012, Magma emplacement process zone preserved in the roof of a large Cordilleran batholith, Wallowa Mountains, northeastern Oregon: Journal of Volcanology and Geothermal Research, v. 227-228, p. 61-75.

Zak, J., Verner, K., Tomek, F., Holub, F.V., Johnson, K., and Schwartz, J.J., 2015, Simultaneous batholith emplacement, terrane/continent collision, and oroclinal bending in the Blue Mountains Province, North American Cordillera: Tectonics, v. 34, p. 1107-1128.

Zeck, H.P., Monie, P., Villa, I.M., and Hansen, B.T., 1992, Very high rates of cooling and uplift in the alpine belt of Betic Cordilleras, southern Spain: Geology, v. 20, p. 1052- 1054.

APPENDICES

Appendix A. UTM Coordinates for samples found in the Salmon River suture zone in zone 11T using WGS 84 datum

Sample ID	Easting	Northing
01A	565884	5030297
06	561316	5027613
07	562248	5027758
07B	564949	5029790
11A	563289	5028756
27	560672	5027707
30A	563648	5029115
61C	562199	5027753
61D	562199	5027753
61E	562199	5027753
63A	563286	5028745
64	563446	5028930
67	546887	5029791
68	565889	5029750
69	569718	5030292
70A	569718	5027905
401A	554486	5028868
PMG	545586	5003550

Appendix A continued. UTM Coordinates for samples found in the Salmon River suture zone in zone 11T using WGS 84 datum

Sample ID	Easting	Northing
ID03	545410	5003487
ID07	558557	5029042
ID26	551980	5028503
ID23	546401	5008963
PRC01	575960	5030665
R18	555667	5030056
R16	557366	5029728
R14	560672	5027707
R12	566649	5030876
R10	569718	5027905
R11	569718	5027905

Appendix B. U-Pb Zircon Ages

Sample Name	Source File	Final Pb206/U238 age (Ma)	± (Ma)	Final Pb206/U238 age (207Pb-corr) (Ma)	± (Ma)	Final U/Th mean	±
67	20ID67.ZR.07	109.00	3.98	-	-	4.49	4.492
	20ID67.ZR.02	143.44	3.14	-	-	54.67	54.67
	20ID67.ZR.03	174.43	8.05	-	-	29.60	29.60
	20ID67.ZR.04	173.90	7.01	-	-	109.67	109.67
	20ID67.ZR.05	173.24	5.84	-	-	9.38	9.38
	20ID67.ZR.06	163.84	6.76	-	-	25.31	25.31
	20ID67.ZR.08	136.50	3.29	-	-	72.65	72.65

Appendix B Continued. U-Pb Zircon Ages

Sample Name	Source File	Final Pb206/U238 age (Ma)	± (Ma)	Final Pb206/U238 age (207Pb-corr) (Ma)	± (Ma)	Final U/Th mean	±
	20ID67.ZR.10	174.00	8.72	-	-	44.95	44.95
404A	21ID404A.ZR.15	109.21	2.69	-	-	10.64	0.79
	20ID404A.AP.04	160.43	10.38	-	-	5.61	0.96
	20ID404A.AP.10	130.59	3.03	-	-	4.57	0.08
	21ID404A.ZR.01	174.98	23.70	-	-	2.73	0.22
	21ID404A.ZR.03	125.65	2.82	-	-	5.76	0.12
	21ID404A.ZR.04	130.49	2.77	-	-	6.07	0.26

Appendix B Continued. U-Pb Zircon Ages

Sample Name	Source File	Final Pb206/U238 age (Ma)	± (Ma)	Final Pb206/U238 age (207Pb-corr) (Ma)	± (Ma)	Final U/Th mean	±
	21ID404A.ZR.05	124.11	2.21	-	-	4.52	0.19
	21ID404A.ZR.06	128.42	3.02	-	-	5.96	0.16
	21ID404A.ZR.07	116.28	2.33	-	-	5.22	0.10
	21ID404A.ZR.08	125.34	2.17	-	-	4.00	0.07
	21ID404A.ZR.09	116.81	2.20	-	-	9.29	1.28
	21ID404A.ZR.10	121.88	1.76	-	-	4.72	0.06
	21ID404A.ZR.11	118.70	2.43	-	-	6.93	0.15

Appendix B Continued. U-Pb Zircon Ages

Sample Name	Source File	Final Pb206/U238 age (Ma)	± (Ma)	Final Pb206/U238 age (207Pb-corr) (Ma)	± (Ma)	Final U/Th mean	±
	21ID404A.ZR.12	124.41	2.88	-	-	6.18	0.13
	21ID404A.ZR.13	124.28	2.25	-	-	3.53	0.22
	21ID404A.ZR.14	131.73	3.00	-	-	5.53	0.09
	21ID404A.ZR. 16	117.47	2.18	-	-	16.44	1.94
	21ID404A.ZR. 17	123.10	2.55	-	-	5.95	0.13
	21ID404A.ZR. 18	129.19	2.78	-	-	5.96	0.11

Appendix B Continued. U-Pb Zircon Ages

Sample Name	Source File	Final Pb206/U238 age (Ma)	± (Ma)	Final Pb206/U238 age (207Pb-corr) (Ma)	± (Ma)	Final U/Th mean	±
	21ID404A. ZR. 19	134.29	3.06	-	-	4.47	0.12
	21ID404A. ZR. 20	120.53	2.85	-	-	6.26	0.17
	21ID404A ZR.21	117.91	2.65	-	-	6.66	0.13
	21ID404A. ZR.01	129.86	2.62	-	-	3.40	0.07
	21ID404A. ZR.02	117.44	3.34	130.97	3.37	7.20	0.44
	21ID404A. ZR.03	118.23	2.72	118.36	2.78	6.00	0.17

Appendix B Continued. U-Pb Zircon Ages

Sample Name	Source File	Final Pb206/U238 age (Ma)	± (Ma)	Final Pb206/U238 age (207Pb-corr) (Ma)	± (Ma)	Final U/Th mean	±
	21ID404A.ZR.04	137.90	3.32	120.53	3.32	4.40	0.33
	21ID404A.ZR.05	118.17	2.70	137.85	2.77	5.66	0.70
	21ID404A.ZR.06	137.40	5.95	121.52	6.12	6.43	0.19
	21ID404A.ZR.07	130.46	2.61	141.48	2.61	3.04	0.19
	21ID404A.ZR.08	118.38	2.45	130.65	2.46	18.43	1.83
	21ID404A.ZR.09	125.37	2.36	118.66	2.39	4.08	0.42

Appendix B Continued. U-Pb Zircon Ages

Sample Name	Source File	Final Pb206/U238 age (Ma)	± (Ma)	Final Pb206/U238 age (207Pb-corr) (Ma)	± (Ma)	Final U/Th mean	±
	21ID404A .ZR.10	117.22	3.43	126.70	3.47	16.18	1.26
	21ID404A .ZR.11	122.10	2.47	118.43	2.47	4.23	0.31
	21ID404A. ZR.12	126.44	3.14	122.19	3.14	11.56	2.62
	21ID404A. ZR.13	125.68	2.34	126.34	2.34	4.20	0.23
	21ID404A. ZR.14	126.20	2.80	125.77	2.78	6.70	0.22
	21ID404A. ZR.15	112.07	2.38	125.67	2.39	7.67	0.53

Appendix B Continued. U-Pb Zircon Ages

Sample Name	Source File	Final Pb206/U238 age (Ma)	± (Ma)	Final Pb206/U238 age (207Pb-corr) (Ma)	± (Ma)	Final U/Th mean	±
	21ID404A.ZR.16	129.01	2.51	112.73	2.53	3.35	0.10
	21ID404A.ZR.17	147.70	7.73	130.26	7.73	4.43	0.57
	21ID404A.ZR.18	127.40	2.17	147.80	2.17	4.44	0.17
	21ID404A.ZR.19	125.53	2.87	127.00	2.94	3.95	0.09
	21ID404A.20	121.10	2.79	128.58	2.78	8.75	0.46
	21ID404A.21	145.92	5.77	120.82	5.77	3.93	0.15

Appendix B Continued. U-Pb Zircon Ages

Sample Name	Source File	Final Pb206/U238 age (Ma)	± (Ma)	Final Pb206/U238 age (207Pb-corr) (Ma)	± (Ma)	Final U/Th mean	±
	21ID404A.22	126.56	2.37	145.94	2.38	4.94	0.17
	21ID404A.23	128.66	2.18	126.85	2.17	6.81	0.26
	21ID404A.24	116.98	2.80	128.28	2.82	6.35	0.35
	21ID404A.25	124.26	2.19	117.85	2.19	4.68	0.11
	21ID404A.26	119.49	3.05	124.38	3.07	5.07	0.18
	21ID404A.27	120.06	2.67	120.45	2.67	3.94	0.22
	21ID404A.28	123.89	2.14	119.94	2.14	4.60	0.20

Appendix B Continued. U-Pb Zircon Ages

Sample Name	Source File	Final Pb206/U238 age (Ma)	± (Ma)	Final Pb206/U238 age (207Pb-corr) (Ma)	± (Ma)	Final U/Th mean	±
70A	20ID70A.ZR.01	120.90	6.89	-	-	118.69	8.46
	20ID70A.ZR.06	159.94	6.83	-	-	71.38	7.26
	20ID70A.ZR.08	135.95	7.56	-	-	3.76	0.14
	20ID70A.ZR.09	137.42	2.82	-	-	138.93	5.62
	20ID70A.ZR.15	121.39	4.33	-	-	113.13	6.02
	20ID70A.ZR.17	94.02	2.12	-	-	82.13	3.32
	20ID70A.ZR.19	139.80	4.55	-	-	110.51	6.86

Appendix B Continued. U-Pb Zircon Ages

Sample Name	Source File	Final Pb206/U238 age (Ma)	± (Ma)	Final Pb206/U238 age (207Pb-corr) (Ma)	± (Ma)	Final U/Th mean	±
	20ID70A.ZR.21	105.08	3.82	-	-	87.34	6.73
	20ID70A.ZR.22	137.55	4.76	-	-	2.47	0.12
	20ID70A.ZR.23	86.44	1.78	-	-	119.94	13.12
	20ID70A.ZR.24	148.35	7.07	-	-	109.77	8.46
30A	21IDCR30A.ZR.05	99.38	1.56	-	-	28.02	0.47
	21IDCR30A.AP.01	100.83	1.40	-	-	17.96	0.63
	21IDCR30A.ZR.01	102.18	1.54	-	-	22.14	0.20

Appendix B Continued. U-Pb Zircon Ages

Sample Name	Source File	Final Pb206/U238 age (Ma)	± (Ma)	Final Pb206/U238 age (207Pb-corr) (Ma)	± (Ma)	Final U/Th mean	±
	21IDCR30A.ZR.02	102.58	1.53	-	-	34.11	0.42
	21IDCR30A.ZR.04	107.92	1.66	-	-	30.70	4.44
	21IDCR30A.ZR.06	107.92	1.83	-	-	30.70	4.44
	21IDCR30A.ZR.07	105.74	1.66	-	-	30.33	2.62
	21IDCR30A.ZR.08	104.77	2.06	-	-	27.54	0.50
	21IDCR30A.ZR.09	101.75	2.06	-	-	27.33	0.66
	21IDCR30A.ZR.10	103.59	2.94	-	-	29.67	0.78

Appendix B Continued. U-Pb Zircon Ages

Sample Name	Source File	Final Pb206/U238 age (Ma)	± (Ma)	Final Pb206/U238 age (207Pb-corr) (Ma)	± (Ma)	Final U/Th mean	±
06	20ID06.01	94.80	670	-	-	22.70	1.30
	20ID06.10	143.00	13.0	-	-	29.20	2.10
07B	20ID07B.05	93.74	15.38	-	-	9.11	3.53
	20ID07B.01	116.82	3.76	-	-	22.67	0.75
	20ID07B.01	131.30	7.60	-	-	25.10	1.30
	20ID07B.02	132.00	2.90	-	-	9.00	1.80
	20ID07B.03	132.00	7.20	-	-	3.86	0.08
	20ID07B.04	127.41	3.92	-	-	22.56	1.32
	20ID07B.08	115.00	3.60	-	-	8.82	0.77

Appendix B Continued. U-Pb Zircon Ages

Sample Name	Source File	Final Pb206/U238 age (Ma)	± (Ma)	Final Pb206/U238 age (207Pb-corr) (Ma)	± (Ma)	Final U/Th mean	±
63A	20ID63A.01	142.40	9.20	-	-	8.33	0.55
64	20ID64.02	103.70	2.40	-	-	49.00	5.70
	20ID64.07	-	-	109.41	26.75	15.94	2.71
	20ID64.07	-	-	138.36	4.24	29.95	6.96
PMG	PMG.13	83.50	5.70	-	-	13.50	2.30
	PMG.07	102.40	8.40	-	-	130.00	50.00
	PMG.01	153.50	9.80	-	-	4.71	0.16

Appendix B Continued. U-Pb Zircon Ages

Sample Name	Source File	Final Pb206/U238 age (Ma)	± (Ma)	Final Pb206/U238 age (207Pb-corr) (Ma)	± (Ma)	Final U/Th mean	±
	PMG.02	178.00	14.00	-	-	28.50	3.90
	PMG.06	187.00	16.00	-	-	11.00	1.90
	PMG.09	186.00	14.00	-	-	5.71	0.31
	PMG.12	181.00	20.00	-	-	124.00	29.00
61C	20ID61C.AP.15	128.65	5.82	98.31	4.48	29.19	1.02
	20ID61C.AP.05	488.71	43.01	103.48	11.50	9.69	0.54
	20ID61C.AP.02	511.71	61.92	130.19	18.01	8.74	0.60
68	20ID68.12	-	-	138.44	5.31	3.58	0.27

Appendix B Continued. U-Pb Zircon Ages

Sample Name	Source File	Final Pb206/U238 age (Ma)	± (Ma)	Final Pb206/U238 age (207Pb-corr) (Ma)	± (Ma)	Final U/Th mean	±
	20ID68.24	-	-	152.44	3.71	2.84	0.26

Appendix C. U-Pb Rutile Ages

Sample Name	Source File	Final Pb206/U238 age (Ma)	± (Ma)	Final Pb206/U238 age (207Pb-corr) (Ma)	± (Ma)	Zr90 (ppm)	Temperature (°C) (+)	Temperature (°C) (-)
401A	21ID401A.01	338.95	78.81	166.32	56.76	4358.74	928.37	928.45
07	21ID07.01	122.10	11.27	92.20	8.65	4249.70	924.92	924.81
	21ID07.02	109.97	13.00	77.74	9.39	4282.67	925.97	925.91
	21ID07.03	111.78	9.97	91.89	8.26	4269.38	925.55	925.47
	21ID07.04	118.66	13.69	93.51	10.91	4258.65	925.21	925.11
	21ID07.05	154.93	23.30	116.90	17.91	4274.77	925.72	925.65
	21ID07.06	117.09	16.39	114.59	16.06	4252.89	925.02	924.91
01A	21ID01A.04	91.89	5.42	89.60	5.29	4262.73	925.34	925.24
27	21ID27.07	122.69	19.65	143.48	22.91	4281.23	925.92	925.87

Appendix D. U-Pb Apatite Ages and Closure Temperatures

Sample Name	Source File	Ca43_ mean (ppm)	± (ppm)	Zr91_ mean (ppm)	± (ppm)	Final Pb206/ U238 age (Ma)	± (Ma)	Final Pb206/ U238 age (207Pb -corr) (Ma)	± (Ma)	C long (um)	a2 short (um)	ESR (um)	Closure Tempe -rature (°C)
67	20ID67. 01	-	-	-	-	286.57	17.43	103.74	12.03	142.04	116.80	55.94	456.86
	20ID67. 02	-	-	-	-	369.15	10.54	106.96	3.83	156.86	79.57	42.37	446.77
	20ID67. 03	-	-	-	-	137.61	3.34	79.49	2.33	294.93	146.95	78.51	469.54
	20ID67. 07	-	-	-	-	210.09	12.47	152.14	15.27	209.44	123.57	63.93	461.80
	20ID67. 12	-	-	-	-	239.07	22.46	174.93	26.04	138.13	82.59	42.61	446.97
	20ID67. 13	-	-	-	-	183.74	5.54	101.39	4.15	195.94	99.76	53.09	454.94

Appendix D Continued. U-Pb Apatite Ages and Closure Temperatures

Sample Name	Source File	Ca43_ mean (ppm)	± (ppm)	Zr91_ mean (ppm)	± (ppm)	Final Pb206/ U238 age (Ma)	± (Ma)	Final Pb206/ U238 age (207Pb -corr) (Ma)	± (Ma)	C long (um)	a2 short (um)	ESR (um)	Closure Tempe -rature (°C)
	20ID67.14	-	-	-	-	96.16	7.87	125.79	17.90	147.71	99.62	50.08	452.80
	20ID67.14	-	-	-	-	66559.35	2729.89	128.37	71.17	180.10	76.59	42.01	446.46
	20ID67.14	-	-	-	-	136.61	4.36	96.69	3.46	95.51	45.09	24.32	439.68
	20ID67.14	-	-	-	-	348.56	13.40	94.70	5.23	117.51	75.86	38.51	443.36
	20ID67.14	-	-	-	-	109.16	2.69	89.94	2.45	406.05	188.13	101.78	493.71
	20ID67.AP.13	291987.80	11914.24	0	0	386.67	62.89	161.42	65.90	233.24	186.31	89.91	474.74

Appendix D Continued. U-Pb Apatite Ages and Closure Temperatures

Sample Name	Source File	Ca43_ mean (ppm)	±	Zr91_ mean (ppm)	± (ppm)	Final Pb206/ U238 age (Ma)	± (Ma)	Final Pb206/ U238 age (207Pb -corr) (Ma)	± (Ma)	C long (um)	a2 short (um)	ESR (um)	Closure Tempe -rature (°C)
	20ID67. AP.14	313115 .30	13767.5 3	120.37	62.91	239.81	20.46	121.09	11.46	175.69	123.65	61.55	460.39
68	20ID68. 02	-	-	-	-	379.78	7.99	85.75	2.17	77.41	54.69	27.20	431.22
	20ID68. 06	-	-	-	-	1147. 67	238.91	67.71	1.93	249.31	100.71	55.67	470.00
	20ID68. 08	-	-	-	-	521.57	17.16	134.95	20.06	160.14	94.71	48.97	465.15
	20ID68. 09	-	-	-	-	330.61	7.45	81.41	2.13	149.71	108.08	53.48	455.21
	20ID68. 13	-	-	-	-	1732.4 1	360.65	93.71	15.14	150.15	80.12	42.27	446.68
	20ID68.1 5	-	-	-	-	426.26	14.66	93.45	3.70	120.78	80.81	40.70	458.24

Appendix D Continued. U-Pb Apatite Ages and Closure Temperatures

Sample Name	Source File	Ca43_ mean (ppm)	±	Zr91_ mean (ppm)	± (ppm)	Final Pb206/ U238 age (Ma)	± (Ma)	Final Pb206/ U238 age (207Pb -corr) (Ma)	± (Ma)	C long (um)	a2 short (um)	ESR (um)	Closure Tempe -rature (°C)
	20ID68. 17	-	-	-	-	866.99	142.21	114.94	13.16	81.79	59.26	29.30	433.78
	20ID68. 20	-	-	-	-	4055.0	634.11	100.48	7.49	149.43	53.42	30.05	434.66
	20ID68. 21	-	-	-	-	3537.4	561.52	76.25	9.76	135.51	42.99	24.55	440.02
	20ID68. 22	-	-	-	-	156.29	1.24	172.45	1.41	407.22	188.13	101.82	479.57
	20ID68. 25	-	-	-	-	608.25	10.38	91.13	2.48	134.74	112.44	53.65	468.59
	20ID68. 26	-	-	-	-	619.16	66.73	105.08	2.57	226.12	115.14	61.28	473.67
	20ID68. 33	-	-	-	-	423.76	10.75	94.90	3.27	206.32	112.44	59.09	458.88

Appendix D Continued. U-Pb Apatite Ages and Closure Temperatures

Sample Name	Source File	Ca43_ mean (ppm)	±	Zr91_ mean (ppm)	± (ppm)	Final Pb206/ U238 age (Ma)	± (Ma)	Final Pb206/ U238 age (207Pb -corr) (Ma)	± (Ma)	C long (um)	a2 short (um)	ESR (um)	Closure Tempe -rature (°C)
	20ID68.38	-	-	-	-	423.76	10.75	94.90	3.27	206.32	112.44	59.09	458.88
	20ID68.39	-	-	-	-	39716.	4281.2	181.00	149.27	109.49	69.22	35.30	440.28
	20ID68.46	-	-	-	-	1320.8	336.59	73.42	3.82	153.72	98.44	50.06	452.29
	20ID68.47	-	-	-	-	773.21	19.67	164.96	21.67	88.17	72.14	34.60	430.54
	20ID68.49	-	-	-	-	540.41	31.72	138.90	11.77	78.16	53.14	26.67	459.46
	20ID68.50	-	-	-	-	305.84	5.69	89.88	3.85	233.46	111.52	60.02	435.87
	20ID68.54	-	-	-	-	5412.7	691.29	97.09	7.67	200.88	53.43	31.12	455.40

Appendix D Continued. U-Pb Apatite Ages and Closure Temperatures

Sample Name	Source File	Ca43_ mean (ppm)	±	Zr91_ mean (ppm)	± (ppm)	Final Pb206/ U238 age (Ma)	± (Ma)	Final Pb206/ U238 age (207Pb -corr) (Ma)	± (Ma)	C long (um)	a2 short (um)	ESR (um)	Closure Tempe -rature (°C)
	20ID68. 56	-	-	-	-	3348.3	535.37	173.63	19.29	159.58	68.84	37.68	425.40
	20ID68 .57	-	-	-	-	1194.0 7	161.52	118.50	12.14	148.26	39.15	22.82	424.24
	20ID68 .58	-	-	-	-	830.69	17.23	128.63	7.21	146.35	103.8	51.58	453.88
30A	21ID 30A.05	-	-	-	-	249.27	6.72	92.48	3.19	83.44	24.07	13.90	408.88
	21ID 30A.02	-	-	-	-	114.06	2.56	106.17	1.59	415.95	153.74	86.08	486.98
	21ID 30A.09	-	-	-	-	73.09	0.96	111.02	1.43	126.91	24.60	14.74	410.70
	21ID30A. 10	-	-	-	-	70.95	0.74	113.03	1.18	414.02	94.74	55.99	470.22

Appendix D Continued. U-Pb Apatite Ages and Closure Temperatures

Sample Name	Source File	Ca43_ mean (ppm)	±	Zr91_ mean (ppm)	± (ppm)	Final Pb206/ U238 age (Ma)	± (Ma)	Final Pb206/ U238 age (207Pb -corr) (Ma)	± (Ma)	C long (um)	a2 short (um)	ESR (um)	Closure Tempe -rature (°C)
	21ID30A.01	-	-	-	-	107.81	1.26	114.40	1.33	166.98	77.87	42.09	459.48
	21ID 30A.08	-	-	-	-	108.31	1.17	114.75	1.20	279.45	120.90	66.14	476.62
	21ID 30A.04	-	-	-	-	1271.32	191.60	116.38	2.37	113.14	62.57	32.79	437.70
	21ID 30A.03	-	-	-	-	111.06	1.17	117.40	1.26	218.84	120.90	63.37	461.47
27	21ID27 .01	-	-	-	-	239.59	12.91	76.76	8.99	169.63	131.9	64.09	461.60
	21ID27 .02	-	-	-	-	292.98	10.78	83.50	3.82	183.00	104	54.21	455.70
	21ID27.04	-	-	-	-	331.20	14.10	82.69	9.39	118.50	89.5	43.81	447.96

Appendix D Continued. U-Pb Apatite Ages and Closure Temperatures

Sample Name	Source File	Ca43_ mean (ppm)	±	Zr91_ mean (ppm)	± (ppm)	Final Pb206/ U238 age (Ma)	± (Ma)	Final Pb206/ U238 age (207Pb -corr) (Ma)	± (Ma)	C long (um)	a2 short (um)	ESR (um)	Closure Tempe -rature (°C)
	21ID27.05	-	-	-	-	313.68	10.31	84.29	3.49	118.43	51.62	28.20	432.47
	21ID27.06	-	-	-	-	329.10	9.53	85.91	3.20	49.05	35.16	17.43	416.26
	21ID27.07	-	-	-	-	358.38	11.86	92.11	4.37	197.97	186.26	85.96	473.01
07	21ID07.01	-	-	-	-	478.52	15.55	108.50	4.91	64.07	50.55	24.47	427.61
	21ID07.02	-	-	-	-	516.78	13.43	126.54	5.45	55.16	43.27	20.98	422.42
	21ID07.03	-	-	-	-	428.14	18.08	113.92	6.14	70.5	51.44	25.39	441.21
	21ID07.04	-	-	-	-	403.82	7.63	99.65	2.51	78.52	56.3	27.90	432.10

Appendix D Continued. U-Pb Apatite Ages and Closure Temperatures

Sample Name	Source File	Ca43_ mean (ppm)	±	Zr91_ mean (ppm)	± (ppm)	Final Pb206/ U238 age (Ma)	± (Ma)	Final Pb206/ U238 age (207Pb -corr) (Ma)	± (Ma)	C long (um)	a2 short (um)	ESR (um)	Closure Tempe -rature (°C)
	21ID07.05	-	-	-	-	678.19	19.33	169.79	7.45	62.26	39.55	20.15	433.14
	21ID07.06	-	-	-	-	631.35	14.04	133.53	4.77	103.54	61.14	31.63	436.43
	21ID07.07	-	-	-	-	425.70	13.26	93.11	3.93	105.23	35.25	20.00	420.81
	21ID07.08	-	-	-	-	153.48	4.85	120.30	4.86	67.19	48.62	24.05	427.01
	21ID07.09	-	-	-	-	434.82	10.41	111.38	3.33	49.97	30.21	15.55	412.53
	21ID07.10	-	-	-	-	500.28	11.46	93.91	3.20	79.9	63.46	30.67	435.37
	21ID07.11	-	-	-	-	766.59	23.08	178.62	27.93	71.62	45.61	23.22	425.83

Appendix D Continued. U-Pb Apatite Ages and Closure Temperatures

Sample Name	Source File	Ca43_ mean (ppm)	±	Zr91_ mean (ppm)	± (ppm)	Final Pb206/ U238 age (Ma)	± (Ma)	Final Pb206/ U238 age (207Pb -corr) (Ma)	± (Ma)	C long (um)	a2 short (um)	ESR (um)	Closure Tempe -rature (°C)
	21ID07. 12	-	-	-	-	431.29	9.89	125.53	3.84	62.17	32.28	17.12	415.67
	21ID07 .13	-	-	-	-	568.01	12.50	138.94	4.90	75.14	35.5	19.14	419.36
	21ID07 .14	-	-	-	-	368.08	8.89	107.36	3.27	68.5	43.35	22.10	424.16
	21ID07 .15	-	-	-	-	420.67	8.15	117.95	3.26	69.71	43.49	22.24	424.38
11A	21ID 11A.08	-	-	-	-	196.74	5.37	86.44	2.61	117.41	40.23	22.75	437.36
	21ID 11A.01	-	-	-	-	90.65	2.53	133.96	4.59	288.41	125.91	68.78	478.15
	21ID11A.	-	-	-	-	129.15	2.92	87.85	1.94	120.61	107.20	50.28	452.95

Appendix D Continued. U-Pb Apatite Ages and Closure Temperatures

Sample Name	Source File	Ca43_ mean (ppm)	±	Zr91_ mean (ppm)	± (ppm)	Final Pb206/ U238 age (Ma)	± (Ma)	Final Pb206/ U238 age (207Pb -corr) (Ma)	± (Ma)	C long (um)	a2 short (um)	ESR (um)	Closure Tempe -rature (°C)
	21ID11A.03	-	-	-	-	136.09	3.62	98.95	2.92	175.77	84.86	45.59	449.40
	21ID 11A.04	-	-	-	-	101.01	2.05	91.20	1.88	171.92	100.12	51.93	454.13
	21ID 11A.05	-	-	-	-	134.49	8.32	133.70	8.13	231.10	150.28	76.16	468.39
	21ID 11A.06	-	-	-	-	186.51	6.33	94.60	3.57	91.01	47.22	25.04	440.72
	21ID 11A.07	-	-	-	-	179.10	3.03	95.40	1.68	147.20	68.06	36.83	441.78
	21ID 11A.09	-	-	-	-	157.32	3.44	91.09	2.19	205.72	102.60	54.81	456.10
	21ID11A.11	-	-	-	-	296.77	5.55	92.22	2.14	143.84	61.00	33.47	438.42

Appendix D Continued. U-Pb Apatite Ages and Closure Temperatures

Sample Name	Source File	Ca43_ mean (ppm)	±	Zr91_ mean (ppm)	± (ppm)	Final Pb206/ U238 age (Ma)	± (Ma)	Final Pb206/ U238 age (207Pb -corr) (Ma)	± (Ma)	C long (um)	a2 short (um)	ESR (um)	Closure Tempe -rature (°C)
	21ID11A. 12	-	-	-	-	141.26	3.24	94.24	2.29	225.87	61.64	35.81	440.78
PMG	PMG.02	-	-	-	-	145.17	5.00	108.27	3.75	170.27	104.2	53.50	460.53
	PMG. 03	-	-	-	-	382.32	21.43	123.36	7.55	525.26	267.88	142.52	498.80
	PMG. 06	-	-	-	-	214.65	13.79	123.47	8.14	429.08	199.01	107.64	501.89
	PMG. 07	-	-	-	-	211.92	11.62	126.84	7.13	631.1	203.39	115.93	504.97
	PMG. 08	-	-	-	-	225.15	12.44	104.60	6.01	245.25	101.51	55.91	475.69
	PMG. 10	-	-	-	-	313.39	13.36	112.54	5.10	160.24	111.36	55.60	461.96

Appendix D Continued. U-Pb Apatite Ages and Closure Temperatures

Sample Name	Source File	Ca43_ mean (ppm)	±	Zr91_ mean (ppm)	± (ppm)	Final Pb206/ U238 age (Ma)	± (Ma)	Final Pb206/ U238 age (207Pb -corr) (Ma)	± (Ma)	C long (um)	a2 short (um)	ESR (um)	Closure Tempe -rature (°C)
	PMG.11	-	-	-	-	190.60	7.94	112.55	4.77	161.59	85.67	45.26	454.36
	PMG.15	-	-	-	-	218.75	12.31	112.41	6.50	203.3	133.03	67.33	469.17
	PMG.16	-	-	-	-	158.88	4.68	106.52	3.04	104.48	73.06	36.42	446.50
	PMG.17	-	-	-	-	199.65	5.75	108.67	3.19	136.6	104.89	51.13	458.58
	PMG.19	-	-	-	-	264.41	19.88	109.21	8.61	189.39	55.89	32.19	454.91
	PMG.20	-	-	-	-	272.07	14.41	104.16	5.97	208.9	115.82	60.66	465.23
	PMG.23	-	-	-	-	387.55	21.73	109.13	6.76	165.55	80.66	43.26	465.89
	PMG.24	-	-	-	-	423.10	27.66	120.70	8.74	165.55	80.66	43.26	465.89

Appendix D Continued. U-Pb Apatite Ages and Closure Temperatures

Sample Name	Source File	Ca43_ mean (ppm)	± (ppm)	Zr91_ mean (ppm)	± (ppm)	Final Pb206/ U238 age (Ma)	± (Ma)	Final Pb206/ U238 age (207Pb -corr) (Ma)	± (Ma)	C long (um)	a2 short (um)	ESR (um)	Closure Tempe -rature (°C)
	PMG. AP.01	213486	11057.	0	0	236.87	35.78	129.17	19.94	162.86	86.68	45.76	454.76
	PMG.AP. 02	207862	10380.	0	0	170.56	14.33	102.82	8.85	178.04	67.82	37.81	460.85
	PMG.AP. 03	213333	12219.	0	0	189.47	16.73	121.92	11.92	156.92	52.26	29.67	451.93
	PMG.AP. 04	214954	9945.4	0	0	178.33	15.11	112.69	9.47	100.56	35.57	20.03	437.94
	PMG.AP. 05	253854	12819.	0	0	184.97	15.98	114.87	10.09	140.97	80.17	41.78	446.37
	PMG.AP. 06	192646	12800.	0	0	164.44	12.23	101.33	7.70	132.76	76.04	39.57	449.48
	PMG.AP. 07	215647	10337.	0	0	167.54	13.72	108.32	9.87	109.73	45.72	25.16	445.99
	PMG.AP. 08	204136 .70	9330.6	0	0	207.02	29.08	135.52	20.15	175.76	74.31	40.80	463.69

Appendix D Continued. U-Pb Apatite Ages and Closure Temperatures

Sample Name	Source File	Ca43_ mean (ppm)	±	Zr91_ mean (ppm)	± (ppm)	Final Pb206/ U238 age (Ma)	± (Ma)	Final Pb206/ U238 age (207Pb -corr) (Ma)	± (Ma)	C long (um)	a2 short (um)	ESR (um)	Closure Tempe -rature (°C)
	PMG. AP.09	237504 .6	13079. 2	0	0	167.92	12.70	109.45	9.06	167.91	76.13	41.33	445.88
	PMG. AP.13	233385 .9	10940. 5	0	0	299.50	33.74	186.87	21.34	401.69	168.51	92.63	495.73
	PMG. AP.14	278631 .8	12891. 5	0	0	276.18	31.33	177.41	20.46	447.78	242.32	127.51	494.26
	PMG. AP.17	162084 .5	7463.0	0	0	244.30	27.19	161.47	21.04	209.09	85.78	47.31	469.28
06	20ID06 .03	-	-	-	-	405.22	13.31	69.93	2.70	177.95	100.17	52.31	459.69
	20ID06. 06	-	-	-	-	379.58	10.65	70.79	2.30	131.26	195.37	77.16	474.39

Appendix D Continued. U-Pb Apatite Ages and Closure Temperatures

Sample Name	Source File	Ca43_ mean (ppm)	±	Zr91_ mean (ppm)	± (ppm)	Final Pb206/ U238 age (Ma)	± (Ma)	Final Pb206/ U238 age (207Pb -corr) (Ma)	± (Ma)	C long (um)	a2 short (um)	ESR (um)	Closure Tempe -rature (°C)
	20ID06.24	-	-	-	-	197.17	4.98	74.14	1.94	153.87	104.41	52.42	459.77
	20ID06.02	-	-	-	-	437.65	16.53	76.30	3.53	257.26	104.04	57.51	476.79
	20ID06.14	-	-	-	-	306.73	9.82	77.21	2.71	270.49	88.93	50.56	476.90
	20ID06.08	-	-	-	-	224.44	7.03	78.37	2.57	209.63	108.41	57.53	463.24
	20ID06.09	-	-	-	-	379.09	10.64	78.67	5.59	294.92	108.89	60.98	465.42
	20ID06.23	-	-	-	-	322.12	8.75	82.64	2.46	203.85	105.68	56.06	462.27
	20ID06.25	-	-	-	-	363.39	12.29	82.74	3.18	261.57	108.69	59.83	464.71

Appendix D Continued. U-Pb Apatite Ages and Closure Temperatures

Sample Name	Source File	Ca43_ mean (ppm)	±	Zr91_ mean (ppm)	± (ppm)	Final Pb206/ U238 age (Ma)	± (Ma)	Final Pb206/ U238 age (207Pb -corr) (Ma)	± (Ma)	C long (um)	a2 short (um)	ESR (um)	Closure Tempe -rature (°C)
	20ID06.19	-	-	-	-	253.19	9.50	84.73	3.34	100.66	50.86	27.10	436.07
	20ID06.11	-	-	-	-	426.69	17.35	87.36	4.08	126.35	68.28	35.94	446.02
	20ID06.04	-	-	-	-	197.44	8.86	87.51	4.04	295.25	88.80	51.03	472.17
	20ID06.15	-	-	-	-	602.73	19.04	87.83	3.75	249.58	130.87	69.27	470.26
	20ID06.01	-	-	-	-	298.76	10.14	88.36	3.22	152.76	78.97	41.91	451.56
	20ID06.10	-	-	-	-	201.52	8.73	92.26	4.10	160.15	83.49	44.24	453.53
	20ID06.07	-	-	-	-	714.89	28.52	93.16	5.22	187.95	99.65	52.64	459.92

Appendix D Continued. U-Pb Apatite Ages and Closure Temperatures

Sample Name	Source File	Ca43_ mean (ppm)	±	Zr91_ mean (ppm)	± (ppm)	Final Pb206/ U238 age (Ma)	± (Ma)	Final Pb206/ U238 age (207Pb -corr) (Ma)	± (Ma)	C long (um)	a2 short (um)	ESR (um)	Closure Tempe -rature (°C)
	20ID06.13	-	-	-	-	354.60	24.48	96.61	7.69	176.19	128.92	63.50	467.00
	20ID06.12	-	-	-	-	555.67	38.02	100.13	8.78	100.66	50.86	27.10	436.07
	20ID06.18	-	-	-	-	413.93	13.43	102.30	3.77	141.48	99.24	49.44	457.61
	20ID06.21	-	-	-	-	342.46	20.72	102.57	6.72	91.35	88.18	40.39	450.22
	20ID06.05	-	-	-	-	736.38	32.80	103.38	6.98	175.40	123.77	61.57	465.79
	20ID06.17	-	-	-	-	432.90	14.89	104.51	4.10	199.83	111.03	58.13	436.63
	20ID06.20	-	-	-	-	212.32	10.49	111.68	5.66	166.99	132.75	64.14	467.33

Appendix D Continued. U-Pb Apatite Ages and Closure Temperatures

Sample Name	Source File	Ca43_ mean (ppm)	±	Zr91_ mean (ppm)	± (ppm)	Final Pb206/ U238 age (Ma)	± (Ma)	Final Pb206/ U238 age (207Pb -corr) (Ma)	± (Ma)	C long (um)	a2 short (um)	ESR (um)	Closure Tempe -rature (°C)
64	20ID64 .13	-	-	-	-	737.84	29.30	65.59	4.71	118.66	62.51	33.06	443.05
	20ID64 .21	-	-	-	-	502.86	24.94	69.13	4.53	158.89	133.27	63.50	466.95
	20ID64 .01	-	-	-	-	322.33	22.56	100.12	7.79	160.83	69.68	38.11	464.14
	20ID64 .02	-	-	-	-	303.42	12.65	83.84	3.81	252.19	152.87	78.65	475.13
	20ID64 .03	-	-	-	-	439.66	14.42	83.52	3.42	158.38	120.19	58.76	464.03
	20ID64 .05	-	-	-	-	784.08	39.92	138.73	10.90	153.38	107.57	53.59	460.59
	20ID64. 07	-	-	-	-	356.76	13.36	89.02	3.73	190.0	91.86	49.37	470.91

Appendix D Continued. U-Pb Apatite Ages and Closure Temperatures

Sample Name	Source File	Ca43_ mean (ppm)	±	Zr91_ mean (ppm)	± (ppm)	Final Pb206/ U238 age (Ma)	± (Ma)	Final Pb206/ U238 age (207Pb -corr) (Ma)	± (Ma)	C long (um)	a2 short (um)	ESR (um)	Closure Tempe -rature (°C)
	20ID64 .08	-	-	-	-	343.18	21.93	87.27	6.26	248.87	113.8	61.70	479.52
	20ID64 .09	-	-	-	-	365.39	10.41	89.48	2.83	98.74	95.09	43.59	452.99
	20ID64 .10	-	-	-	-	762.70	30.82	91.32	5.84	143.17	84.07	43.54	452.94
	20ID64 .11	-	-	-	-	444.83	30.82	83.26	5.42	192.75	94.81	50.77	471.97
	20ID64 .12	-	-	-	-	1093.7 4	23.25	185.11	16.72	152.62	112.48	55.38	461.82
	20ID64 .14	-	-	-	-	339.38	62.77	84.29	3.15	144.57	98.04	49.22	457.44

Appendix D Continued. U-Pb Apatite Ages and Closure Temperatures

Sample Name	Source File	Ca43_ mean (ppm)	±	Zr91_ mean (ppm)	± (ppm)	Final Pb206/ U238 age (Ma)	± (Ma)	Final Pb206/ U238 age (207Pb -corr) (Ma)	± (Ma)	C long (um)	a2 short (um)	ESR (um)	Closure Tempe -rature (°C)
	20ID64.15	-	-	-	-	807.78	90.57	198.24	66.07	275.62	93.01	52.71	473.41
	20ID64.16	-	-	-	-	298.93	9.71	78.68	2.75	167.75	127.34	62.25	466.20
	20ID64.17	-	-	-	-	529.51	21.28	109.38	5.35	244.55	148.78	76.49	474.05
	20ID64.18	-	-	-	-	412.82	22.63	77.72	4.88	177.16	91.68	48.65	457.10
	20ID64.19	-	-	-	-	306.75	10.13	77.45	2.79	132.72	60.42	32.78	466.20
	20ID64.20	-	-	-	-	1110.71	41.79	179.16	11.74	171.53	133.27	64.77	467.70
	20ID64.22	-	-	-	-	348.55	18.74	90.49	5.49	179.90	71.74	39.74	462.70

Appendix D Continued. U-Pb Apatite Ages and Closure Temperatures

Sample Name	Source File	Ca43_ mean (ppm)	±	Zr91_ mean (ppm)	± (ppm)	Final Pb206/ U238 age (Ma)	± (Ma)	Final Pb206/ U238 age (207Pb -corr) (Ma)	± (Ma)	C long (um)	a2 short (um)	ESR (um)	Closure Tempe -rature (°C)
	20ID64. 23	-	-	-	-	417.79	28.32	109.29	8.64	118.74	105.02	49.32	457.52
69	20ID69 .92	-	-	-	-	431.75	16.78	60.08	2.91	141.41	127.97	59.72	476.89
	20ID69 .01	-	-	-	-	121.55	3.32	71.23	1.97	407.22	189.52	102.45	499.85
	20ID69 .02	-	-	-	-	172.94	7.13	74.13	3.15	232.2	106.40	57.67	460.90
	20ID69 .03	-	-	-	-	151.04	3.84	81.30	2.10	132.8	114.16	54.04	469.89
	20ID69 .05	-	-	-	-	421.15	12.22	74.71	2.55	250.43	97.50	54.19	474.48
	20ID69. 08	-	-	-	-	1063.5	36.73	112.93	7.53	145.75	142.02	64.87	448.67

Appendix D Continued. U-Pb Apatite Ages and Closure Temperatures

Sample Name	Source File	Ca43_ mean (ppm)	±	Zr91_ mean (ppm)	± (ppm)	Final Pb206/ U238 age (Ma)	± (Ma)	Final Pb206/ U238 age (207Pb -corr) (Ma)	± (Ma)	C long (um)	a2 short (um)	ESR (um)	Closure Tempe -rature (°C)
	20ID69.09	-	-	-	-	201.91	5.43	81.53	2.26	338.52	126.83	70.88	473.12
	20ID69.10	-	-	-	-	163.50	17.88	91.02	10.25	160.19	157.42	71.73	470.98
	20ID69.11	-	-	-	-	377.80	14.04	88.09	3.67	326.85	126.00	70.13	447.45
	20ID69.17	-	-	-	-	621.40	59.93	113.37	14.28	365.60	213.39	110.64	468.93
	20ID69.20	-	-	-	-	1068.63	49.68	162.84	13.06	236.31	130.97	68.60	446.09
	20ID69.21	-	-	-	-	647.15	53.40	130.75	13.67	204.25	62.56	35.88	449.96
	20ID69.2	-	-	-	-	1221.4	49.34	163.17	12.45	228.56	146.95	74.66	476.19

Appendix D Continued. U-Pb Apatite Ages and Closure Temperatures

Sample Name	Source File	Ca43_ mean (ppm)	±	Zr91_ mean (ppm)	± (ppm)	Final Pb206/ U238 age (Ma)	± (Ma)	Final Pb206/ U238 age (207Pb -corr) (Ma)	± (Ma)	C long (um)	a2 short (um)	ESR (um)	Closure Tempe -rature (°C)
	20ID69.23	-	-	-	-	543.28	24.04	80.40	4.53	173.15	97.00	50.70	488.54
	20ID69.24	-	-	-	-	543.28	24.04	80.40	4.53	173.15	97.00	50.70	488.54
	20ID69.27	-	-	-	-	415.72	25.39	76.65	5.58	313.78	113.18	63.58	467.76
	20ID69.30	-	-	-	-	1247.9	52.87	180.89	13.99	103.73	78.54	38.42	480.54
	20ID69.32	-	-	-	-	283.12	13.28	81.60	4.08	244.00	113.8	61.50	468.91
	20ID69.33	-	-	-	-	824.02	109.72	157.93	29.43	300.83	135.33	73.57	472.09
	20ID69.34	-	-	-	-	419.92	58.39	141.83	20.66	266.79	79.99	45.98	468.22

Appendix D Continued. U-Pb Apatite Ages and Closure Temperatures

Sample Name	Source File	Ca43_ mean (ppm)	±	Zr91_ mean (ppm)	± (ppm)	Final Pb206/ U238 age (Ma)	± (Ma)	Final Pb206/ U238 age (207Pb -corr) (Ma)	± (Ma)	C long (um)	a2 short (um)	ESR (um)	Closure Tempe -rature (°C)
	20ID69.35	-	-	-	-	204.09	25.34	83.81	11.20	207.07	105.19	56.00	480.69
	20ID69.36	-	-	-	-	522.97	57.00	115.24	14.98	146.15	69.43	37.40	447.72
	20ID69.38	-	-	-	-	233.60	22.79	101.72	10.40	141.31	80.88	42.10	460.73
	20ID69.39	-	-	-	-	456.17	75.82	122.76	23.64	263.87	133.73	71.23	459.06
	20ID69.40	-	-	-	-	272.07	28.13	85.44	9.63	281.67	222.02	107.51	486.45
	20ID69.43	-	-	-	-	215.85	14.95	81.52	6.18	175.77	168.62	77.38	458.90
	20ID69.44	-	-	-	-	205.00	11.24	87.47	4.97	210.41	90.63	49.46	460.45

Appendix D Continued. U-Pb Apatite Ages and Closure Temperatures

Sample Name	Source File	Ca43_ mean (ppm)	±	Zr91_ mean (ppm)	± (ppm)	Final Pb206/ U238 age (Ma)	± (Ma)	Final Pb206/ U238 age (207Pb -corr) (Ma)	± (Ma)	C long (um)	a2 short (um)	ESR (um)	Closure Tempe -rature (°C)
	20ID69.47	-	-	-	-	608.04	86.76	120.84	21.79	277.83	154.63	80.93	479.71
	20ID69.50	-	-	-	-	768.18	29.80	114.89	6.19	104.83	84.60	40.72	446.60
	20ID69.51	-	-	-	-	289.28	14.15	96.95	4.74	202.13	95.69	51.58	472.58
	20ID69.52	-	-	-	-	331.73	64.26	123.13	27.05	194.57	101.55	53.80	454.01
	20ID69.54	-	-	-	-	312.47	86.14	143.77	46.67	529.98	308.73	160.13	481.06
	20ID69.55	-	-	-	-	276.94	10.94	82.12	3.48	124.70	75.11	38.69	478.48
	20ID69.56	-	-	-	-	1275.8	95.75	170.82	26.84	201.82	132.24	66.91	464.28

Appendix D Continued. U-Pb Apatite Ages and Closure Temperatures

Sample Name	Source File	Ca43_ mean (ppm)	±	Zr91_ mean (ppm)	± (ppm)	Final Pb206/ U238 age (Ma)	± (Ma)	Final Pb206/ U238 age (207Pb -corr) (Ma)	± (Ma)	C long (um)	a2 short (um)	ESR (um)	Closure Tempe -rature (°C)
	20ID69. 57	-	-	-	-	164.54	6.86	95.41	4.04	93.74	75.97	36.53	450.52
	20ID69. 59	-	-	-	-	154.19	8.33	79.62	4.41	121.62	73.11	37.68	471.59
	20ID69. 62	-	-	-	-	421.08	36.91	88.83	9.53	160.23	102.94	52.31	471.32
	20ID69. 64	-	-	-	-	330.45	23.15	88.28	6.92	251.27	178.07	88.50	451.72
	20ID69. 66	-	-	-	-	1206.5	59.29	165.02	15.71	184.45	97.93	51.43	455.62
	20ID69. 70	-	-	-	-	197.02	7.14	80.06	3.00	143.03	56.65	31.41	484.56
	20ID69. 72	-	-	-	-	796.24	80.02	152.16	21.51	150.11	75.12	40.10	451.39

Appendix D Continued. U-Pb Apatite Ages and Closure Temperatures

Sample Name	Source File	Ca43_ mean (ppm)	±	Zr91_ mean (ppm)	± (ppm)	Final Pb206/ U238 age (Ma)	± (Ma)	Final Pb206/ U238 age (207Pb -corr) (Ma)	± (Ma)	C long (um)	a2 short (um)	ESR (um)	Closure Tempe -rature (°C)
	20ID69.74	-	-	-	-	369.74	13.18	79.04	3.19	299.25	78.93	46.01	484.98
	20ID69.76	-	-	-	-	265.26	12.43	85.39	4.25	337.88	133.14	64.18	479.39
	20ID69.77	-	-	-	-	202.01	23.76	104.36	12.75	137.97	80.43	41.71	503.61
	20ID69.78	-	-	-	-	584.77	76.24	119.62	20.60	138.6	72.04	38.19	459.69
	20ID69.80	-	-	-	-	500.84	24.08	86.00	5.16	115.32	70.00	36.00	468.20
	20ID69.81	-	-	-	-	266.24	9.02	86.99	3.12	285.49	100.49	56.64	454.94
	20ID69.82	-	-	-	-	657.10	41.60	92.67	8.50	190.51	54.23	31.36	476.23

Appendix D Continued. U-Pb Apatite Ages and Closure Temperatures

Sample Name	Source File	Ca43_ mean (ppm)	±	Zr91_ mean (ppm)	± (ppm)	Final Pb206/ U238 age (Ma)	± (Ma)	Final Pb206/ U238 age (207Pb -corr) (Ma)	± (Ma)	C long (um)	a2 short (um)	ESR (um)	Closure Tempe -rature (°C)
	20ID69.83	-	-	-	-	557.55	113.69	190.81	44.79	124.93	96.15	46.84	464.64
	20ID69.84	-	-	-	-	237.11	8.86	90.21	3.52	211.40	73.40	41.44	474.50
	20ID69.88	-	-	-	-	900.75	64.61	164.43	17.29	207.32	196.16	90.38	453.95
70A	20ID70A.ZR.04	16.53	23.18	0	0	88.62	7.88	90.51	8.05	120.17	41.58	23.49	489.47
	20ID70A.ZR.07	49.59	39.47	0	0	118.51	13.20	123.29	13.73	248.16	155.26	79.35	475.47
	20ID70A.ZR.16	140.50	82.01	0	0	85.57	3.20	88.30	3.33	140.00	111.44	53.83	460.76

Appendix D Continued. U-Pb Apatite Ages and Closure Temperatures

Sample Name	Source File	Ca43_ mean (ppm)	±	Zr91_ mean (ppm)	± (ppm)	Final Pb206/ U238 age (Ma)	± (Ma)	Final Pb206/ U238 age (207Pb -corr) (Ma)	± (Ma)	C long (um)	a2 short (um)	ESR (um)	Closure Tempe -rature (°C)
404A	21ID404A.01	341575.2	12918.1	56.07	51.51	174.21	10.53	52.03	52.03	4.53	155.90	78.92	469.74
	21ID404A.02	268829	10957.	0	0	407.28	31.28	52.30	52.30	5.16	93.92	46.97	463.58
	21ID404A.03	239239	9502.8	0	0	218.25	17.69	67.99	67.99	4.26	128.83	70.47	479.09
	21ID404A.04	37.04	36.35	0	0	167.25	10.82	69.68	69.68	3.79	37.61	21.01	434.59
	21ID404A.05	300448	10712.	495390	148154	157.30	9.00	69.95	69.95	5.42	85.76	44.14	448.24
	21ID404A.06	292120	10547.	91	6	237.10	14.11	72.07	72.07	4.53	65.20	36.30	454.05

Appendix D Continued. U-Pb Apatite Ages and Closure Temperatures

Sample Name	Source File	Ca43_ mean (ppm)	±	Zr91_ mean (ppm)	± (ppm)	Final Pb206/ U238 age (Ma)	± (Ma)	Final Pb206/ U238 age (207Pb -corr) (Ma)	± (Ma)	C long (um)	a2 short (um)	ESR (um)	Closure Tempe -rature (°C)
	21ID404A.07	214332	9966.8	0	0	124.03	8.54	72.36	72.36	5.05	71.95	40.15	444.85
	21ID404A.08	233269	6774.9	420.58	118.33	191.15	14.25	77.60	77.60	4.53	86.06	45.76	449.53
	21ID404A.09	198567.70	8707.02	28	89	109.16	5.90	84.54	84.54	5.10	118.35	68.80	478.16
	21ID404A.10	0	0	0	0	136.84	3.18	136.60	136.60	3.17	55.40	26.87	430.80
	21ID404A.11	212958.98	6152.73	47.171	40.995	148.06	8.80	167.01	167.01	10.81	78.62	41.27	445.83
61E	20ID61E.93	-	-	-	-	387.92	18.59	51.33	3.01	111.78	56.87	30.27	439.94
	20ID61E.99	-	-	-	-	307.89	14.67	64.61	3.43	106.78	53.85	28.71	438.06

Appendix D Continued. U-Pb Apatite Ages and Closure Temperatures

Sample Name	Source File	Ca43_ mean (ppm)	±	Zr91_ mean (ppm)	± (ppm)	Final Pb206/ U238 age (Ma)	± (Ma)	Final Pb206/ U238 age (207Pb -corr) (Ma)	± (Ma)	C long (um)	a2 short (um)	ESR (um)	Closure Tempe -rature (°C)
	20ID 61E.01	-	-	-	-	118.18	2.44	136.33	3.28	156.97	85.39	44.89	454.06
	20ID61E. 02	-	-	-	-	344.44	17.22	94.93	5.19	73.74	63.22	29.95	439.56
	20ID61E. 03	-	-	-	-	392.63	17.78	84.77	4.37	83.47	59.87	29.67	439.23
	20ID61E. 04	-	-	-	-	295.15	22.29	135.93	10.58	163.13	72.02	39.27	462.26
	20ID61E. 05	-	-	-	-	583.02	33.40	81.71	6.58	114.67	79.05	39.54	449.45
	20ID61E. 06	-	-	-	-	409.07	17.88	68.89	3.58	96.92	73.73	36.02	446.11
	20ID61E. 08	-	-	-	-	483.72	24.27	78.87	4.96	77.89	42.23	22.21	429.21

Appendix D Continued. U-Pb Apatite Ages and Closure Temperatures

Sample Name	Source File	Ca43_ mean (ppm)	±	Zr91_ mean (ppm)	± (ppm)	Final Pb206/ U238 age (Ma)	± (Ma)	Final Pb206/ U238 age (207Pb -corr) (Ma)	± (Ma)	C long (um)	a2 short (um)	ESR (um)	Closure Tempe -rature (°C)
	20ID61E.9	-	-	-	-	347.78	24.27	102.25	9.14	112.48	77.46	38.76	448.73
	20ID61E.10	-	-	-	-	682.67	27.76	107.34	12.64	97.71	77.02	37.30	447.35
	20ID61E.102	-	-	-	-	355.46	17.94	101.75	5.66	144.79	66.84	36.18	459.21
	20ID61E.106	-	-	-	-	235.31	11.75	75.44	3.96	118.37	65.41	34.28	444.34
	20ID61E.10107	-	-	-	-	377.11	19.52	75.74	4.74	136.01	60.93	33.15	455.98
	20ID61E.108	-	-	-	-	604.15	49.86	136.10	14.79	83.67	79.85	36.70	446.77
	20ID61E.11	-	-	-	-	379.54	16.61	73.05	3.70	114.33	75.10	37.98	448.00

Appendix D Continued. U-Pb Apatite Ages and Closure Temperatures

Sample Name	Source File	Ca43_ mean (ppm)	±	Zr91_ mean (ppm)	± (ppm)	Final Pb206/ U238 age (Ma)	± (Ma)	Final Pb206/ U238 age (207Pb -corr) (Ma)	± (Ma)	C long (um)	a2 short (um)	ESR (um)	Closure Tempe -rature (°C)
	20ID61E. 110	-	-	-	-	326.54	18.13	84.40	5.25	121.8	75.79	38.78	448.75
	20ID61E. 12	-	-	-	-	518.61	28.35	69.74	5.20	58.18	46.79	22.54	429.71
	20ID61E. 14	-	-	-	-	414.99	28.34	108.13	8.35	84.31	48.87	25.37	433.78
	20ID61E. 17	-	-	-	-	414.40	20.30	105.50	5.87	141.38	57.21	31.62	454.25
	20ID61E. 18	-	-	-	-	587.93	35.74	80.63	7.31	114.88	70.97	36.37	446.45
	20ID61E. 19	-	-	-	-	846.10	49.93	128.73	4.03	156.97	85.39	44.89	454.06
	20ID61E. 20	-	-	-	-	576.83	33.17	109.03	7.73	182.04	77.82	42.65	465.36

Appendix D Continued. U-Pb Apatite Ages and Closure Temperatures

Sample Name	Source File	Ca43_ mean (ppm)	±	Zr91_ mean (ppm)	± (ppm)	Final Pb206/ U238 age (Ma)	± (Ma)	Final Pb206/ U238 age (207Pb -corr) (Ma)	± (Ma)	C long (um)	a2 short (um)	ESR (um)	Closure Tempe -rature (°C)
	20ID61E.21	-	-	-	-	463.13	22.76	87.78	5.16	117.78	66.37	34.65	444.72
	20ID61E.22	-	-	-	-	462.97	24.73	107.11	6.64	152.67	66.37	44.47	453.72
	20ID61E.23	-	-	-	-	394.27	32.86	71.84	7.24	107.19	84.97	35.83	445.91
	20ID61E.25	-	-	-	-	275.68	13.40	83.23	4.31	143.19	70.97	37.16	460.20
	20ID61E.27	-	-	-	-	478.00	37.98	108.04	18.41	111.48	69.18	38.47	448.46
	20ID61E.33	-	-	-	-	252.74	11.47	85.97	4.11	154.32	76.92	42.03	451.66
	20ID61E.35	-	-	-	-	352.50	58.79	102.67	16.54	170.28	79.06	39.61	462.58

Appendix D Continued. U-Pb Apatite Ages and Closure Temperatures

Sample Name	Source File	Ca43_ mean (ppm)	±	Zr91_ mean (ppm)	± (ppm)	Final Pb206/ U238 age (Ma)	± (Ma)	Final Pb206/ U238 age (207Pb -corr) (Ma)	± (Ma)	C long (um)	a2 short (um)	ESR (um)	Closure Tempe -rature (°C)
	20ID61E. 36	-	-	-	-	318.00	27.26	98.06	9.72	141.75	72.17	40.40	450.23
	20ID61E. 38	-	-	-	-	447.09	34.09	108.70	9.98	96.53	76.78	31.34	441.16
	20ID61E. 39	-	-	-	-	417.55	23.39	103.94	6.55	88.95	61.59	30.80	440.54
	20ID61E. 43	--	-	-	-	411.83	18.68	70.36	3.82	87.08	61.64	33.51	443.53
	20ID61E. 44	-	-	-	-	319.08	23.93	88.11	7.32	136.37	69.40	35.39	458.39
	20ID61E. 47	-	-	-	-	362.69	26.53	102.39	8.71	162.97	65.80	43.62	453.01
	20ID61E. 48	-	-	-	-	468.23	86.18	142.71	38.81	154.06	81.74	33.12	455.96
	20ID61E. 50	-	-	-	-	390.08	36.76	100.08	10.87	123.53	59.53	33.90	443.95

Appendix D Continued. U-Pb Apatite Ages and Closure Temperatures

Sample Name	Source File	Ca43_ mean (ppm)	±	Zr91_ mean (ppm)	± (ppm)	Final Pb206/ U238 age (Ma)	± (Ma)	Final Pb206/ U238 age (207Pb -corr) (Ma)	± (Ma)	C long (um)	a2 short (um)	ESR (um)	Closure Tempe -rature (°C)
	20ID61E.51	-	-	-	-	331.35	20.25	69.86	4.90	165.82	63.89	42.97	465.64
	20ID61E.52	-	-	-	-	526.98	33.57	100.37	7.97	89.30	79.97	29.60	439.15
	20ID61E.54	-	-	-	-	526.98	33.57	100.37	7.97	89.30	79.97	29.60	439.15
	20ID61E.57	-	-	-	-	305.67	14.53	83.90	4.33	93.82	58.51	31.02	440.80
	20ID61E.59	-	-	-	-	909.40	49.61	126.31	12.29	100.57	61.26	31.27	432.08
	20ID61E.60	-	-	-	-	406.58	35.37	102.57	10.34	100.57	60.72	31.27	441.08
	20ID61E.61	-	-	-	-	216.59	20.56	110.97	10.82	121.9	60.72	40.86	441.08
	20ID61E.62	-	-	-	-	303.31	14.05	90.63	4.50	176.15	81.02	39.36	462.35

Appendix D Continued. U-Pb Apatite Ages and Closure Temperatures

Sample Name	Source File	Ca43_ mean (ppm)	±	Zr91_ mean (ppm)	± (ppm)	Final Pb206/ U238 age (Ma)	± (Ma)	Final Pb206/ U238 age (207Pb -corr) (Ma)	± (Ma)	C long (um)	a2 short (um)	ESR (um)	Closure Tempe -rature (°C)
	20ID61E. 63	-	-	-	-	397.76	20.34	89.37	5.20	202.73	68.91	58.90	445.33
	20ID61E. 64	-	-	-	-	475.57	37.10	109.72	9.31	106.45	112.46	34.14	464.12
	20ID61E. 65	-	-	-	-	598.15	27.84	86.99	5.26	151.09	66.86	46.19	444.19
	20ID61E. 68	-	-	-	-	678.36	130.52	124.52	42.43	80.69	89.32	30.06	455.11
	20ID61E. 69	-	-	-	-	640.53	52.68	137.75	14.53	74.75	61.58	30.41	439.69
	20ID61E. 70	-	-	-	-	417.22	24.19	98.96	6.79	100.87	64.25	35.64	440.10
	20ID61E. 71	-	-	-	-	500.53	18.26	107.54	4.43	169.7	71.77	47.57	445.72
	20ID61E. 73	-	-	-	-	476.41	34.22	83.22	7.88	146.16	90.07	43.24	456.18

Appendix D Continued. U-Pb Apatite Ages and Closure Temperatures

Sample Name	Source File	Ca43_ mean (ppm)	±	Zr91_ mean (ppm)	± (ppm)	Final Pb206/ U238 age (Ma)	± (Ma)	Final Pb206/ U238 age (207Pb -corr) (Ma)	± (Ma)	C long (um)	a2 short (um)	ESR (um)	Closure Tempe -rature (°C)
	20ID61E.81	-	-	-	-	498.32	20.04	94.32	4.58	270.19	82.93	104.68	452.70
	20ID61E.83	-	-	-	-	242.41	9.60	71.65	3.08	71.36	217.3	24.94	486.33
	20ID61E.84	-	-	-	-	477.22	39.75	130.70	43.68	77.65	50.07	28.59	433.19
	20ID61E.85	-	-	-	-	323.69	19.02	89.52	5.80	88.09	75.68	35.83	437.94
	20ID61E.86	-	-	-	-	288.12	17.74	94.33	6.24	84.93	50.52	26.09	445.91
	20ID61E.87	-	-	-	-	366.77	28.15	75.84	6.55	82.42	54.58	27.55	434.75
	20ID61E.92	-	-	-	-	432.33	25.09	101.89	6.87	93.55	45.87	24.58	445.15
	20ID61E.95	-	-	-	-	260.14	23.19	120.03	11.02	93.80	66.14	32.91	432.68

Appendix D Continued. U-Pb Apatite Ages and Closure Temperatures

Sample Name	Source File	Ca43_ mean (ppm)	±	Zr91_ mean (ppm)	± (ppm)	Final Pb206/ U238 age (Ma)	± (Ma)	Final Pb206/ U238 age (207Pb -corr) (Ma)	± (Ma)	C long (um)	a2 short (um)	ESR (um)	Closure Tempe -rature (°C)
	20ID61E.96	-	-	-	-	419.95	15.89	98.57	4.24	154.82	75.19	40.67	463.57
	20ID61E.98	-	-	-	-	368.11	42.74	107.71	12.83	192.60	99.05	52.62	442.89
61D	20ID61D.ZR.01	226450.05	223989	-	-	126.55	11.62	78.69	7.32	98.73	81.11	38.86	443.68
	20ID61D.01	-	-	-	-	178.46	4.60	95.98	2.78	150.00	90.00	46.40	463.12
	20ID61D.03	-	-	-	-	293.82	7.16	95.29	2.94	294.44	167.77	87.40	487.59
	20ID61D.04	-	-	-	-	284.24	15.52	145.45	8.48	161.22	98.37	50.54	466.33
	20ID61D.6	-	-	-	-	346.95	8.36	101.51	2.70	120.00	80.00	40.32	445.00

Appendix D Continued. U-Pb Apatite Ages and Closure Temperatures

Sample Name	Source File	Ca43_ mean (ppm)	±	Zr91_ mean (ppm)	± (ppm)	Final Pb206/ U238 age (Ma)	± (Ma)	Final Pb206/ U238 age (207Pb -corr) (Ma)	± (Ma)	C long (um)	a2 short (um)	ESR (um)	Closure Tempe -rature (°C)
	20ID6D.07	-	-	-	-	539.14	23.01	134.99	8.06	160.00	90.00	47.01	450.51
	20ID61D.08	-	-	-	-	584.07	18.90	103.58	7.49	166.62	92.04	48.24	451.45
	20ID61D.09	-	-	-	-	544.39	18.14	118.29	5.20	169.62	73.12	40.02	444.73
	20ID61D.10	-	-	-	-	276.41	10.05	91.70	3.78	89.11	40.90	22.16	424.26
	20ID61D.11	-	-	-	-	1014.2	20.85	159.48	5.97	104.04	63.50	32.62	437.52
	20ID61D.12	-	-	-	-	582.99	28.20	140.40	9.25	169.15	59.02	33.30	450.91
	20ID61D.14	-	-	-	-	282.85	18.59	134.91	9.67	153.20	81.34	42.96	447.26

Appendix D Continued. U-Pb Apatite Ages and Closure Temperatures

Sample Name	Source File	Ca43_ mean (ppm)	±	Zr91_ mean (ppm)	± (ppm)	Final Pb206/ U238 age (Ma)	± (Ma)	Final Pb206/ U238 age (207Pb -corr) (Ma)	± (Ma)	C long (um)	a2 short (um)	ESR (um)	Closure Tempe -rature (°C)
	21ID61D.15	-	-	-	-	276.24	5.59	88.54	2.02	120.76	49.38	27.25	431.28
	20ID61D.16	-	-	-	-	350.42	8.47	93.12	2.65	137.24	67.88	36.31	441.28
	20ID61D.ZR.05	256761.62	256607.1	-	-	365.41	27.83	154.81	12.93	186.02	119.14	60.58	459.80
	20ID61D.ZR.07	273768.27	262732.4	-	-	298.94	22.26	103.29	7.95	117.35	57.38	30.76	448.04
61C	20ID61C.11	-	-	-	-	481.59	11.85	70.14	2.17	283.76	196.67	98.25	439.83
	20ID61C.14	-	-	-	-	570.80	18.29	79.86	3.49	255.79	180.56	89.82	444.56

Appendix D Continued. U-Pb Apatite Ages and Closure Temperatures

Sample Name	Source File	Ca43_ mean (ppm)	±	Zr91_ mean (ppm)	± (ppm)	Final Pb206/ U238 age (Ma)	± (Ma)	Final Pb206/ U238 age (207Pb -corr) (Ma)	± (Ma)	C long (um)	a2 short (um)	ESR (um)	Closure Tempe -rature (°C)
	20ID61 C.01	-	-	-	-	814.53	29.03	107.59	6.29	243.12	100.94	55.57	461.32
	20ID61 C.05	-	-	-	-	1037.4	48.00	145.11	11.17	258.97	139.52	73.48	434.88
	20ID61 C.06	-	-	-	-	642.83	20.97	89.66	4.03	258.78	150.06	77.91	459.85
	20ID61 C.07	-	-	-	-	772.98	32.42	91.17	5.69	278.84	149.47	78.79	460.80
	20ID61 C.8	-	-	-	-	805.79	25.87	99.51	5.14	210.01	187.73	87.91	446.80
	20ID61 C.10	-	-	-	-	739.05	18.27	102.76	3.69	240.17	178.53	87.72	449.93
	20ID61 C.15	-	-	-	-	738.48	29.48	92.75	5.17	207.31	167.43	80.57	462.34
	20ID61 C.16	-	-	-	-	894.70	33.33	121.66	8.16	226.00	174.14	84.81	444.58

Appendix D Continued. U-Pb Apatite Ages and Closure Temperatures

Sample Name	Source File	Ca43_ mean (ppm)	±	Zr91_ mean (ppm)	± (ppm)	Final Pb206/ U238 age (Ma)	± (Ma)	Final Pb206/ U238 age (207Pb -corr) (Ma)	± (Ma)	C long (um)	a2 short (um)	ESR (um)	Closure Tempe -rature (°C)
	20ID61C.AP.01	278385.6	11554.50	0	0	1599.4	80.13	174.09	23.93	132.83	65.02	34.85	433.86
	20ID61C.AP.02	296707.2	11774.94	116183	27004.	536.39	64.80	125.32	17.27	215.54	69.95	39.84	492.28
	20ID61C.AP.03	323806.7	12610.79	0	0	1175.4	94.59	95.11	32.38	183.93	125.99	63.11	474.70
	20ID61C.AP.04	310375.3	15206.67	0	0	1130.3	68.87	170.06	17.20	88.81	60.23	30.24	456.61
	20ID61C.AP.05	288354.7	12272.07	70799.	10136.	513.21	45.04	99.88	11.45	155.82	79.99	42.51	467.03
	20ID61C.AP.06	319817.6	14020.00	0	0	1452.3	114.04	134.15	30.13	260.86	113.93	62.23	469.25
	20ID61C.AP.07	305508	11366.15	0	0	1227.4	84.45	100.87	15.59	130.61	83.32	42.40	469.68

Appendix D Continued. U-Pb Apatite Ages and Closure Temperatures

Sample Name	Source File	Ca43_ mean (ppm)	±	Zr91_ mean (ppm)	± (ppm)	Final Pb206/ U238 age (Ma)	± (Ma)	Final Pb206/ U238 age (207Pb -corr) (Ma)	± (Ma)	C long (um)	a2 short (um)	ESR (um)	Closure Tempe -rature (°C)
	20ID61C.AP.08	208576.80	11718.10.	0	0	1103.0	113.34	104.42	30.63	132.89	92.76	46.27	473.87
	20ID61C.AP.09	322056.20	13598.81	0	0	937.93	67.88	83.21	25.30	156.42	86.76	45.44	473.79
	20ID61C.AP.12	292401.50	13260.53	0	0	976.49	70.74	91.20	22.88	93.58	53.67	27.92	470.53
	20ID61C.AP.16	308977	12808.05	0	0	986.58	66.60	87.40	21.42	124.22	53.67	29.37	472.49